WEATHERING OF SULFIDE ORES IN MODEL SOILS, POTENTIALLY TOXIC ELEMENT RELEASE AND BIOAVAILABILITY

by

THOMAS CHARLES ROBSON

A thesis submitted to Plymouth University in partial fulfilment for the degree of

DOCTOR OF PHILOSOPHY

School of Geography, Earth and Environmental Sciences

Faculty of Science and Environment

September 2013

AUTHOR'S DECLARATION

At no time during the registration for the degree of Doctor of Philosophy has the author been registered for any other University award without prior agreement of the Graduate Committee. Work submitted for this research degree at the Plymouth University has not formed part of any other degree either at Plymouth University or at another establishment.

This study was financed with the aid of a studentship from Plymouth University and additional funding from the Seale Hayne Educational Trust. The work presented in this Thesis was primarily the work of the author unless acknowledged otherwise.

Relevant scientific seminars and conferences were regularly attended at which work was often presented; external institutions were visited for consultation purposes and several papers were prepared for publication.

Word count of main body of thesis: 44,198

Signed .....

Date .....

Weathering of Sulfide Ores in Model Soils, Potentially Toxic Element Release and Bioavailability

Thomas Robson

The exploitation of metallic sulfide ores produces vast quantities of fine-grained wastes hosting potentially toxic elements (PTEs). There are concerns that, if improperly disposed of and managed, waste mineral particles can behave as vectors that disperse PTEs via aeolian and fluvial transport, subsequently contaminating soils and crops used to support human populations. The importance of these particles, as sources and influencers of PTE biogeochemistry in productive soils, has received limited research.

Long-term (365 d) batch incubation experiments, field weathering experiments and phytoavailability trials, were performed to establish the rate, patterns and factors limiting PTE (Cd, As, Hg) release from grains of sphalerite (Zn(Fe,Cd)S), arsenopyrite (FeAsS) and cinnabar (HgS) into soil matrices (0.1 % mineral:soil m/m), and the bioavailability of the liberated PTEs to important food crops (*Tricitum aestivum*, wheat and *Oryza sativa*, rice).

All three of the ores underwent chemical weathering in oxic agricultural soils of both temperate and sub-tropical provenance, during which nonessential PTEs (cadmium, mercury, arsenic) were released in bioavailable forms, at rates relevant to agricultural production. Sphalerite weathered at a rate of 0.6 to 1.2 % a^{-1} (Cd basis) in the experimental soils, releasing 0.5 to 1 μmol Cd g^{-1} ZnS a^{-1} into the soil matrix. Cinnabar weathering reached a maximum of 12.0 – 13.5 % (Hg basis) after 90 days exposure in oxic soils, whereas arsenopyrite weathering was rapid and extensive, reaching 56 to 66 % (S basis) after 180 days. The PTE concentrations accumulated in edible grains of wheat and rice grown in the sulfide-contaminated soils were higher than international food safety limits by factors of 8 (Cd in rice), 10 – 30 (Hg in wheat and rice) and 8 – 12 (As in wheat and rice).

The primary geochemical factors controlling PTE release and bioavailability were solid-phase associations (i.e. PTEs complexed by clays, metal oxyhydroxides and organic matter) and the precipitation of secondary mineral phases. Weathering arsenopyrite grains were passivated from further oxidation by secondary iron-arsenate phases, which also co-precipitated arsenic liberated from the ore. Secondary phase formation was identified as the cause of decreasing extractable Hg (liberated from cinnabar) after mercury release from cinnabar peaked (≤ 90 days exposure). For sphalerite, the evidence indicates that secondary sulfide phases formed under flooded (sulfate-reducing) soil conditions (paddy rice), limited the bioavailability of cadmium previously liberated under oxic conditions.

These key findings demonstrate a potential human health hazard relating to the dispersal of PTE-hosting sulfide ore particles produced by mining activities into soils supporting human populations via crop contamination. This work also highlights differences in ore geochemistry, showing the need for additional research on different ore minerals and their alteration products.

Acknowledgements

I am eternally grateful to my supervisors, Dr. Charly Braungardt, Dr. John Rieuwerts, Prof. Paul Worsfold and Dr. Miranda Keith-Roach for their guidance, wisdom and support throughout my PhD studies. I have to say that Charly has been the most committed and selfless mentor anybody could wish for.

I would also like to say a big 'thank you' to Dr. Claire Williams and the many Andy's of Plymouth University (Dr. Andy Fisher, Andy Arnold, Andy Atfield and Andrew Tonkin) for the great technical assistance, inventiveness and tolerance they have shown me over the years.

It has been a pleasure to be part of the Biogeochemistry Research Centre (BGC) community. Thanks to PhD students past and present (Jane, Luke, Estella, Holly, Neil, Apha) for the banter, the pep talks and comradeship.

I would also like to acknowledge my family, especially my partner, Alice, for their love and companionship during challenging times.

Conference presentations and publications

Oral presentations

T. Robson, C. Braungardt, J. Rieuwerts, P. Worsfold. "Sphalerite weathering in soils: Implications for Cd contamination of crops". 23rd SETAC Europe Annual Meeting, SECC, Glasgow, UK. 12 – 16 May 2013.

T. Robson, C. Braungardt, J. Rieuwerts, P. Worsfold. "Sphalerite in agricultural soils: Implications for Cd contamination of crops". 4th Annual Biogeochemistry Conference (BGC), National Marine Aquarium, Plymouth, UK. 17 December 2012.

T. Robson, C. Braungardt, M. Keith-Roach, P. Worsfold. "Weathering of arsenopyrite in agricultural soils". Goldschmidt 2011, Prague Congress Centre, Prague, Czech Republic. 14 – 19 August 2011.

T. Robson, C. Braungardt, M. Keith-Roach, P. Worsfold. "Risks from the weathering of arsenopyrite in agricultural soils". 2nd Annual Biogeochemistry Conference (BGC), Plymouth University, UK. 18 December 2010.

International peer-reviewed journal publications

T.C. Robson, C.B. Braungardt, J. Rieuwerts P. Worsfold (2014). "Cadmium contamination of agricultural soils and crops resulting from sphalerite weathering". *in press Environmental Pollution*, 184, 283-289, DOI: 10.1016/j.envpol.2013.09.001.

Thomas C. Robson, Charlotte B. Braungardt, Miranda J. Keith-Roach, John R. Rieuwerts and Paul J. Worsfold (2013). "Impacts of arsenopyrite contamination on agricultural soils and crops". *Journal of Geochemical Exploration*, 125, 102-109.

List of contents

List of figures

List of tables

List of abbreviations

AFM	Atomic force microscopy
ANOVA	Analysis of variance
ATR-IR	Attenuated total reflectance [coupled with] infrared spectroscopy
AVS	Acid-volatile sulfide
BCF	Bioconcentration factor
CHNS	Carbon, hydrogen, nitrogen, sulfur [elemental analyser]
DOC	Dissolved organic carbon
DOM	Dissolved organic matter
DW / DWE	Dry weight [equivalent]
eCEC	Effective cation exchange capacity
EDTA	Ethylenediaminetetraacetic acid
Eh	Redox potential
EXAFS	Extended X-ray absorption fine-edge structure
FAO	United Nations Food and Agriculture Organisation
HDPE	High density polyethylene
HEPES	4-(2-hydroxyethyl)-1-piperazineethanesulfonic acid
ICP-MS	Inductively coupled plasma mass spectrometry
ICP-OES	Inductively coupled plasma optical emission spectrometry
K	Equilibrium constant
LOD	Limit of detection
log K	Stability constant
OM	Organic matter

ORP	Oxidation-reduction potential [electrode]
PM_{10}	Particles with nominal aerodynamic diameter of less than 10 μm
$PM_{2.5}$	Particles with nominal aerodynamic diameter of less than 2.5 μm
PMTMI / PWTMI	Provisional [monthly/weekly] tolerable maximum intake
PP	Polypropylene
PTE	Potentially toxic element
PTFE	Polytetrafluoroethylene
RSD	Relative standard deviation
SEM	Scanning electron microscopy
SEM-EDXS	Scanning electron microscopy [coupled with] energy dispersive X-ray spectroscopy
SRI	System of rice intensification
TF	Transfer factor
UHP	Ultra-high purity [water]
WHO	World Health Organisation
XANES	X-ray absorption near-edge structure
XPS	X-ray photoelectron spectroscopy
XRD	X-ray diffraction

Chapter 1

Introduction

1.1 Environmental and human health risks associated with mineral exploitation

Sulfide ore minerals, which are rich in desirable but potentially toxic elements (PTEs) such as copper, lead, cadmium, arsenic and mercury, have been extensively exploited around the world for thousands of years (Qiu et al., 2012; Oyarzun et al., 2013). The extractive processes (e.g. drilling, blasting) and processing activities (e.g. crushing, milling, separation, transport) used produce vast quantities of fine-grained material (Higueras et al., 2006; Castillo et al., 2013). This significantly increases the surface area of the mineral resources, which aids metal recovery, and also generates granular wastes consisting of gangue, uneconomic grades of ores and guest minerals and incompletely recovered ores (Roussel et al., 2000; Kim et al., 2004; Parviainen et al., 2012a). It is estimated that over 1 million abandoned mines exist in the world (UNEP, 2001). Waste material tips, pits and lagoons represent key sources of PTEs in the surface environment due to their often high residual metal content, abundance, physical and chemical instability, improper disposal and maintenance (Candeias et al., 2010). These wastes are often toxic and devoid of organic matter, which inhibits plant succession and soil development, leaving their surfaces exposed to erosion (Mendez & Maier, 2007) and enabling particle dispersal into the wider surface environment. These dispersed particles are vectors for toxic metals and metalloids, connecting mines and soils. This material can degrade soil function by acidification and introduction of bioavailable PTE species to soils (Ramsey et al., 2005), and raises concerns over human health risks arising from consumption of contaminated crops (Dudka et al., 1995; Yu et al., 2006; Peralta-Videa et al., 2009), especially in developing and rapidly industrialising countries, where environmental regulations (i.e. for waste disposal management) may be either weak or poorly enforced and communities depend on

soils impacted by mining (Miller et al., 2004; Zhuang et al., 2009). However, the weathering behaviour and influence of mining waste particles upon biogeochemical cycling of PTEs and the associated environmental and human health risks, is poorly understood.

1.2 Dispersal of mineral particles into the environment

Aeolian (wind-blown dusts) and fluvial (surface run-off; transport in streams, rivers and flood plains) transport (Figure 1.1) are generally agreed to be the dominant environmental dispersal pathways for mineral particles produced by mining. It is suggested that, in a semi-arid climate, the impact of these two pathways is roughly equal but that fluvial and aeolian transport are favoured by wet and dry climates, respectively (Blight & Da Costa, 2001).

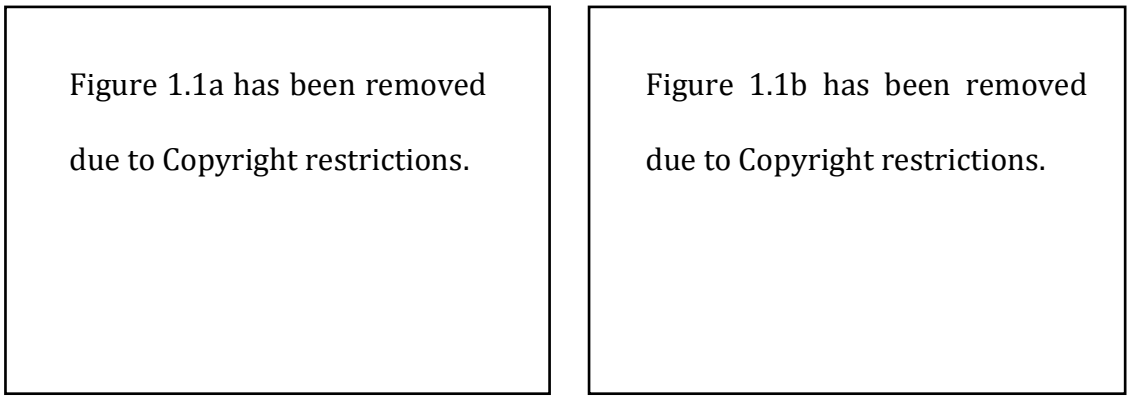

Figure 1.1 Images illustrating (a) gullies formed by surface run-off erosion of waste piles[1] and (b) dust plume emanating from a tailings impoundment as the result of wind erosion[2].

[1] Reprinted from Science of the Total Environment, 449, Castillo et al., Contribution of mine wastes to atmospheric metal deposition in the surrounding area of an abandoned heavily polluted mining district (Rio Tinto Mines, Spain), 363-372, Copyright (2013), with permission from Elsevier.

[2] Reproduced from Water, Air and Soil Pollution, 152, 2004, 133, Arsenic and Heavy Metal Pollution of Soil, Water and Sediments in a Semi-Arid Climate Mining Area in Mexico, Razo et al., figure 2 with kind permission from Springer Science and Business Media.

Particles are eroded from exposed tailings piles and impoundments by the surface impact of wind-blown rain droplets and, if the water storage and infiltration capacity of the wastes are exceeded, by surface run-off (Dorren & Blight, 1986), after which they may enter surface waters and be transported further afield (order of kilometres to tens of kilometres), resulting in the contamination of floodplain soils (Miller et al., 2004; Razo et al., 2004) and agricultural soils where river waters are used for irrigation (Simmons et al., 2005; Zhuang et al., 2009; Razo et al., 2004). In addition, wastes have been released directly into surface waters by improper disposal to rivers and river banks (Kossoff et al., 2012; Lavazzo et al., 2012) and dam failures (Albering et al., 1999; Lopez et al., 2008; Hudson-Edwards et al., 2005).

Aeolian particle dispersal is evidenced both indirectly, by the spatial distributions of soil contamination in mining areas (Lopez et al., 2008; Zhuang et al., 2009; Razo et al., 2004), and directly by means of air quality monitoring data showing that grains (sulfides and other metal-rich forms), including those of respirable diameter, are dispersed from mining wastes (Moreno et al., 2005; Zota et al., 2009; Moreno et al., 2006; Kocman et al., 2011; Castillo et al., 2013).

The probability of wastes being eroded by winds and the distances over which they can be transported depend on many factors, such as the physical properties of the particles (size, density, morphology), wind velocity, land surface morphology and vegetation cover (Lawrence & Neff, 2009). The finest particles (< 20 μm) are most likely to be transported in suspension by turbulent air, travelling large distances (order of kilometres), whereas larger grains (20 – 70 μm) may be suspended for a short time (order of hundreds of metres). Larger grains either successively hop (saltation, 60 – 500 μm) or creep (> 500 μm) along the ground (Figure 1.2).

Figure 1.2: The modes of aeolian particle transport.[3]

Saltating and creeping grains also bombard very fine material, overcoming inter-particle cohesion and aiding suspension (Lancaster, 2009a; Bagnold, 1941; Kon et al., 2007) (Lancaster, 2009b; Bagnold, 1941; Kon et al., 2007). Mass loss occurs predominantly from the uppermost slopes of elevated waste impoundments, and the majority of erosion is thought to occur during infrequent weather events where winds are sufficiently energetic to suspend the material (Blight & Da Costa, 2001).

1.3 Chemical weathering of minerals in soils

Sulfides are chemically reactive in oxic environments, as demonstrated by pyrite (FeS_2) oxidation and resulting supergene processes and acid mine drainage observed in many waste tips (Schippers, 2004). Sulfide minerals are formed under conditions that differ considerably from surficial environments (i.e. heat, pressure, supersaturated hydrothermal fluids). In addition, the sulfur moiety of sulfide minerals is reduced (S^{-2} or S^{-1}) and therefore vulnerable to oxidation (Schippers,

[3] Reproduced from Greeley and Iversen (1985) with permission from Cambridge University Press.

2004). As a result, many sulfides are considered metastable under surficial, oxic and biologically active conditions (Figure 1.3).

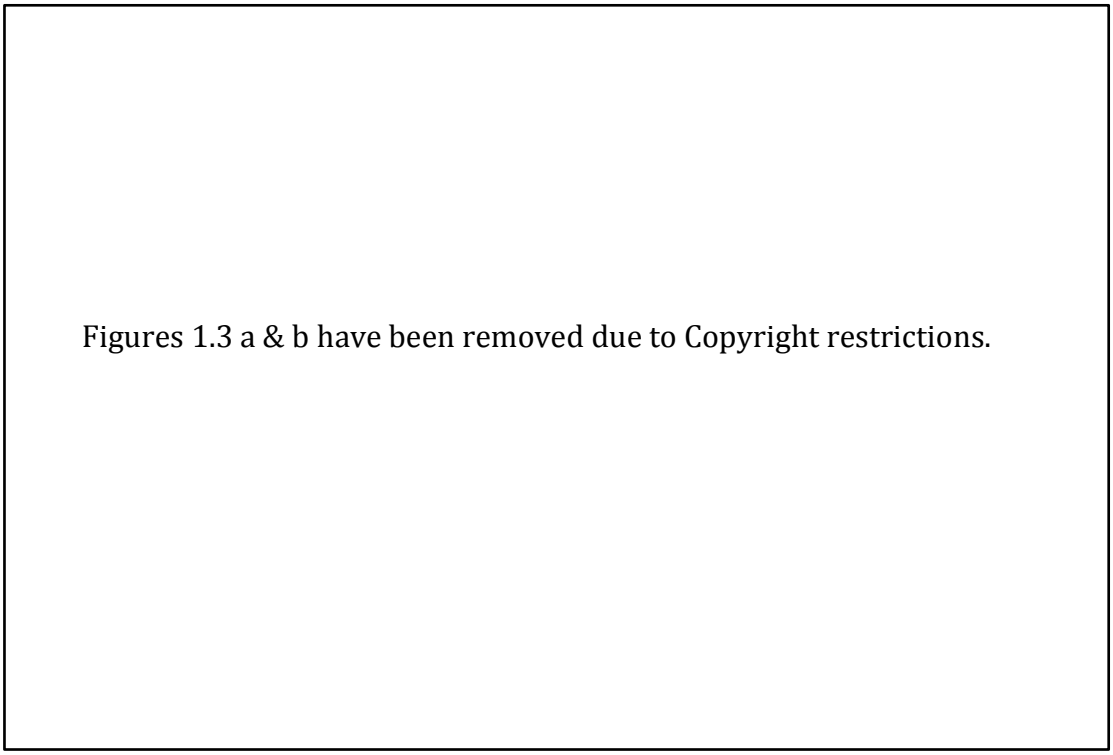

(a) (b)

Figure 1.3: (a) Eh-pH diagrams for the Fe-As-S-O system at 25 ˚C and 1 atm.[4] (b) Eh-pH phase diagram for Hg-O-H-S-Cl system (Hg = 10^{-8} mol L^{-1}, Cl=$10^{-3.5}$ mol L^{-1}, S=10^{-3} mol L^{-1}).[5]

Crucially, the weathering of sulfide grains in soils may release PTEs, providing a source of potentially bioavailable species for plant uptake (Chamon et al., 2005). In addition, the liberation of PTEs from the mineral matrices enhances the ecotoxicological risk of surface and groundwater pollution (Robles-Arenas et al., 2006) and degraded soil function (Ramsey et al., 2005). A conceptual model for the interaction of sulfide ores, the PTEs they host, and soils is provided in Figure 1.4.

[4] ~~Reprinted from Applied Geochemistry, 24/12, Corkhill et al., Arsenopyrite oxidation - A review, Pages 2342 – 2361, Copyright (2009), with permission from Elsevier.~~

[5] ~~Produced from Arbestain et al. (2009) under open license.~~

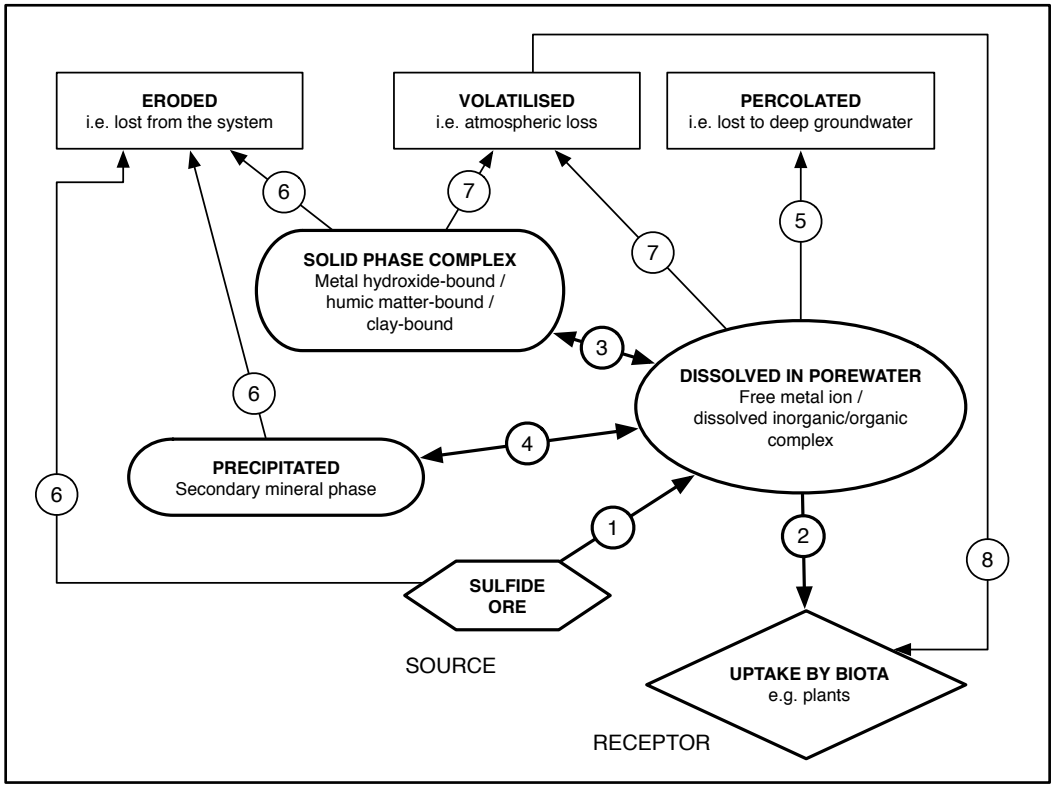

Figure 1.4 Conceptual model of a soil – sulfide – plant system. Biogeochemical processes represented by each pathway are discussed by number in the text. The processes most relevant to this study are emboldened.

It is proposed that this chemical weathering, resulting in the dissolution of the mineral phase, releases PTEs into the soil solution, where they may become part of a dissolved inorganic or organic complex (Figure 1.4 process 1) and rendered available for plant uptake (2). Alternatively, they may form surface complexes with solid soil phases (3) or precipitate as part of a secondary mineral phase (4). The PTEs may be effectively lost from the system by percolation of the dissolved fraction to deep groundwater (5), where they are effectively unavailable for uptake by biota in the soil. Losses, or rather transference, may also be attributed to the soil erosion (6) and, for volatile elements (i.e. mercury), by vapour loss to the atmosphere (7). These loss factors could also constitute pollutant linkages with other receptors, which are not the focus of this study (e.g. groundwater pollution).

A potential pollutant linkage may exist between the source (sulfide ores) and the receptor of interest, plants (human consumers by proxy), via processes (1) and (2) for non-volatiles, or (1) and (8) via (7) for mercury. The key factors determining the magnitude of this hazard are the rate of mineral weathering (1), the solid-liquid distribution (3 and 4) and the rate of plant uptake (2). In addition, plants are known to modify the geochemical conditions in the rhizosphere to regulate the bioavailability of metals (discussed in section 1.4), therefore mediating processes (3) and (4).

1.4 PTE uptake by plants

Plant species, such as wheat and rice, provide the primary source of carbohydrate to humans and are cultivated globally. As such, they represent an important pathway between soil-borne contaminants and humans (Lee et al., 2008; Liu et al., 2010). Several studies link mining, the contamination of soils by PTEs and crop contamination. For example, rice grown in the Dabaoshan mining area, China, accumulated 1.2 – 3.9 nmol Pb g^{-1} and 3.4 – 62 nmol Cd g^{-1} in edible tissues (Zhuang et al., 2009). The estimated daily intake of lead and cadmium for local populations consuming that rice is higher than guideline values (WHO, 2005; WHO, 1999) by factors of 2.3 and 6.8, respectively. The grains of rice grown near Myungbong mine, South Korea, contained 4.5 times the national average of arsenic (5.47 nmol As g^{-1} compared with 1.2 nmol As g^{-1}) and may present an excess cancer risk to long-term consumers (Lee et al., 2008).

With the possible exception of mercury, which may be absorbed directly from the atmosphere (Niu et al., 2011), higher plants obtain metals and metalloids directly from soils. In addition to macronutrients (e.g. potassium, magnesium), plants also obtain micronutrient metals (e.g. iron, zinc, nickel) that are biologically

essential but which may become toxic at excessive concentrations. The abundance and bioavailability of these nutrients in soil porewater will not, in most cases, match the requirements of plants. Furthermore, those requirements vary widely between tissue, cell and sub-cellular components. Consequently, plants actively influence metal bioavailability in the rhizosphere, and regulate root uptake, translocation and storage (Figure 1.5), a phenomena termed metal homeostasis (Clemens et al., 2002). The uptake of biologically nonessential elements (e.g. cadmium and arsenic) can be regarded as a side effect of nonspecific metal homeostatic processes, as will be discussed.

Plants modify rhizospheric geochemical conditions both to enhance and diminish metal availability. For example, iron solubility is severely limited by the formation of oxyhydroxide minerals in circum-neutral oxic soils. Iron, phosphorus and zinc-deficient plants (e.g. *Zhea mays*) have been shown to enhance iron availability by exuding hexadentate phytosiderophore chelants (Figure 1.5 process a), which scavenge Fe(III) from solid phases (Meda et al., 2007). However, root exudates express a broad mobilising effect and can also increase the bioavailability of potentially toxic essential (e.g. zinc, copper, nickel) and non-essential (e.g. cadmium, lead, arsenic) elements (Luo et al., 2008). Conversely, the rhizosphere oxidising capabilities of *Oryza sativa* promote the precipitation of iron oxyhydroxide root plaques. Not only does this limit the bioavailability (i.e. phytotoxicity) of the iron, which is much more soluble (Fe^{2+}) under flooded reducing soils compared with oxic conditions, but the process may also benefit the plant by co-precipitating cadmium (Wang et al., 2011) and arsenic (Xu et al., 2008).

Root uptake (Figure 1.5 process b) is an active process, mediated by transporter proteins that bind and transport metal ions and hydrated complexes across the root membrane and into cell vacuoles for storage (Clemens et al., 2002).

Several studies have demonstrated that, in common with rhizosphere exudate strategies, transporter proteins express variable metal specificity. For example the plasma membrane protein OsNRAMP5, which is important for iron and manganese uptake, is also the dominant cadmium transporter in *Oryza sativa* (Clemens et al., 2013).

A key determinant of metal accumulation in aerial (i.e. edible) tissues is root-to-stem translocation via the xylem (Figure 1.5 process c) (Uraguchi et al., 2009). The processes retarding root-to-stem translocation are root vacuolar storage and the transport of metals into the xylem, the general effectiveness of which is reflected by the consistent observation that nonessential metal concentrations in plants decrease in the order: roots > stems > leaves & grains. Again, these processes are controlled by chelants and transporter proteins (Clemens et al., 2013), which are not always specific. For instance, important proteins for silicon (silicic acid) xylem transport are also permeable to arsenic (arsenous acid) in *Oryza sativa* (Ma et al., 2008).

Figure 1.5 has been removed due to Copyright restrictions.

Figure 1.5 Illustration of the key biogeochemical processes controlling metal mobilisation, root uptake, upward translocation and storage in higher plants. CW = cell wall; M = metal; filled circles = chelants; filled ovals = transporters; bean-shaped structures = metallochaperones.[6]

[6] ~~Reprinted from Trends in Plant Science, 7, Stephan Clemens, Michael G Palmgren, and Ute Krämer, A long way ahead: understanding and engineering plant metal accumulation, Pages 309 – 315, Copyright (2002), with permission from Elsevier.~~

1.5 Toxicity of PTEs to humans

The risk posed to humans by consumption of plants contaminated with PTEs is dependent upon several factors: (a) concentration accumulated in edible tissues of plants, which is a function of the element speciation, environmental conditions and plant physiology; (b) consumption rates of those plants and (c) systematic absorption of PTEs, toxic dose and severity of health effects (Table 1.1). Reviews on the risk posed by PTEs in the food chain have highlighted arsenic, cadmium, mercury, lead, chromium and selenium as priority elements for research (McLaughlin et al., 1999; Peralta-Videa et al., 2009).

Table 1.1: Summary of medical symptoms (chronic exposure), concentrations indicative of toxic doses and intake guidelines relating to exposure to major and trace metals. Modified after Soghoian and Sinert (2009). Daily intake guidelines, where provided, are based on the WHO/FAO provisional weekly tolerable daily intake values. 1dL = 0.1 L

Metal	Symptoms	Toxic Concentration	Daily intake guideline
Arsenic	Diabetes, hypopigmentation/ hyperkeratosis, cancer: lung, bladder, skin, encephalopathy	24-h urine: ≥50 μg L^{-1} urine, or 100 μg g^{-1} creatinine	0.20 μmol kg^{-1} body weight $week^{-1}$ (WHO/FAO, 1989)
Cadmium	Proteinuria, lung cancer, osteomalacia	Proteinuria and/or ≥ 15 μg g^{-1} creatinine	0.22 μmol kg^{-1} body weight $month^{-1}$ (FAO/WHO, 2011)
Copper	vineyard sprayer's lung (inhaled); Wilson disease (hepatic and basal ganglia degeneration)	Normal excretion: 25 μg per 24 h (urine)	
Iron	Hepatic cirrhosis	Nontoxic: <300 μg dL^{-1} Severe: >500 μg dL^{-1}	
Lead	Encephalopathy, anaemia, abdominal pain, nephropathy, foot-drop/ wrist-drop	Pediatric: symptoms or [Pb] ≥ 45 μg dL^{-1} (blood); Adult: symptoms or [Pb] ≥ 70 μg/dL^{-1}	
Mercury	Nausea, metallic taste, gingivo-stomatitis, tremor, neurasthenia, nephrotic syndrome; hypersensitivity (Pink disease)	Background exposure "normal" limits: 10 μg L^{-1} (whole blood); 20 μg L^{-1} (24-h urine)	Total Hg: 20 nmol kg^{-1} body weight $week^{-1}$, MeHg: 8 nmol kg^{-1} body weight $week^{-1}$ (FAO/WHO, 2010; WHO/FAO, 2003)
Nickel	Occupational (inhaled): pulmonary fibrosis, reduced sperm count, nasopharyngeal tumours	Excessive exposure: ≥8 μg L^{-1} (blood) Severe poisoning: ≥500 μg L^{-1} (8-h urine)	
Silver	Argyria: blue-grey discoloration of skin, nails, mucosae	Asymptomatic workers have mean [Ag] of 11 μg L^{-1} (serum) and 2.6 μg L^{-1} (spot urine)	
Zinc	Copper deficiency: anaemia, neurologic degeneration, osteoporosis	Normal range: 0.6 – 1.1 mg L^{-1} (plasma) 10 – 14 mg L^{-1} (red cells)	

1.6 Minerals selected for study

Three sulfide minerals were selected for study, based on their widespread global distribution, record of exploitation, evidence of contemporary dispersal and/or presence in abandoned wastes, the chronic toxicity of their associated nonessential PTEs at relatively low concentrations, our existing understanding of plant metal uptake and evidence implicating mine waste in relation to adverse human health and/or ecotoxicological effects.

1.6.1 Sphalerite

Apart from iron sulfides (e.g. chalcopyrite, $CuFeS_2$), sphalerite (ZnS) is the most common of the naturally occurring sulfide minerals, the principal ore of zinc and the primary source of cadmium. Sphalerite is formed under a range of hydrothermal conditions, in coal, limestone, and other sedimentary deposits, and often associated with galena (PbS) (Anthony et al., 1990). In the sphalerite crystal structure, zinc is often isomorphically substituted by other metals, and common impurities include Fe (≤ 26 %), Mn (≤ 6 %) and Cd (≤ 2 %) (Cook et al., 2009; Smolders & Mertens, 2013). For this reason, sphalerite is a major source of cadmium, the PTE of concern in this case. Sphalerite, which is processed by smelting or electrolytic methods, is produced by many countries (Figure 1.6). Annual global zinc production from mining (all minerals) was 13 million tonnes in 2012 and the global resource is estimated to be 1.9 billion tonnes (US Geological Survey, 2013).

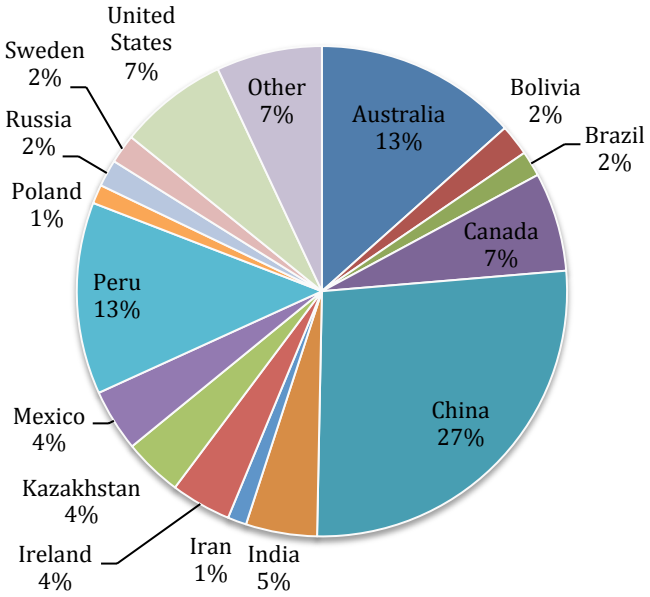

Figure 1.6 Mean mine production of zinc between 2004 and 2008. Based on USGS Minerals Yearbook data (United States Geological Survey, 2008).

1.6.2 Cinnabar

Cinnabar (HgS) is the primary mineral ore of mercury in the world's 26 mercury mining belts (Holley et al., 2007). It forms from low-temperature hydrothermal solutions in veins and in sedimentary, igneous, and metamorphic host rocks (Anthony et al., 1990; King, 2002). An estimated 1200 sites have been used for mercury extraction and ore processing in the world (UNEP, 2009) but falling demand and an increasing awareness of the deleterious environmental and human health implications of mercury contamination have resulted in a collapse of mercury mining since the 1970s (Loredo et al., 2006). As a result, many of the world's largest production centres (e.g. Almaden, Spain; Wuchan, China; Idrija, Slovenia; Californian Coastal Belt, USA) ceased production before 2005 (Horvat et al., 1999; Gray et al., 2000; Rytuba, 2000; Moreno et al., 2005; Li et al., 2012). For the most part, only small-scale 'artisanal' mercury mining continues (Qiu et al., 2006), but mercury is also indirectly sourced as a by-product in other ores (Rytuba, 2003). Mercury production by mining was 1600 tonnes in 2012 and global resources are estimated at 600000 tonnes (US Geological Survey, 2013). Crushed cinnabar is roasted to produce sulphur dioxide (SO_2) and mercury vapour, which is then condensed to the liquid state.

1.6.3 Arsenopyrite

Arsenopyrite (FeAsS) is the most abundant arsenic-containing mineral and occurs worldwide. Global arsenic production was 52,700 tons in 2009 (as As_2O_3), of which the primary producers were China (47 %), Chile (19 %), Morocco (17 %) and Peru (8 %). Global arsenic resources are estimated at 880000 tonnes (US Geological Survey, 2013). Arsenic may be obtained from roasting arsenopyrite as well as from copper, gold and lead smelter dust (USGS, 2010). Arsenopyrite forms

at high temperatures and is often found in hydrothermal vein systems and contact metamorphic systems, where it is associated with other high-temperature formation sulfides, such as chalcopyrite and sphalerite (King, 2002a) and also gold deposits (Roussel et al., 2000).

1.7 Investigative approaches used to study mineral weathering

The relevant investigative approaches previously applied to study the weathering behaviour of minerals and their weathering products, and to predict their environmental behaviour, are summarised in this section. The benefits and limitations of the approaches are briefly discussed with an emphasis on studying mineral-soil interactions.

1.7.1 Mixed flow reactors

Numerous mineral dissolution experiments have been designed around mixed-flow reactors, whereby a mineral sample is exposed to a constantly flowing solution (variable pH and purging with air, pure O_2 or pure N_2) and comparisons of inlet and outlet solution chemistry supports inferences on mineral alteration behaviour (Stanton et al., 2008; Asta et al., 2010; Barnett et al., 2001). The reactors have also been coupled with mineralogical examination of the weathered material using, for example, X-ray photoelectron spectroscopy and attenuated total reflectance infrared spectroscopy, to provide additional insights into the speciation of secondary products and dissolution mechanisms (Holley et al., 2007; Asta et al., 2010).

The advantages of this approach are that investigators can monitor the release, solution chemistry and precipitation of metals originating from the target

mineral under tightly controlled and replicable conditions. This makes these approaches suitable for producing thermodynamic data for equilibrium models and predicting rock-water interactions (i.e. flooded mine shafts). The mechanistic understanding afforded by such studies can also complement the interpretation of data from other experimental approaches. The primary limitation is that this experimental approach cannot be applied to soil-mineral mixtures unless stirred soil slurries are used (de Livera et al., 2011), which is not satisfactorily representative of environmental conditions.

1.7.2 Humidity cells

Humidity cells are laboratory-scale reactors designed to model the weathering of waste rock by enhancing (accelerating) oxidative processes, therefore providing indications of the sample's acid generation, neutralisation potential and leachate chemistry. Samples (typically 1 kg) are generally incubated in sealed containers for 16 – 24 weeks, exposed to cycles of moist and dry air, and periodically (e.g. weekly) saturated with deionised water, which is drained and analysed (e.g. pH, conductivity, sulfate, metals) (ASTM International, 2012).

The advantages of humidity cells are that they are a fast (relatively) and cost-effective means of acquiring experimental data for predictions of oxidative dissolution rates and stability of environmentally exposed waste rock. The experiments are readily replicated to quantify the uncertainties, which is crucial for predictive applications. The drawbacks of this approach are that the methods are not designed for mineral-soil mixtures and the artificial enhancement of oxidative processes may produce misleading results (Sapsford et al., 2009).

1.7.3 Soil incubations

The term 'soil incubations' is used here to describe experimental approaches involving the exposure of minerals to soils under specific environmental conditions to investigate their weathering behaviour. Data describing mineral alterations and metal behaviour are obtained by aqueous extraction, sometimes in combination with spectroscopic analyses.

Static batch incubations, also referred to as microcosms, have been used to simulate the influence of oxic and reducing soil conditions upon minerals (Han et al., 2006) and metallic alloys (Handley-Sidhu et al., 2009). Batches of small closed (e.g. serum bottles) or open (e.g. pots) systems are incubated and analysed (chemically, physically and spectroscopically) at varying exposure intervals in these experiments.

Column experiments, either with waste rock and waste rock-soil mixtures (Kossoff et al., 2011) or mineral-sand mixtures (Barnett et al., 2001), have been used to investigate the environmental stability of minerals, soil-mineral interactions and the transport of weathering products. Deionised water or artificial rainwater are usually either pumped upwards through the column (avoiding preferential flow pathways) or fed from above and allowed to percolate through the column. As with mixed flow reactors (section 1.7.1), the effluent is analysed at regular intervals and inferences are made from those data.

Field incubations involve the deposition of experimental minerals in soils and sediments under real environmental conditions. The samples are excavated after a specific exposure (i.e. 'incubation') duration and examined or analysed. This approach has been used to investigate the formation of secondary mineral phases (Mihaljevic et al., 2010; Robson et al., 2013) and the bacterial colonisation of minerals (Vazquez-Rodriguez et al., 2012).

Soil incubations incorporate the complexity of soil matrices and the influence of those matrices upon the biogeochemistry of metals released from minerals into the experimental system (Figure 1.4). Within this category, each approach has specific benefits and limitations. Field incubations provide the most environmentally realistic weathering conditions but the conditions cannot be controlled and are difficult to monitor; therefore field incubations are suitable when investigating the formation of secondary weathering phases (i.e. after a long exposure duration) is the top priority. Static batch incubations are efficient and versatile because numerous batches can be maintained simultaneously and incubations may be sacrificed from the experiment for destructive analytical techniques while the experiment continues. This approach lends itself to replication, providing data with well-defined uncertainties, which is important because the experiments are usually performed to predict the environmental behaviour of minerals over long timescales (months – decades). Static batch incubations also allow investigators to control the weathering conditions and are relatively easy to monitor. As the name denotes, these incubations are hydraulically static, except for evaporation or evapotranspiration (plants), and do not simulate water movement of freely-draining soils. Column experiments do not share this limitation and are the most effective approach for studying mineral-soil interactions under dynamic flow conditions. More specifically, columns are best suited to investigating the transport of dissolved alteration products in soils and predicting the subsequent ecotoxic effects of groundwater and surface water contamination. The limitations of column experiments are that they are time-consuming and resource-intensive compared with static batch incubations, which limits the number of replicates undertaken in practice. In addition, destructive

analytical techniques (e.g. selective aqueous extraction, spectroscopic examination) require the entire column to be sacrificed from the experiment.

1.8 Aims and objectives

Sulfide ore particles dispersed from mining areas may behave as vectors for PTEs, connecting mines and soils. This material can degrade soil function by acidification and the introduction of bioavailable PTE species to soils (Ramsey et al., 2005), and this raises concerns over human health risks arising from consumption of contaminated crops (Dudka et al., 1995; Yu et al., 2006; Peralta-Videa et al., 2009). This issue is especially relevant to developing and rapidly industrialising countries, where environmental regulations may be either weak or poorly enforced and communities depend on soils impacted by mining (Miller et al., 2004; Zhuang et al., 2009). However, how these particles behave in soils and influence biogeochemical cycling of PTEs and the associated environmental and human health risks, is poorly understood.

The working hypothesis for this project was: Sulfide ore minerals undergo chemical weathering in soils, releasing non-essential PTEs at rates relevant to crop production and creating a hazard by producing contaminated crops. The overall project aim was to investigate the potential impacts of mining on agricultural soils through the contamination of soils with mineral waste particles. The primary objective was to investigate the chemical weathering of several sulfide ores in soils and the geochemical associations and bioavailability of toxic metals, liberated during weathering, to crops under conditions relevant to agriculture. More specific objectives were:

- Using soils collected from contrasting geological and climatic provenance, perform static batch incubation experiments of soil-sulfide mixtures lasting up to one year.

- Use selective aqueous extraction of batch incubation soils to determine the kinetics of PTE release and the geochemical associations of liberated PTEs in soils.

- Construct plant microcosms to investigate the bioavailability of liberated PTEs to key crop species (spring wheat, *Triticum aestivum* and lowland rice, *Oryza sativa*) under both oxic and reducing (i.e. flooded soil) conditions.

- Identify secondary weathering phases that may form during sulfide ore weathering under field and laboratory conditions using complimentary spectroscopic techniques, i.e. scanning electron microscopy – energy dispersive X-ray spectroscopy (SEM-EDXS) and X-ray diffraction (XRD).

- Explore relationships between weathering behaviour, secondary phase formation, soil physicochemical factors, agricultural practices and the bioavailability of weathering products.

- Evaluate the hazard to human health associated with the consumption of PTE-contaminated crops produced during this project.

1.9 Organisation of thesis

Chapter 2 describes the experimental methods employed to meet the objectives outlined above, with respect to three sulfide ores minerals studied: sphalerite, cinnabar and arsenopyrite. In chapters 3 – 5, the specific mineralogy, PTE biogeochemistry, toxicology and experimental results are discussed for the three ore minerals in turn. In chapter 6, the key findings are synthesised and suggestions are provided for furthering this work.

Chapter 2

Experimental methods

2.1 Introduction

This chapter describes the sample collection, characterisation and experimental methods used throughout this project. Chapters 3 – 5 provide a summary of the experimental approaches and, where relevant, refer back to the detailed method descriptions laid out in this chapter.

2.2 Reagents and apparatus

All reagents were of analytical grade or higher (ROMIL, Sigma-Aldrich, Fisher). Ultra-high purity water (UHP, ≥ 18.2 MΩ cm^{-1}, Maxima Analytical, Elga) was used for all applications unless otherwise stated. General good practice was observed when handling trace concentrations of metals: Aqueous metal solutions were handled under a class 5 laminar flow hood (Bassaire 06VB, BS EN15014644) and polypropylene (PP) or high density polyethylene (HDPE) centrifuge tubes, bottles, syringes and sieves were used for sample preparation, storage and analyses for trace metal applications. Plastics were sequentially cleaned (2% v/v Decon 90 ≥ 12 h soak; 10% v/v HCl ≥ 24 h soak) and repeatedly rinsed (≥ 5 times) with water between and after soaks, then dried under laminar flow prior to use. Laboratory glassware (volumetric flasks, conical flasks etc.) was used for some other applications, including the preparation of extractant solutions, instrumental eluents and major ion analytical standards. Glassware was also cleaned as previously described. Disposable polypropylene spatulas (Smart Spatulas, Cole-Parmer) was used for all sample preparation and material transfer unless otherwise stated.

2.3 Experimental soils sampling, preparation and characterisation

2.3.1 Site selection and sampling

Soils formed under contrasting geological and climatic conditions were required to broaden the geographic relevance of the projected research outputs; therefore two sampling locations were selected to represent temperate and sub-tropical to tropical soils.

The temperate soil was sourced from the Tamar Valley, Cornwall, United Kingdom (50°28'20.11"N, 4°13'56.81"W). The freely draining, slightly acid loamy soil resides on slate bedrock (Tavy series) in an area also abundant in mudstone and sandstones. The soil supported low-intensity grassland, used only for haymaking for the past decade. A large bulked sample (~ 40 kg dry weight, DW) was collected in HDPE sacks from the A horizon using a stainless steel trowel.

The sub-tropical soil was collected from the University of Hong Kong Kadoorie Centre, New Territories, Hong Kong SAR (22°25'42.98"N, 114° 6'46.12"E). The ultisols in this area are underlain by volcanic tuff and breccia as well as sandstone, siltstone and mudstone (Shing Mun formation). The soils were occupied by secondary hillside forest and also used for organic horticulture. A composite of organic horticultural (5 – 30 cm depth) and secondary forest subsoil (30 – 100 cm) were collected in approximately equal parts by volume, using a stainless steel shovel. The soils were oven dried (40˚C, ≥ 48 h) prior to shipping to the UK in polythene bags.

2.3.2 Sample preparation and storage

Soils were oven-dried (40 – 50 ˚C, ≥ 48 h) in plastic-lined trays, disaggregated using a pestle and mortar and sieved (plastic) to < 2 mm. The gravel and detritus were discarded. Well-rotted cow dung was oven-dried (50 ˚C, ≥ 72 h), comminuted using a garden waste shredder and sieved to < 2 mm. The soils were split into four portions (5 – 10 kg) and fertilised with shredded dung at 10 % m/m, bringing their organic matter content to the upper range for productive soils. After amendment, the soils were homogenised by 5 cycles of mixing, mechanical splitting (Type 1 rotary divider, Endecotts Ltd.) and recombination (Figure 2.1). The same process was used to divide the bulk into homogenous portions (~ 1.5 kg), which were sealed in resealable polythene bags and stored at room temperature (darkness) until required.

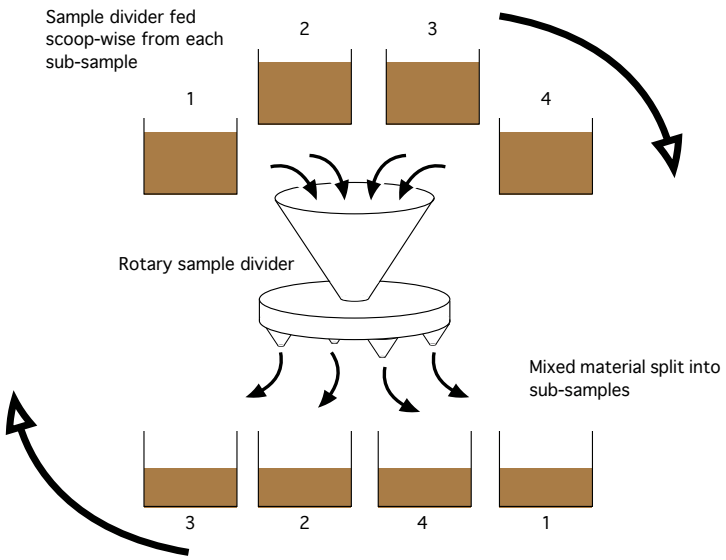

Figure 2.1 Illustration of experimental soil homogenization process. Four large sub-samples (~ 5 kg) were fed scoop-wise into a rotary sample mixer to produce four new sub-samples from the combined material. The process was repeated to produce homogenous portions.

Care was taken to ensure representative sub-division of the homogenous portions throughout the project. The rotary separation approach was used to prepare 100 g aliquots for laboratory batch incubation experiments (section 2.6). The cone-and-quarter technique was used to further split those portions when smaller amounts were required (< 10 g).

2.3.3 Characterisation

A wide range of techniques were employed to determine the physical and chemical character of the experimental soils, as described in the following sub-sections.

2.3.3.1 pH and Eh

Soil pH and Eh (redox potential) were measured in aqueous slurries at a 1:1 solid:solution ratio (10 ± 0.1 g dry weight equivalent, DWE, soil and 10.0 mL water) according to US EPA method 9045D (United States Environmental Protection Agency, 2004). Slurries were shaken (20 s) and allowed to settle (1 h) before determination, using electrochemical probes (section 2.10.1).

2.3.3.2 Preparation for particle size analysis

Samples (5 – 10 g) were moistened and mixed to a coarse paste before sub-samples (1 – 2 g DW, n = 5) were transferred into plastic serum tubes and mixed with dilute hydrogen peroxide (3 – 6 % v/v, Fisher Scientific). The samples were digested overnight at room temperature, followed by overnight digestion in a water bath at 80 ± 1 ˚C. Additional peroxide and digestion steps were applied until gaseous evolution ceased. Particle size analyses were performed using laser diffractometry (section 2.10.8) on the remaining inorganic fraction.

2.3.3.3 Effective cation exchange capacity

Effective cation exchange capacity (eCEC) was determined according to the Hendershot and Duquette method (Carter & Gregorich, 2007). Soil sub-samples (1.5 ± 0.01 g, n = 5) were accurately weighed into 50 mL centrifuge tubes, shaken with 0.1 mol $BaCl_2$ L^{-1} (30 ± 0.01 mL) for 2 hours, and then centrifuged (3000 G, 30 min). Supernatant solutions were syringe-filtered (0.45 µm Millex MF membrane, Millipore Corporation) and elemental concentrations (Ca, Mg, K, Na, Al, Fe, Mn) were determined using inductively coupled plasma optical emission spectrometry (ICP-OES) (section 2.10.3). The concentration of desorbed major cations was used to calculate eCEC (Eqn. 2.1).

$$eCEC\ (cmol(+)\ kg^{-1}) = \sum \frac{cation\ M \times valence \times L}{kg\ sample} \times 100 \qquad \textbf{(Eqn. 2.1)}$$

where: cation M = molarity of analyte cation (Ca, Mg, K, Na, Al, Fe, Mn); valance = valance of cation (e.g. Ca^{2+} = 2); L = litres of extraction solution (0.03).

2.3.3.4 Organic/inorganic particulate carbon and organic matter

Samples (n = 5) of finely ground (< 100 µm) soil were split into two aliquots, one of which was gently heated in concentrated HCl for 30 minutes to evolve inorganic carbon (carbonate) as CO_2, vacuum-filtered (0.45 µm polyester, Millipore Corporation), repeatedly rinsed with water and then freeze-dried. Between 2 – 4 mg DW of the treated and untreated samples was accurately weighed (± 0.01 mg) into tin foil capsules in readiness for total carbon determination using a CHNS elemental analyser (section 2.10.2). Inorganic carbon was calculated by difference between total and organic carbon concentrations. Organic matter was determined

gravimetrically by weighing dry samples (5 – 10 g, n = 3) before and after combustion at 450 ˚C for 4 h in a muffle furnace (loss on ignition).

2.3.3.5 Elemental composition

Finely ground (< 100 µm) freeze-dried soil samples (0.5 ± 0.01 g, n = 3) were accurately weighed into 120 mL closed PTFE (polytetrafluoroethylene) reaction vessels (CEM Corporation), combined with 10 ± 0.01 mL acid mixture (50 % v/v 1:3 mixture of HNO_3 and HCl + 1 mg Au L^{-1}) and then subjected to microwave-assisted digestion (MarsXpress, CEM Corporation) at 1600 W and 175 ˚C for at least 15 min.

The digestates were diluted two-fold in the reaction vessels, centrifuged (3000 G, 20 min) and then the supernatants were refrigerated until analyses using ICP-OES or inductively coupled plasma mass spectrometry (ICP-MS) (section 2.10.3). A certified reference material (BCR 320R Channel sediment) was digested to verify the efficiency of the digestion procedure (Table 2.1). Apart from cadmium, which yielded a recovery of approximately 90 %, the determined and certified concentrations fell within their combined uncertainty (Joint Research Centre for Reference Materials, 2012).

Table 2.1 Comparison of certified and determined concentrations (ICP-OES) for the BCR 320R Channel sediment certified reference material. Uncertainties are reported as ± 1 standard deviation (n=3).

Parameter		Certified	Determined	Recovery
As	(µmol kg^{-1})	290 ± 27	279 ± 36	96.3 %
Cd	(µmol kg^{-1})	23.5 ± 1.6	21.1 ± 0.2	90.2 %
Fe	(mmol kg^{-1})	460 ± 23	462 ± 11	100 %
Mn	(mmol kg^{-1})	16.6 ± 0.9	16.3 ± 0.1	98.4 %
Zn	(mmol kg^{-1})	4.88 ± 0.31	4.85 ± 0.19	99.5 %
Hg	(µmol kg^{-1})	4.24 ± 0.45	4.17 ± 0.10	98.3 %

Total sulfur and nitrogen were determined using a combustion-based CHNS elemental analyser (section 2.10.2). Between 0.5 – 4 mg DW of finely ground (< 100 µm) sample (n = 5) was accurately weighed (± 0.01 mg) into tin foil capsules prior to CHNS analyses.

2.3.3.6 Bulk mineralogy

Finely ground freeze-dried soil samples (< 100 µm) were packed into plastic sample plates and smeared with a glass plate to produce a smooth surface for x-ray diffraction (XRD) analysis (section 2.10.4).

2.3.3.7 Field capacity (moisture)

Field capacity was determined experimentally. The apparatus used (Figure 2.2) consisted of an open-bottomed soil chamber and a water collection chamber, separated by a water-permeable mesh. The soil chamber was filled with 100 ± 0.1 g soil, which was saturated with water and left overnight to drain. The wetted soil was re-saturated and subsequently re-weighed the following day.

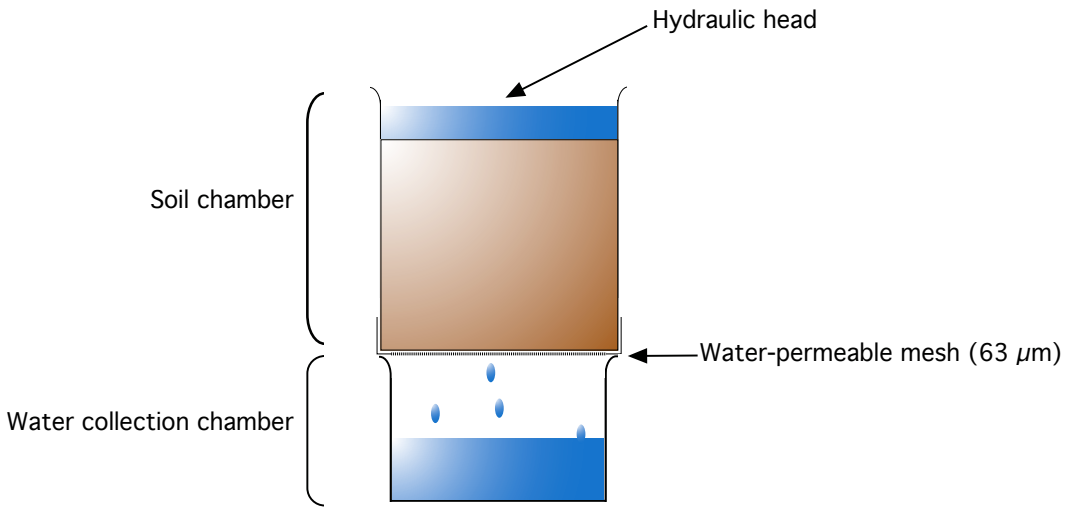

Figure 2.2 Experimental apparatus for the gravimetric determination of soil field capacity.

2.3.3.8 pH buffering behaviour

The pH buffering behaviour of the experimental soils was determined using a modified version of the procedure proposed by Magdoff and Bartlett (1985): 20 ± 0.1 g DW aliquots of the soils were transferred into 50 mL centrifuge tubes and wetted to their field capacity with dilute solutions of H_2SO_4 or Na_2CO_3 formulated to deliver doses of 0–16 cmol kg^{-1} acid or base. After a 24 h equilibration period, water was added to each sample to produce 1:1 slurries and pH was determined (section 2.3.3.1).

2.3.3.9 Oxalate-extractable iron and aluminium

Oxalate-extractable (amorphous) iron and aluminium concentrations were determined after Carter and Gregorich (2007), using 0.5 ± 0.01 g (n = 5) finely ground soil (< 100 μm) extracted in 20 ± 0.1 mL 0.2 mol L^{-1} ammonium oxalate - oxalic acid buffer (pH 3.0 ± 0.1) for 4 h in darkness (reciprocating shaker). Total iron and aluminium concentrations were determined in the supernatant solutions (ICP-OES, section 2.10.3) after centrifugation (3000 G, 15 min) and dilution.

2.4 Experimental minerals preparation and characterisation

2.4.1 Mineral preparation and storage

Specimen sphalerite, arsenopyrite and cinnabar were obtained from a private collection (Richard Tayler Minerals, Cobham, UK). Mineral specimens were sliced into platelets (~ 2 cm^2 × 0.3 cm) using a diamond-edged rotary cutting blade, removing any altered surface phases. To remove coolant residues, the platelets

were sequentially rinsed in water (10 s) and hexane (10 s). The platelets were air-dried, sealed in polyethylene bags and stored in a desiccator until required.

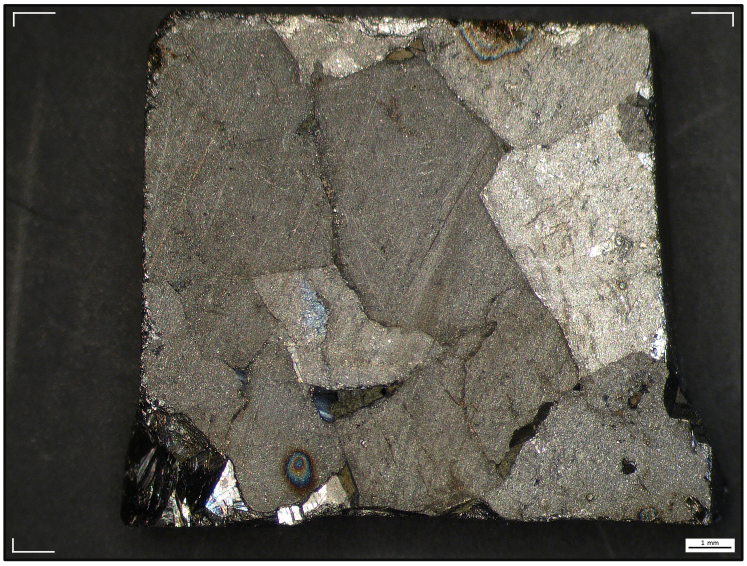

Figure 2.3 An example of a mineral platelet (arsenopyrite) as prepared for experimentation, photographed under visible light microscope. White bar = 1 mm.

Some of the platelets were also finely ground using a ceramic ball mill and sieved to < 63 µm. The < 63 µm fraction represents clay and silt size particles, which are thought to account for the majority of fugitive dust mass flux (Kon et al., 2007). Ground mineral was stored in a desiccating, N_2-purged atmosphere.

2.4.2 Mineral characterisation

2.4.2.1 Elemental composition

Total sulfur was determined in finely ground experimental mineral (< 63 µm) using an elemental analyser (section 2.10.2). Total metal/metalloid concentrations in the arsenopyrite and sphalerite were quantified using ICP-OES (section 2.10.3) after acid digestion (section 2.3.3.5). The cinnabar (1.00 ± 0.01 g) was extracted overnight in pre-weighed 15 mL PP centrifuge tubes (end-over-end mixing, PTR

35, Grant Instruments) at room temperature in 4 ± 0.01 mL 2.3 mol Na_2S L^{-1} (Sigma-Aldrich) after Revis et al. (1989). Extracts were centrifuged (3000 G, 20 min) and then the supernatants were decanted, replaced by 4 mL fresh Na_2S and the slurries were re-suspended. This process was repeated twice more with 4 ± 0.01 mL water and the supernatants were combined, diluted (400 x) and analysed using ICP-OES. The centrifuge tubes were dried (50 ˚C) to constant weight to quantify the solid residue (quartz) and the liquid residue from the extraction procedure.

2.4.2.2 Mineralogical composition

Ground (< 63 μm) experimental minerals were prepared for bulk mineral phase identification (section 2.3.3.6) using XRD (section 2.10.4). Mineral platelets were also examined using SEM-EDXS to characterise the bulk structure (i.e. identify inclusions) of the minerals. Platelets were set in epoxy resin (100:31 SR8100 resin and SD8822 hardener, Sicomin, France), sectioned and polished prior to examination.

2.5 Field weathering experiments

2.5.1 Experiment preparation

An experimental plot, the sampling location for the temperate experimental soil (section 2.3.1), was stripped of existing vegetation and thoroughly worked (to a depth of ≥ 30 cm) to produce a well-mixed substrate resembling freshly ploughed field soil. Specimen arsenopyrite, sphalerite and cinnabar were sliced into platelets to provide a generous, freshly exposed surface area for direct observations of surface alterations and secondary phase formation after the experiment using

SEM-EDXS (section 2.10.5). The platelets were sewn into nylon bags (2 mm mesh) to aid retrieval after Mihaljevič *et al.* (2010), were deposited approximately 0.1 m below ground level within a 0.1 m × 0.1 m horizontal grid and then remained *in situ* for 24 months (Figure 2.4).

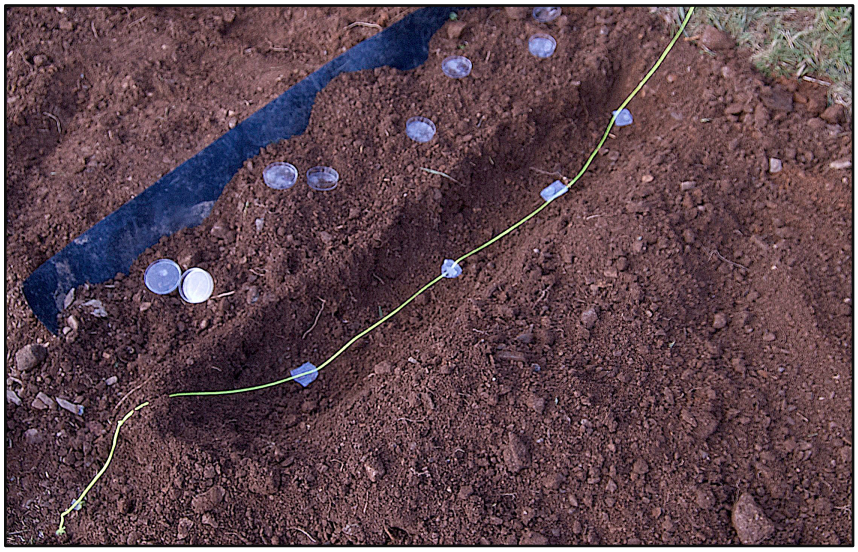

Figure 2.4 Preparation of experimental platelets for deposition within nylon bags. Bags are tethered to high-visibility nylon thread to mark the location and to aid recovery. The petri dishes in the image are 55 mm in diameter.

2.5.2 Platelet recovery and examination

The experimental mineral platelets and host soil were excavated in small plastic corers (∅ 5 cm), which where air-dried (48 h) and then freeze-dried. The platelets and adhered soil were removed from their mesh bags, wrapped in polythene film to preserve their integrity and then set in epoxy resin (100:31 SR8100 resin and SD8822 hardener, Sicomin, France). Care was taken to ensure gaps were left in the film to allow the resin to permeate the pore spaces as the samples were degassed under vacuum (10 mbar). The samples were oven-cured overnight (40 ˚C) and cross-sections were made, bisecting the centre of the platelets and soils, using a

diamond edged cutting disk (Figure 2.5). After polishing, the cross-sections were carbon coated and mounted with copper tape to enhance the conductivity of the surface during SEM analyses.

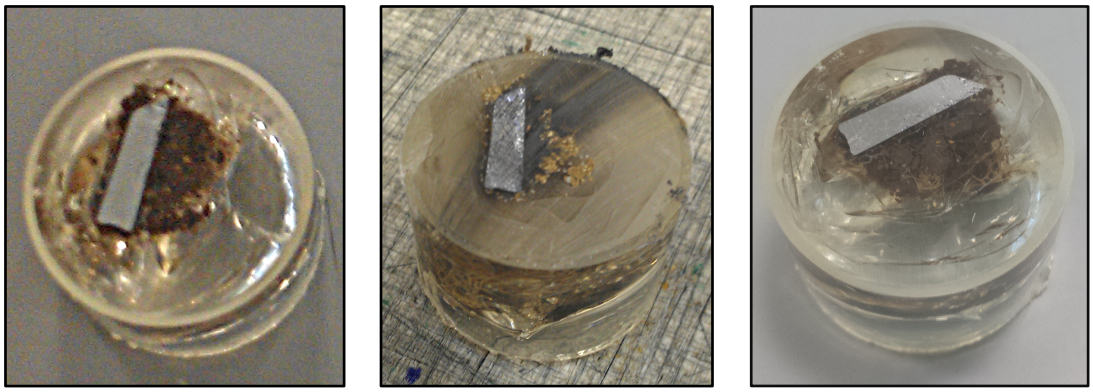

(a) (b) (c)

Figure 2.5 Example of platelet and adjoining soil set in epoxy resin before (a) and after (b) sectioning, and after polishing (c).

2.6 Laboratory incubation experiments

2.6.1 Preparation of incubations

Incubations were prepared in colourless PP beakers (250 mL) using 100 ± 0.1 g aliquots of the temperate or sub-tropical experimental soils, which had been prepared as described in section 2.3. The beakers were filled with soil, after which 0.1 ± 0.005 g of finely ground (< 63 µm) arsenopyrite, sphalerite or cinnabar was accurately weighed in a pre-weighed centrifuge tube, combined with and then thoroughly mixed with the soil using a plastic spatula (replaced between different minerals). The centrifuge tube was re-weighed after each use to check for any mineral residue. Control samples were prepared in the same manner, with the exception of ground mineral.

2.6.2 Maintaining incubations

The incubation soils were moistened to 75 % of their respective field capacity (section 2.3.3.7) with water. This moisture level was maintained on a weekly basis by weighing the incubations and compensating for lost mass by adding water. The incubations were maintained under stable laboratory conditions (21 ± 2 ˚C, 60 % relative humidity) in a polyethylene tunnel to minimise contamination risks. A slight airflow (< 0.2 m s^{-1}) was maintained over the incubations (laminar flow), which were kept in darkness to discourage excessive algal growth in the soils.

2.6.3 Sacrifice and analyses of incubations

After the allocated incubation duration, the incubations were freeze-dried (Modulyo 230 + Savant RV8, Thermo Fisher Scientific) and then homogenized and sub-sampled using the approaches described in section 2.3.2. Soils were stored under low-temperature (-18 ˚C), N_2-purged conditions until analysed. In addition to a pH determination as described in section 2.3.3.1, the soils were subjected to multiple selective aqueous extractions, as described in the following sub-sections. Unless specified, all aqueous extractions were performed in triplicate using 50 mL PP centrifuge tubes and were agitated for 2 h using a reciprocating shaker (60 rpm). Extracts were centrifuged (3600 G, 30 min, 20 ˚C, Legend RT, Sorvall) and supernatants were syringe-filtered (0.45 µm, Puradisc PES, Whatman) and then preserved until analysis, either by freezing for anions (Yorks & McHale, 2000) or acidification to < pH 2 with 50 % v/v HNO_3 for metals.

2.6.3.1 Preparation and analyses for arsenopyrite-spiked incubations

The arsenopyrite-spiked soils and controls were sub-sampled for the extraction of soluble major ions (NO_3^-, SO_4^{2-}) in water and exchangeable arsenic in 0.1 mol L^{-1}

potassium phosphate buffer (K_2HPO_4/KH_2PO_4, Sigma-Aldrich) prepared to pH 7.2 ± 0.1. Both extractions were performed using a 1:5 solid:solution ratio (5 ± 0.01 g soil with 25 ± 0.01 mL solution), based on the optimisation (for maximum recovery) of previously reported methods (Alam et al., 2001; Gleyzes et al., 2001). After filtration, 1.0 mL of the water extracts were transferred to glass chromatography vials (1.8 mL screw-top, pre-slit septa) and frozen (-18°C). The samples were defrosted immediately prior to the determination of sulfate and nitrate using ion chromatography (section 2.10.9). Phosphate buffer samples were refrigerated until dissolved arsenic concentrations were determined using ICP-OES (section 2.10.3) using calibration standards prepared in the buffer matrix. Procedural blanks were prepared with each sample batch, and were treated as per the samples. Analytical figures of merit for the arsenic determinations are given in Table 2.2. The detection limit was calculated by multiplying the standard deviation, taken from multiple determinations (n = 7) of the standard solution with the lowest concentration, by three. The linear range was ascertained from instrumental calibration curves ($R^2 \geq 0.999$).

Table 2.2 Analytical figures of merit for the determination of total arsenic in 0.1 mol L^{-1} phosphate buffer soil extract solutions using ICP-OES. Precision (% relative standard deviation, RSD) and accuracy (% deviation from accepted value) was based on replicate analyses of an independently prepared mixed calibrant solution (130 µmol L^{-1}) in the buffer matrix.

	As
Procedural blank	< LOD (limit of detection)
Detection limit	2.90 µmol L^{-1}
Linear range	5.34 – 267 µmol L^{-1}
Precision (n = 5)	2 %
Accuracy (n = 5)	5.5 %

2.6.3.2 Preparation and analyses for sphalerite-spiked incubations

Sphalerite-spiked soils and controls were sub-sampled for the extraction of soluble major ions (NO_3^-, SO_4^{2-}) in water (section 2.6.3.1), exchangeable cadmium and zinc in 0.01 mol $CaCl_2$ L^{-1} (Fisher Scientific, 1:5 solid:solution) (Pueyo et al., 2003; Rao et al., 2008) and total labile cadmium and zinc in 0.1 mol EDTA L^{-1} (ethylenediaminetetraacetic acid, Fisher Scientific, 1:30 solid:solution - 1 ± 0.01 g soil with 30 ± 0.01 mL solution) (Rumball & Richmond, 1996; Lo & Yang, 1999). The solid:solution ratio used for EDTA extraction was optimised for maximum recovery. The EDTA extracts were diluted fivefold prior to analysis but not acidified, as this was unnecessary for preservation and may have resulted in EDTA salt precipitation. The EDTA and $CaCl_2$ extracts were refrigerated until cadmium and zinc concentrations were determined using ICP-OES and ICP-MS (section 2.10.3), depending on the concentration, using calibration standards prepared in the relevant extractant matrices. The analytical figures of merit for these determinations are given in Table 2.3. Detection limits and linear ranges were determined as previously described.

Table 2.3 Analytical figures of merit for the determination of total cadmium and zinc in 0.1 mol EDTA L^{-1} and 0.01 mol $CaCl_2$ L^{-1} soil extract solutions. Precision (% RSD) and accuracy (% deviation from accepted value) was based on replicate analyses of independently prepared mixed calibrant solutions (concentrations given as 'QA calibrant' in the table) in the appropriate matrices.

	Cd (nmol L^{-1})	Cd (nmol L^{-1})	Zn (nmol L^{-1})	Zn (µmol L^{-1})
Matrix	$CaCl_2$	EDTA	$CaCl_2$	EDTA
Procedural blank	< LOD	0.0538	< LOD	< LOD
Detection limit	0.133	0.0263	1.10	0.0599
Linear range	1.78 – 89.0	0.178 – 3.56	15.3 – 764	1.53 – 9.17
QA calibrant	44.6	0.893	153	3.06
Precision (n = 5)	3.7 %	3.9 %	1.4 %	2.9 %
Accuracy (n = 5)	4.9 %	1.3 %	0.5 %	1.3 %

2.6.3.3 Preparation and analyses for cinnabar-spiked incubations

Cinnabar-spiked soils and controls were sub-sampled for the extraction of soluble major ions (NO_3^-, SO_4^{2-}) in water (section 2.6.3.1), exchangeable mercury in 0.01 mol $CaCl_2$ L^{-1} (Fisher Scientific, 1:5 solid:solution) (Pueyo et al., 2003; Rao et al., 2008) and a two-step sequential extraction to quantify mercury release from cinnabar after Revis et al. (1989). Extraction step (1): Mercury not associated with, or released from, the cinnabar was extracted using 14 mol HNO_3 L^{-1} (Fisher Scientific) (Fernández-Martínez & Rucandio, 2005; Mikac et al., 2003) in pre-weighed 15 mL centrifuge tubes. Soils were extracted overnight in HNO_3 (1 ± 0.01 g soil in 4 ± 0.01 mL HNO_3), after which the centrifuged residues were rinsed (vortex mixed) with a further aliquot of acid and two more of UHP water (4 ± 0.01 mL). The supernatants from each rinse step were combined with the first extract and the soil residues were freeze-dried, after which the extraction tubes were re-weighed to quantify the residual solid mass for the next extraction step. Extraction step (2): The residual, cinnabar-hosted mercury was extracted by repeating the

procedure outlined for step 1, but substituting HNO_3 with saturated (2.3 mol L^{-1}) sodium sulfide (Na_2S, Sigma-Aldrich). The HNO_3 and Na_2S extracts were diluted tenfold (UHP water) and thousandfold (0.2 % v/v NaOH), respectively, prior to mercury determination using ICP-MS (section 2.10.3). The analytical figures of merit for these determinations are given in Table 2.4. Detection limits and linear ranges were determined as previously described.

Table 2.4 Analytical figures of merit for the determination of total mercury in 0.01 mol $CaCl_2$ L^{-1} , 14 mol HNO_3 L^{-1} and 2.3 mol Na_2S L^{-1} soil extract solutions. Precision (% RSD) and accuracy (% deviation from accepted value) was based on replicate analyses of independently prepared mixed calibrant solutions (concentrations given as 'QA calibrant' in the table) in the appropriate matrices.

	Hg (nmol L^{-1})	**Hg (nmol L^{-1})**	**Hg (nmol L^{-1})**
Matrix	0.01 mol L^{-1} $CaCl_2$	14 mol L^{-1} HNO_3	2.3 mol L^{-1} Na_2S
Procedural blank	1.77	4.58	3.05
Detection limit	0.194	2.38	38.8
Linear range	0.499 – 49.9	100 - 1000	500 - 5000
QA calibrant	9.97	200	1000
Precision (n = 5)	1.78 %	0.84 %	0.59 %
Accuracy (n = 5)	3.43 %	0.32 %	5.32 %

2.7 Abiotic control experiment

Abiotic control experiments, in which un-spiked and arsenopyrite-spiked temperate experimental soil (section 2.3) was incubated under sterile conditions, were designed to assess the influence of microbiotic activity upon the geochemical conditions prevailing in the soils (pH, Eh, soluble major ions) and mineral weathering rate. The incubations were analogous to those described in section 2.5 and were performed in 250 mL conical flasks sealed with polyurethane foam bungs.

2.7.1 Preparation of sterile materials and abiotic incubations

The experimental soil (section 2.3) and arsenopyrite (section 2.4) were sterilised by tyndallisation: the materials were steam-heated to ~ 95 ˚C for 1 hour and then incubated at 37 ˚C overnight. This process was repeated twice more to completely kill all bacteria and spores. Conical flasks were topped with polyurethane foam bungs and autoclaved (≥ 121 ˚C, ≥ 100 kPa, ≥ 30 min) prior to use.

Precautions were taken to preserve the sterility of the materials: open flasks, soils and arsenopyrite were handled within a 30 cm radius of a Bunsen burner flame, which provides a physical barrier to organisms floating in the air. Implements (e.g. spatulas) were heat-sterilised (≥ 1 min, 250 ˚C) in a glass bead steriliser (Steri 250, Inotech Biosystems Inc., Maryland, USA) or using the Bunsen flame.

The incubations were prepared as described in section 2.6.1 and were moistened to 75 % field capacity with filter-sterilised (0.22 μm sterile packaged PES, Whatman) water.

2.7.2 Maintaining, sacrificing and analysing abiotic incubations

The incubations were maintained as described for the batch incubation experiments (section 2.6.2). The samples were freeze-dried after the designated incubation duration, after which no additional precautions were taken to preserve sample sterility. The samples were analysed for pH, Eh, and water-soluble major ions (NO_3^-, SO_4^{2-}) as previously described (section 2.6.3).

2.8 High-concentration incubations for secondary phase identification

Soil incubations were prepared with a high concentration (10 % m/m) of experimental minerals with the aim of detecting secondary mineral phases using XRD and SEM-EDXS. Incubations were prepared with 1 ± 0.01 g sphalerite, cinnabar or arsenopyrite (< 63 µm) and 9 ± 0.01 g DW temperate and sub-tropical experimental soil (n = 5 for each soil/mineral combination) in 50 mL PP tubes. The spiked soils were incubated as described in section 2.6.2 for 180 days prior to freeze-drying. Both incubated and un-incubated samples were amended with an internal standard (10 % m/m ≥ 98 % Al_2O_3, Sigma-Aldrich) and then finely ground (< 100 µm) using a planetary mill (zirconium oxide grinding bowls, Pulverisette 5, Fritsch) in preparation for XRD analyses (section 2.10.4). The diffractograms were normalised using the intensity of the internal standard peak (2θ = 35.14 °), allowing for comparison of incubated and unincubated samples. Samples were also infused with epoxy resin, sectioned and polished (section 2.5.2). The polished sections were examined using SEM-EDXS (section 2.10.5) to identify the presence, elemental composition and morphology of any secondary phases that formed during the incubation period.

2.9 Phytoavailability experiments

2.9.1 Preparation of phytoavailability experiment soils

The phytoavailability experiment incubations were prepared in colourless polypropylene tubs (4 L) as described for the batch laboratory incubations described in section 2.6, except for their larger mass of soil (2 ± 0.005 kg) and

finely ground (< 63 μm) arsenopyrite, sphalerite or cinnabar (2 ± 0.005 g), and the use of plastic shovels to thoroughly mix the minerals and soils.

2.9.2 Maintenance and planting of incubations

The phytoavailability experiment incubations were maintained in parallel, and under the same conditions, as the batch laboratory incubations (section 2.6.2) for the first 180 days of the experiment.

After 180 days, 10 day-old spring wheat (*Triticum aestivum*) seedlings, which had been grown in vermiculite, were transplanted into tubs containing temperate experimental soil (350 seeds m^{-2}). The plants were matured to ripeness (a further 112 days) under glasshouse conditions (24 ± 3 ˚C, 66 ± 3 % RH). The soils were gravimetrically maintained at 75 % field capacity (± 20%) during this period.

The tubs containing sub-tropical experimental soil received 14 day-old rice seedlings, which were grown in un-spiked, saturated sub-tropical experimental soil. The tubs were flooded, leaving around 6 cm standing water, and maintained inside an environmental growth chamber (Fitotron PG660, Sanyo) under diurnal lighting and controlled temperature (16 h light, 8 h dark at 27 ˚C, followed by 12 h light, 12 h dark at 24 ˚C) until the grains had ripened (152 days). The standing water level was maintained twice weekly.

2.9.3 Plant harvesting, preparation and analyses

The mature wheat and rice plants were uprooted and their stems and ears were rinsed (≥ 5 times) with water to remove adhered particles, separated from the roots and then freeze-dried. The seed and chaff were separated by agitating the grains under a low airflow and allowing the lighter chaff to be blown away from

the seed. The weighed stems and seeds were finely comminuted using a stainless steel coffee grinder, which was wiped down with methanol-soaked tissue between samples. Tissue samples (0.5 ± 0.01 g, n = 3) were accurately weighed into PTFE digestion vessels, combined with 10 ± 0.01 mL 8 mol L^{-1} high-purity HNO_3 (Romil Pure Chemistry) and then microwave-digested (section 2.3.3.5). The digests were analysed for arsenic, cadmium, zinc and mercury using ICP-OES/ICP-MS (section 2.10.3). In addition to procedural blanks, a certified reference material (IRMM 804 Rice flour) was also digested (0.5 ± 0.01 g, n = 3). The CRM moisture content was determined and the elemental concentrations were corrected accordingly. The determined and certified tissue concentrations (Table 2.5) fell within their combined uncertainty (Joint Research Centre for Reference Materials, 2012). The analytical figures of merit are given in Table 2.6.

Table 2.5 Comparison of exemplary concentrations determined for biological tissue certified reference materials and the certified values. Uncertainties are reported as ± 1 standard deviation (n = 3).

Material	Parameters (μmol kg^{-1})	Certified	Determined
IRMM 804 Rice flour	As	0.654 ± 0.053	0.651 ± 0.057
	Cd	14.3 ± 0.6	14.3 ± 1.1
	Zn	353 ± 29	360 ± 32
BCR 60 aquatic plant	Hg	1.69 ± 0.20	1.78 ± 0.04
DOLT-4 dogfish liver	Hg	12.9 ± 1.1	12.2 ± 0.2

Table 2.6 Analytical figures of merit for the determination of total arsenic, cadmium and mercury in plant tissue digests. Precision (%RSD) and accuracy (% deviation from accepted value) was based on replicate analyses of independently prepared mixed calibrant solutions (concentrations given as 'QA calibrant' in the table) in the appropriate matrices (n = 7).

	As (nmol L^{-1})	As (µmol L^{-1})	Cd (nmol L^{-1})	Hg (nmol L^{-1})
Procedural blank	1.95	<LOD	<LOD	1.83
Detection limit	0.921	1.20	2.70	0.249
Linear range	13.3 – 66.7	6.67 – 66.7	44.5 – 356	4.99 – 499
QA calibrant	26.7	13.3	90.0	49.9
Precision (n = 7)	7.8 %	4.2 %	3.7 %	1.6 %
Accuracy (n = 7)	6.8 %	4.8 %	3.5 %	2.7 %

2.9.4 Analysis of the flooded sub-tropical soils

The standing water was drained from the sub-tropical soil incubations just prior to uprooting the rice plants, after which the tubs were transferred to an anoxic chamber (Vinyl anaerobic chamber, Coy laboratory products) purged with nitrogen and hydrogen/helium mixture (95:5). The saturated soils were sampled with polypropylene corers (∅ 2.5 cm, n = 5) under sub-oxic conditions (≤ 400 ppm O_2) and porewater pH and Eh were determined in the water that collected in the core voids (section 2.10.1). Bulked cores were centrifuged in airtight buckets (2000 G, 10 min) to remove excess water, drained and then thoroughly mixed with a plastic spatula (replaced between soil treatments). Moisture content was determined in the first soil treatment to be prepared (control soils): 10 ± 0.5 g wet sample was transferred to pre-weighed porcelain crucibles (n = 3), oven-dried (105˚C, ≥ 1 h) and periodically re-weighed until constant mass was attained. The moisture content, calculated by mass lost through drying, was used to estimate dry weight equivalents (DWE) for all samples, although determinations were made for

each sample and subsequently used to correct individual DWEs. Each bulked sample was sub-sampled into pre-weighed 50 mL centrifuge tubes for aqueous extraction, using the protocols as outlined in Table 2.7.

Table 2.7 Aqueous extraction protocols applied for each soil treatment after sub-sampling within an anoxic chamber.

Soil treatment	Aqueous extraction protocols
Arsenopyrite	Soluble major ions and exchangeable arsenic (section 2.6.3.1),
Sphalerite	Soluble major ions (section 2.6.3.1), exchangeable cadmium & zinc and total labile cadmium & zinc (section 2.6.3.2)
Cinnabar	Soluble major ions (section 2.6.3.1), exchangeable mercury and liberated mercury (section 2.6.3.3)
Control	All procedures outlined above, plus acid-volatile sulfide (section 2.9.4.1) and Fe(II)/(III) (section 2.9.4.2).

The degassed (O_2-free nitrogen, 15 min) extractant solutions were added and the tubes were capped, sealed with Parafilm and the samples were extracted as previously described in section 2.6.3. The metal extractions were handled under normal laboratory conditions after centrifugation. The water extracts (major anions) were handled exclusively under sub-oxic conditions until analysed to preserve the redox-sensitive speciation.

2.9.4.1 Sulfur speciation

Dissolved sulfate and sulfide was determined in soil water extracts using ion chromatography (section 2.10.9) or the methylene blue method, as described in section 2.10.7. Acid-volatile sulfide (AVS) was extracted from the solid phase after Allen et al. (1993): Samples of moist soil (10 ± 0.5 g DWE) were weighed into 250 mL round-bottom flasks inside the anoxic chamber and sealed with a Parafilm before removal from the chamber. The samples were combined with 50 mL of 6

mol L^{-1} HCl (Fisher Scientific) and then heated (~ 80 ˚C) and magnetically stirred under a flow of O_2-free nitrogen carrier gas for 45 min (Figure 2.6).

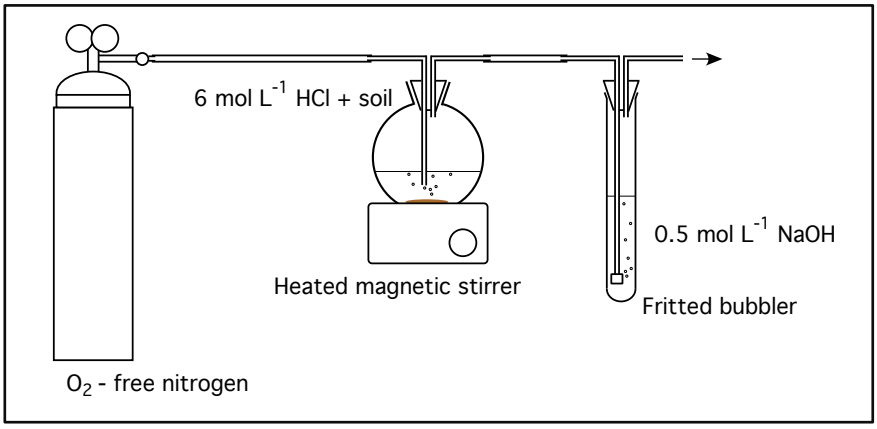

Figure 2.6 Schematic showing apparatus used for acid-volatile sulfide extraction from soils.

Any evolved H_2S in the carrier gas was trapped in 40 mL of 0.5 mol NaOH L^{-1} (Fisher Scientific). After extraction, 5 ± 0.01 mL of the NaOH solution was mixed with 0.4 ± 0.01 mL diamine colour-developing reagent, acidified to < pH 1 (6 mol HCL L^{-1}), a requirement of the methylene blue colorimetric technique, and then dissolved sulfide concentrations were determined as described in section 2.10.7. The solutions were acidified after combination with the colour-developing reagent to minimise loss of sulfur as H_2S gas.

2.9.4.2 Iron speciation

Iron(II) and Fe(III) were extracted from the solid phase after Loveley and Phillips (1986). Wet soil sub-samples (1 ± 0.05 g DWE) were combined with 50 ± 0.02 mL 0.5 mol HCl L^{-1} (Fisher Scientific) inside the anoxic chamber, sealed with Parafilm, agitated for one hour at room temperature (60 rpm, reciprocating shaker) and then centrifuged (3600 G, 20 min). The Fe(II) concentration was determined using

the Ferrozine technique (section 2.10.6) and the total iron concentration was determined using ICP-OES (section 2.10.3), allowing Fe(III) concentrations to be calculated by difference.

2.10 Analytical measurement techniques

2.10.1 pH and Eh

Electrochemical probes (temperature-compensated) and meters were used to determine slurry pH (pHC2051-8 probe, Radiometer analytical with PHM210 meter, MeterLab) and Eh (Gelplas ORP, BDR with HI9025 meter, Hanna). The pH instrument was calibrated through two points using certified buffer solutions (pH 4.01 and 7.01, Fisher Scientific) and potentials from the oxidation-reduction potential (ORP) electrode were corrected to the standard hydrogen electrode after checking the instrumental response in freshly prepared ZoBell's solution (Nordstrom & Wilde, 2008).

2.10.2 CHNS elemental analysis

Total particulate carbon, nitrogen and sulfur were determined using combustion-based elemental analysers (NC2500, Carlo Erba) calibrated (single point) with either cyclohexanone-2,4-dinitrophenylhydrazone for C & N analysis or L-cysteine ($C_3H_7NO_2S$) for sulfur analysis (OEA Labs Ltd., Cornwall, UK). Replicate analyses, check standards and the PACS-1 marine sediment certified reference material (National Research Council, Canada) were used to verify precision and accuracy. The analytical figures of merit and standard operating conditions used are summarised in Table 2.8 and Table 2.9.

Table 2.8 Standard operating conditions used for NC2500 Elemental Analyser, Carlo Erba.

Parameter	Configuration
Carrier gas	Helium, 100 mL min^{-1}
Combustion gas	Oxygen, 10 mL dosing loop
Compressed air pressure	150 kPa
Oxidation furnace temperature	1000 °C
Reduction furnace temperature	650 °C
Chromatographic column temperature	65 °C
Detector	Thermal conductivity

Table 2.9 Analytical figures of merit for total carbon, nitrogen and sulfur determination in soils and minerals by CHNS elemental analysis. Precision values represent the %RSD of replicate sample analyses (n ≥ 5).

	Carbon	Nitrogen	Sulfur
Procedural blank	Undetectable	Undetectable	Undetectable
Detection limit	~ 0.01 wt. % for all elements		
Linear range (mg)	0.001 – 3.6	0.001 – 6.0	0.001 – 2.0
Precision (soils)	< 7 %	< 15 %	< 10 %
Precision (minerals)	-	-	< 5 %
PACS-1 certified	3.69 ± 0.11 %	-	-
PACS-1 determined	3.53 ± 0.04 %	-	-

2.10.3 Determination of elemental concentrations in aqueous solutions

Elemental concentrations in aqueous solutions were determined using inductively coupled plasma mass spectrometry, ICP-MS (X-series 2 with Collision Cell Technology, Thermo Scientific) and inductively coupled plasma optical emission spectrometry, ICP-OES (725-ES ICP-OES, Varian) at the ISO9001 accredited Analytical Research Facility, Plymouth University, UK. The standard operating conditions used for these instruments are given in Table 2.10 and Table 2.11.

Table 2.10 Standard operating configuration for ICP-MS.

Parameter	Configuration
Nebuliser gas	Argon
Power	1.40 kW
Coolant flow	13 L min^{-1}
Nebuliser flow	0.85 L min^{-1}
Nebuliser	Glass concentric and HDPE V-grove
Auxiliary flow	0.8 L min^{-1}
Collision cell gas	7 % v/v H_2 in He at 3.5 mL min^{-1}

Table 2.11 Standard operating configuration for ICP-OES.

Parameter	Configuration
Nebuliser gas	Argon
Power	1.40 kW
Coolant flow	12 L min^{-1}
Nebuliser flow	0.68 L min^{-1}
Nebuliser	HDPE V-groove
Auxiliary flow	1.5 L min^{-1}
Viewing height	8 mm

The isotopes and emission lines selected for the determination of elemental concentrations (Table 2.12), using ICP-MS and/or ICP-OES, was chosen for optimal sensitivity (i.e. most abundant isotope or responsive emission line) and minimal interference.

Table 2.12 Isotopes and emission lines selected for the determination of elementals of interest, using ICP-MS and ICP-OES.

Element	Isotope (ICP-MS)	Emission line (ICP-OES)
As	^{75}As	193.696 nm
Cd	^{111}Cd	
Hg	^{202}Hg ^{199}Hg (Na_2S matrix only)	
Zn	^{66}Zn	213.857 nm

Unless otherwise stated, samples were acidified (20 µL 50 % v/v ultra-pure HNO_3 per 10 mL sample) and spiked to 50 µg In L^{-1} (Fisher Scientific) and/or 1 mg Y L^{-1} (ROMIL Pure Chemistry) for internal standardisation during ICP-MS and ICP-OES analyses, respectively. Instruments were calibrated using a series of 5 matrix-matched multi-elemental calibration standards (PrimAg, ROMIL Pure Chemistry). Procedural blanks, replicate determinations, quality control standards (QC-19, CPI International) and certified reference materials were used to verify precision and accuracy.

Special procedures were applied when determining mercury concentrations. An excess of gold (1 mg L^{-1}) and chloride (HCl) was ensured in samples intended for mercury analyses to prevent mercury deposition on the instrument sample introduction interfaces (Butler, 2003), which results in unwanted memory effects. In addition, a 2 % v/v HCl solution spiked with 1 mg L^{-1} gold was used as the wash solution, which significantly reduced mercury stabilisation and washout times. No sample acidification was used for Na_2S extracts (section 2.6.3.3) because of the incompatibility between the reagent and acids, and the instruments were flushed with UHP water between samples. Mercury determinations were carried out using the standard additions method of calibration to mitigate matrix effects. A calibration, using five standards as previously described, was also performed to ascertain the instrument detection limit and linear range prior to standard additions.

2.10.4 Powder X-ray diffraction (XRD)

Sample powder mounts were analysed using a Siemens D5000 X-ray diffractometer at Camborne School of Mines, Exeter University Cornwall Campus, Tremough, UK. The instrument was calibrated using a silica standard and was

configured with a Cu-Kα source, a 2θ operating range of 2 – 70° and a 0.02° s^{-1} angle interval/dwell time. Baseline-subtracted diffractograms were compared with diffraction pattern libraries for phase identification, using the EVA software package (DIFFRACplus suite, Bruker Corporation).

2.10.5 Scanning electron microscopy - energy dispersive X-ray spectroscopy

After infusion with epoxy resin, samples were sectioned, polished and carbon-coated. The samples were examined using a JEOL 7001 field emission scanning electron microscope operated at 15 kV (accelerator voltage), equipped with an X-Max 80 mm silicon drift detector and Oxford Analytical AzTec 350 energy-dispersive X-ray microanalysis suite (Oxford Instruments, Abingdon, UK). A combination of electron micrographs, electron backscatter images, spot-based and map-based elemental determination and element maps were performed.

2.10.6 Determination of Fe(II) in aqueous solution

Iron(II) concentrations in aqueous solutions were determined spectrophotometrically (8453 UV-Vis, Agilent) using the ferrozine colorimetric method (Stookey, 1970). A 100 µL aliquot of 0.5 mol HCl L^{-1} soil extract was mixed with 5 mL of 1 mg ferrozine L^{-1} solution (Lovley & Phillips, 1986), which was prepared in 50 mmol L^{-1} HEPES (4-(2-hydroxyethyl)-1-piperazineethanesulfonic acid) buffer at pH 7.3 ± 0.1 (VWR BDH). The absorbance was determined at λ_{max} 562 nm after 1 min for colour development. Calibration standards (0.1 – 1.0 mmol Fe L^{-1}) were prepared from ferrous ethylenediammonium sulfate (VWR BDH) in a 0.5 mol HCl L^{-1} matrix (R^2 = 0.999). The analytical figures of merit for this technique are given in Table 2.13.

Table 2.13 Analytical figures of merit for the spectrophotometric determination of Fe(II) using the ferrozine method. Precision (%RSD) is based on replicate (n = 5) determinations of a 1 mmol Fe(II) L^{-1} standard.

	Fe(II) (mmol L^{-1})
Procedural blank	0.04
Detection limit	0.01
Precision	0.1 %
Linear range	0.1 – 1.0

2.10.7 Determination of sulfide (S^{2-}) in aqueous solution

Sulfide concentrations in aqueous solutions were determined spectrophotometrically (8453 UV-Vis, Agilent) using the methylene blue colorimetric method (Cline, 1969). Diamine colour-developing reagent was prepared using N-N-dimethyl-p-phenylenediamine sulfate (Sigma-Aldrich) and ferric chloride (VWR BDH) in 50 % v/v HCl (Fisher Analytical). Prior to absorbance determination (λ_{max} 670 nm), 0.4 ± 0.01 mL diamine reagent was mixed with 5 ± 0.01 mL of sample and the samples were diluted ten times with water after 20 minutes development time. Five calibration standards (50 – 150 µmol L^{-1}) were prepared in water using sodium sulfide nonahydrate (Sigma-Aldrich) ($R^2 \geq 0.99$). The analytical figures of merit for this method are given in Table 2.14.

Table 2.14 Analytical figures of merit for the spectrophotometric determination of dissolved sulfide using the methylene blue method. Precision (%RSD) is based on replicate determinations of the 100 µmol L^{-1} standard (n = 7).

	Dissolved sulfide (S^{2-}) (µmol L^{-1})
Procedural blank	< LOD
Detection limit	10
Precision	1 %
Linear range	50 – 250

2.10.8 Laser diffractometry

Soil particle size distribution was determined used laser diffractometry (Mastersizer 2000 with Hydro-G wet sample dispersion unit, Malvern Instruments). The instrumental operating conditions used for the analysis are given in Table 2.15.

Table 2.15 Standard operating conditions used for particle size distribution analysis with Mastersizer 2000.

Parameter	Configuration
Particle diameter range	0.02 – 2000 µm
Detector	Red laser (632 nm) scatter array (46 detectors)
Background measurement	30 s
Sample measurement	30 s (n = 5)
Dispersant	0.1 % m/v sodium hexametaphosphate + 90 s ultrasonic dispersion
Refractive index	1.53
Adsorption value	0.01

2.10.9 Determination of major ions in aqueous solutions

Anion concentrations were determined using ion chromatography (DX-500 chromatographic system, Dionex-Thermo Scientific) configured as described in Table 2.16. The instrument was calibrated using multi-analyte standards (n = 5), prepared from salts (sodium nitrate & sodium sulfate, Fisher Scientific). Concentrated (100 mmol L^{-1}) stocks were kept refrigerated for up to 3 months and standards were freshly prepared prior to each analysis. Drift-control standards (100 µmol L^{-1}) were measured after every 10 samples to verify that the instrumental response was ± 10% of the calibration. Exemplary analytical figures of merit for the technique are given in Table 2.17.

Table 2.16 Standard operating conditions used for major ion determination with the Dionex DX-500 anion chromatographic system.

Parameter	Configuration
Eluent	9 mmol Na_2CO_3 L^{-1}
Flow rate	1 mL min^{-1}
Total elution time	< 20 min
Columns	Dionex IonPac AG9-HC (guard), IonPac AS9-HC (analytical)
Suppressor	ASRA Ultra II 4 mm, 100 mA
Detection	Conductimetric
Background conductance	~ 24 µS
System back-pressure	~ 15.5 MPa

Table 2.17 Analytical figures of merit for the determination of major ions in aqueous solution using the Dionex DX-500 anion chromatographic system. Precision (%RSD) is based on the replicate determination of a 200 µmol L^{-1} mixed standard.

	Nitrate (µmol L^{-1})	Sulfate (µmol L^{-1})
Procedural blank	< LOD	< LOD
Detection limit	3.96	7.50
Precision (n = 5)	1 %	0.6 %
Linear range	20 – 500	20 – 500

Chapter 3

The Implications of Sphalerite Contamination in Agricultural Soils

3.1 Introduction

Cadmium is considerably environmentally mobile, bioavailable and toxic to humans (Smolders & Mertens, 2013) and there are clear linkages between mineral exploitation and cadmium soil contamination, the most widely publicised being the contamination of soils by the Japan's Jinzu River and its association with the debilitating 'itai-itai' disease (Ishihara et al., 2001). The mining region bordering Guangdong and Hunan provinces in southern China serves as a useful case study. Decades of multi-metallic mineral exploitation have been shown to contaminate river sediments and agricultural soils (e.g. Chenzhou) with cadmium on a regional scale. For example, as far as 60 km from the source soils are contaminated (> 9 μmol Cd kg^{-1}) (Limei et al., 2008) and inhabitants are considered at risk of chronic health effects from consuming locally grown rice and vegetables contaminated with cadmium (Zhuang et al., 2009; Zhao et al., 2012).

Crop safety is a concern because the primary human intake routes for cadmium are tobacco smoking and diet (Smolders & Mertens, 2013; Järup, 2003), both of which link human exposure to soil contamination. Because cadmium exists primarily as a free metal ion (Cd^{2+}) in neutral to acidic (pH < 8) oxic (Eh > 200 mV) soils, it is bioavailable under conditions prevailing in agricultural soils (Beesley et al., 2010). Above pH 6, Cd^{2+} may form surface complexes with organic matter and metal oxyhydroxides, be adsorbed by clays or precipitate as carbonate ($CdCO_3$) and phosphate ($Cd_3(PO_4)_2$). Precipitation controls solubility at high concentrations, but adsorption mechanisms are considered to be the primary factor controlling cadmium solubility/bioavailability in soils. The pH-dependence of cadmium solubility is illustrated by the observation that, for each pH unit increase (pH 4 – 7.7), adsorption (removal from soil solution) increases by a factor of 3 (Smolders & Mertens, 2013).

Chronic toxicity may arise because cadmium has a long biological half-life (15 – 30 years) and so accumulates in the body, resulting in kidney disease, osteoporosis, lung and prostate cancer and endocrine disruption (Ishihara et al., 2001; Henson & Chedrese, 2004; Järup, 2003). In addition, cumulative lifetime intake associated with chronic toxicity (≥ 18 mmol) can be less than an order of magnitude above the 'background' level in populations (0.9 – 3.6 mmol) (Limei et al., 2008; Smolders & Mertens, 2013).

Sphalerite is the primary geologic source of zinc and occurs commonly around the world. This zinc ore is notable for its tendency for isomorphic substitution of zinc by other metals, and cadmium is generally present in solid solution at 0.2 – 2 % and is predominantly obtained as a zinc by-product (Smolders & Mertens, 2013). Sphalerite has been reported as an important zinc and cadmium-hosting phase in mining wastes at numerous locations, most often Pb-Zn operations (Robles-Arenas et al., 2006; Gosar & Miler, 2011; Sapsford et al., 2009), but also Au-Ag operations (Chon et al., 2005; Clark et al., 2001) and others. The dispersal of sphalerite has been reported by wind-blown dusts, including the respirable (PM_{10}/$PM_{2.5}$) fraction (Zota et al., 2009; Castillo et al., 2013), in surface streams and rivers (Miler & Gosar, 2012; Concas et al., 2006; Gosar & Miler, 2011), through tailings dam failure (Alastuey et al., 1999; Simón et al., 2001), smelter fallout (Roberts et al., 2002; Sarret et al., 2004; Isaure et al., 2005) and indirectly, from characteristic zinc-cadmium geochemical signatures in contaminated substrates (Navarro et al., 2008).

In common with other sulfides, sphalerite is regarded as metastable in surficial environments. The dissolution mechanisms proposed for sphalerite include oxidative dissolution, either by molecular oxygen (Eqn. 3.1) or Fe(III) (Eqn.

3.2), and acid-promoted dissolution (Eqn. 3.3) (Heidel et al., 2011). Cadmium is released from solid solution during sphalerite dissolution (Stanton et al., 2008).

$$ZnS + 2O_2 \rightarrow Zn^{2+} + SO_4^{2-} \quad \textbf{(Eqn. 3.1)}$$

$$ZnS + 8Fe^{3+} + 4H_2O \rightarrow Zn^{2+} + 8Fe^{2+} + SO_4^{2-} + 8H^+ \quad \textbf{(Eqn. 3.2)}$$

$$ZnS + 2H^+ \rightarrow Zn^{2+} + H_2S_{(aq)} \quad \textbf{(Eqn. 3.3)}$$

Reported sphalerite dissolution rates range over two orders of magnitude under similar pH and temperature conditions (Table 3.1), illustrating the uncertainty of sphalerite dissolution behaviour, even under controlled conditions. Laboratory experiments in aqueous media (Acero et al., 2007; Stanton et al., 2008) showed that sphalerite dissolution follows a first order reaction with respect to [H^+] (pH 1 – 4.2), the rate increases with temperature (25 – 70 ˚C) and is independent of dissolved oxygen concentrations (6.3 – 270 µmol L^{-1} dO_2), suggesting that oxidation by molecular oxygen (Eqn. 3.1) is of minimal importance. In contrast, Kossoff et al. (2011) did not observe a clear relationship between pH and sphalerite dissolution rates, perhaps due to the greater complexity of their experimental system in terms of buffering minerals and adsorption surfaces (mixed waste/soil columns). Apart from differences in experimental design, the iron content of the sphalerite is also proposed to influence the dissolution rate (Weisener et al., 2003).

Table 3.1: Sphalerite dissolution rates for oxic solutions reported in the literature. Rate variable indicates the analyte used to measure mineral dissolution (Zn) and the relative substitute iron content.

Rate variable	Conditions	Rate ($\mu mol\ m^{-2}\ day^{-1}$)	Source
Zn (high Fe)	pH = 4, T = 25 ˚C	9.85 – 11.23	Stanton et al. (2008)
Zn (low Fe)	pH = 4, T = 25 ˚C	1.32	Stanton et al. (2008)
Zn (low Fe)	pH = 1, T = 25 ˚C	121	Weisener et al. (2003)
Zn (no Fe)	pH = 4.2, T = 25 ˚C	0.545	Acero et al. (2007)

Numerous investigators have reported the spatial distribution and concentration of toxic metals in soils affected by mineral exploitation, and expressed concerns about the dispersal of metal-hosting particles into soils and surface waters, citing potential environmental and human health impacts (Conesa et al., 2006; Chopin & Alloway, 2007 and references therein). However, further research is required to enhance our understanding of how transported mineral particles influence soil quality, in terms of the biogeochemical cycling of toxic metals and the subsequent risk they pose to human health through crop contamination.

3.2 Methods

The overall investigative strategy and experiments are summarised in this section, with reference to relevant sub-sections in Chapter 2, where the applied methods are described in detail.

3.2.1 Investigative approach

This study comprised three strands of investigation (Figure 3.1):

(1) A field weathering experiment to investigate secondary mineral phase formation associated with long-term sphalerite soil exposure under environmental conditions.

(2) Laboratory batch incubations (0 – 365 d) of sphalerite-spiked (0.1 % ZnS m/m) soils to determine sphalerite dissolution behaviour in soils under controlled conditions. Additional incubations, with a higher sphalerite concentration (10 % ZnS m/m), were performed with the aim of identifying secondary alteration phases.

(3) Phytoavailability experiments where *Triticum aestivum* and *Oryza sativa* were grown in samples of the temperate and flooded sub-tropical soils, respectively, to evaluate the bioavailability of cadmium released from sphalerite under oxic and sub-oxic conditions.

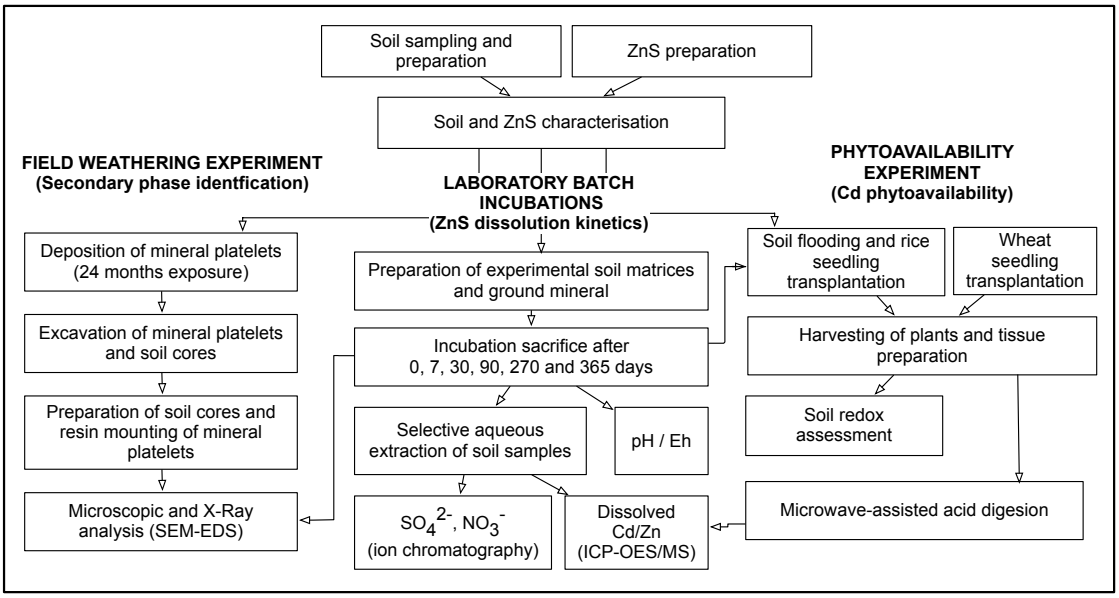

Figure 3.1: Schematic summarising the experimental approaches taken in this study.

3.2.2 Soil and mineral sampling, preparation and characterisation

Soils of temperate and sub-tropical provenance were collected on the basis of their contrasting geological and climatic character (section 2.3.1). The fine soil fraction (< 2 mm) was carefully homogenised to produce what will hereafter be referred to as the temperate and sub-tropical *experimental soils* (section 2.3.2) and these were characterised by determining their physical and chemical features (section 2.3.3).

Small platelets (~ 2 × 2 × 0.3 cm) and a fine powder (< 63 μm) were prepared from specimen sphalerite. The sphalerite was characterised by examining its mineralogy and elemental composition as described in section 2.4.

3.2.3 Field weathering experiment

Sphalerite platelets were deposited approximately 0.1 m below ground level within a 0.1 m × 0.1 m horizontal grid and then remained *in situ* for 24 months at the sampling location for the temperate experimental soil. The platelets were excavated in cores and prepared as polished epoxy resin sections prior to examination for secondary phase formation using SEM-EDXS (section 2.5).

3.2.4 Laboratory batch incubation experiments

Sphalerite-spiked (0.1 % m/m, < 63 μm) and control (not spiked) temperate and sub-tropical experimental soils were incubated under laboratory conditions for durations ranging 0 to 365 days as described in section 2.6. After incubation, the samples were analysed for water-soluble major ions (NO_3^-, SO_4^{2-}), cation-exchangeable cadmium and zinc (0.01 mol $CaCl_2$ L^{-1} extract) and total labile cadmium and zinc (0.1 mol EDTA L^{-1} extract) to determine the release trends and geochemical associations of the sphalerite constituents as weathering progressed during the experiment (section 2.6.3.2).

In response to an unexpected decline in soil pH observed during the initial 30 days of incubation, an abiotic control incubation was conducted to replicate that incubation period under sterile conditions (section 2.7). That experiment was designed to test a hypothesis: the activity of ammonium and sulfate oxidising bacteria produced an excess of protons that were not lost by percolation (impossible) and so acidified the soils.

Additional, highly concentrated sphalerite-spiked (10 % m/m) soils were also incubated for 180 days with the aim of detecting secondary phase formation using SEM-EDXS (section 2.8).

3.2.5 Phytoavailability experiments

Large (4 L) analogues of the laboratory batch incubation samples were incubated for 180 days before *Triticum aestivum* (spring wheat) or *Oryza sativa* (lowland rice) were transplanted into the temperate and sub-tropical experimental soils, respectively (section 2.9). The total cadmium concentration of the stems and grains was determined to evaluate the bioavailability of cadmium released during sphalerite weathering and the hazard posed to human health via the crop contamination pathway. In addition, the biogeochemical conditions prevailing in the flooded sub-tropical soils after rice cultivation were determined to examine relationships between soil conditions and the plant uptake and geochemical associations of cadmium liberated during sphalerite weathering (section 2.9.4).

3.3 Results and discussion

3.3.1 Experimental soil and sphalerite characterisation

Both experimental soils were of circum-neutral pH, rich in organic matter, with a similar moderate eCEC (Table 3.2). Both soils were iron rich (5.5 – 6.3 % Fe m/m) but the sub-tropical soil contained 7 times less manganese, more aluminium (6.2 % vs. 3.9 %) and a lower proportion of poorly crystalline iron and aluminium oxyhydroxides (factor of 2 – 4 times). Both soils had similar sulfur, zinc and cadmium concentrations, which fell within (Cd) or just above (Zn) the range expected for uncontaminated soils (Mertens & Smolders, 2013).

Mineralogical analysis (XRD) showed that the main crystalline phases were clinochlore, muscovite, illite and quartz in the temperate soil (sandy loam), and kaolinite, orthoclase, microcline, gibbsite and quartz in the sub-tropical soil (silt loam).

Elemental analysis (ICP-OES, CHNS) indicated that 99.3 ± 2.2 % of the specimen sphalerite was accounted for by the total zinc, sulfur, cadmium and iron content. Together with X-ray diffractograms (Figure 3.2) and SEM-EDXS analysis, the data showed that the sphalerite was of high purity, consisting of ZnS ($Zn_{1.01}S_{0.99}$) with 0.3 % m/m iron and 0.9 % m/m cadmium. The diffractogram also confirms the crystalline structure of sphalerite and not the polymorph, wurtzite.

Table 3.2: Characterisation data for the temperate and sub-tropical experimental soils. Uncertainties reported as ± 1 standard deviation (n = 5). eCEC = Effective cation exchange capacity; LOI = Organic matter content, determined by loss on ignition.

	Temperate soil	Sub-tropical soil
pH	6.58 ± 0.07	6.83 ± 0.12
eCEC (cmol+ kg^{-1})	14.6 ± 0.3	13.1 ± 0.2
$C_{organic}$ (% m/m)	5.57 ± 0.20	4.62 ± 0.06
$C_{inorganic}$ (% m/m)	< LOD	0.47 ± 0.37
Total N (% m/m)	0.47 ± 0.02	0.39 ± 0.05
LOI (% m/m)	12.3 ± 0.5	13.1 ± 0.7
Sand (%)	49.4 ± 3.2	31.2 ± 2.0
Silt (%)	45.3 ± 2.9	58.5 ± 2.0
Clay (%)	5.29 ± 0.39	10.3 ± 1.3
Al (mol kg^{-1})	1.44 ± 0.11	2.32 ± 0.11
$Al_{oxalate}$ (mol kg^{-1})	0.121 ± 0.001	0.0975 ± 0.0018
Fe (mol kg^{-1})	0.973 ± 0.018	1.13 ± 0.03
$Fe_{oxalate}$ (mol kg^{-1})	0.202 ± 0.002	0.0602 ± 0.0014
Mn (mmol kg^{-1})	37.6 ± 3.2	5.25 ± 0.31
S (mmol kg^{-1})	17.0 ± 2.2	17.1 ± 1.7
Cd (µmol kg^{-1})	2.70 ± 0.55	2.67 ± 0.27
Zn (mmol kg^{-1})	2.05 ± 0.14	2.13 ± 0.17
Hg (µmol kg^{-1})	1.30 ± 0.26	0.78 ± 0.22
As (mmol kg^{-1})	0.579 ± 0.043	0.292 ± 0.014
H_2O-Chloride (µmol kg^{-1})	402 ± 30	560 ± 11
H_2O-Nitrate (mmol kg^{-1})	3.42 ± 0.09	4.03 ± 0.23
H_2O-Sulfate (mmol kg^{-1})	0.756 ± 0.013	1.78 ± 0.01

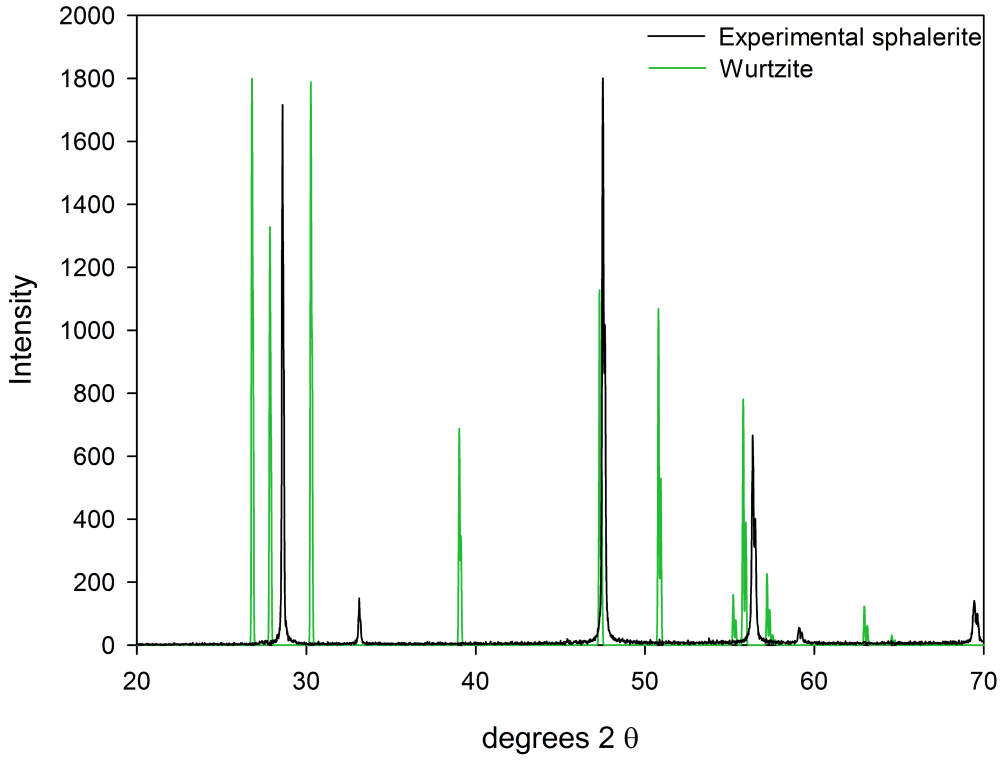

Figure 3.2 X-ray diffractogram for ground sphalerite. All peaks correspond to sphalerite. The peak distribution expected for the sphalerite polymorph, wurtzite, is shown for comparison.

3.3.2 Soil biogeochemical conditions throughout oxic incubations

The pH was not controlled during the experiment and a notable decrease was observed in the pH of both temperate (-1.05 pH units) and sub-tropical (-0.43 pH units) soils during the initial 30 days of incubation. After 30 days, the temperate and sub-tropical soils fluctuated around pH 5.53 ± 0.13 and pH 6.40 ± 0.08, respectively. Experimentally derived (section 2.3.3.8) pH buffering curves (Figure 3.3) demonstrated that the sub-tropical soil had significantly greater buffering capacity (≈ 43% at neutral-acid pH) than the temperate soil, which was devoid of carbonate. This partly explains the disparate pH decline in the early stages of the experiment.

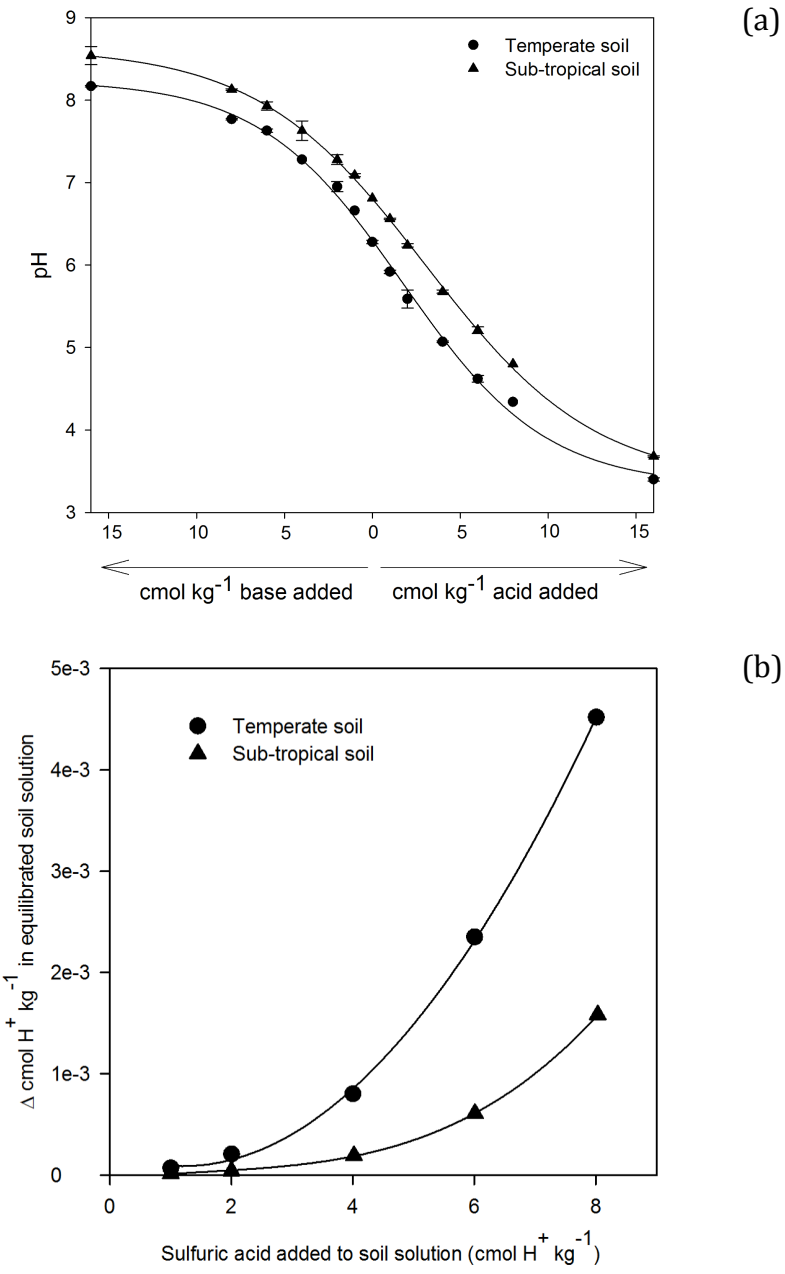

Figure 3.3: (a) Soil pH buffering curves for the temperate and sub-tropical experimental soils. (b) Curves showing delta H^+ activity in soil solution after equilibration versus delta H^+ concentration added to the temperate and sub-tropical experimental soils.

Data from an abiotic control experiment (section 2.7) covering the initial 30 days incubation of the temperate soil indicate that the pH decline was mediated by soil microbiota, as the decline was absent in abiotic controls (Figure 3.4). The data suggest that the decline was coupled with sharp increases in nitrate and sulfate

concentrations under biotic conditions, a trend absent from abiotic controls. These trends reflect the activity of ammonium and sulfur oxidising bacteria, both of which can contribute to soil acidity, especially if percolation is prevented, as was the case in these experiments.

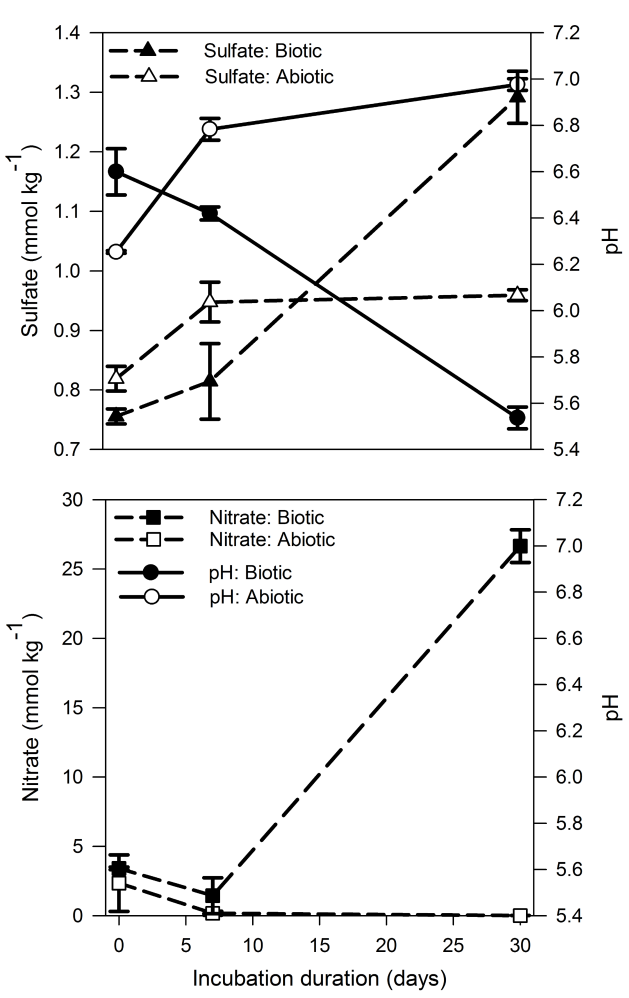

Figure 3.4: Sulfate and pH (a) and nitrate (b) in biotic and abiotic control incubations (first 30 days) of the temperate soil. Lines connecting data points are presented for clarity. Uncertainties are reported as ± 1 standard deviation (n = 3).

Sphalerite dissolution had a negligible effect on soil pH, since control and spiked incubation soil pH generally differed by < 0.1 pH unit throughout the incubations. The soils were periodically checked for redox potential, which indicated consistently oxic conditions (Eh 350 – 400 mV) throughout the incubations.

3.3.3 Geochemical conditions in sub-tropical soil during rice cultivation

For the phytoavailability experiment, the sub-tropical soils that were incubated under oxic conditions for 180 days, were flooded during rice cultivation (a further 152 days). After rice cultivation the sub-tropical soils had attained neutral pH (7.01 ± 0.08) and moderately reducing conditions (Eh = -23 ± 6 mV) (Figure 3.5 b). It is common for flooded acidic paddy soils to attain neutral pH as most important reduction reactions, e.g. iron reduction, consume free protons (Ponnamperuma, 1972).

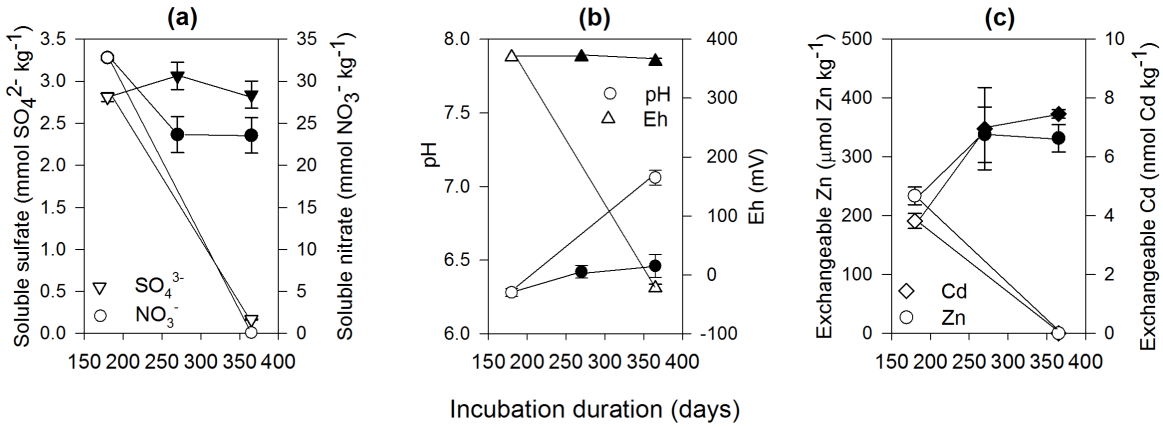

Figure 3.5: Redox indicators (a) SO_4^{2-} and NO_3^-, (b) pH and Eh and (c) exchangeable zinc/cadmium determined over the 180 – 365 days incubation period for the temperate experimental soil, both under oxic (filled symbols) and anoxic (hollow symbols) conditions. Lines connecting data points are shown for clarity. Uncertainties are reported as ± 1 standard deviation (n = 3).

Redox indicators and exchangeable metal concentrations suggest that the availability of cadmium in porewater, and therefore to the rice plants, was limited by the formation of secondary sulfide phases that co-precipitated with cadmium and zinc. Depleted soluble nitrate (> 99 %) and sulfate (≥ 94 %) concentrations (Figure 3.5 a), together with a significant proportion of acid-extractable iron (66 ± 10 %) determined as Fe(II), indicated the influence of nitrate, iron and sulfate-

reducing anaerobic microorganisms (Inglett et al., 2005). Dissolved sulfide was not detected in soil extracts but acid-volatile sulfide (AVS) was found in the reduced control soils (200 ± 16 μmol S^{2-} kg^{-1}), showing the formation of poorly ordered secondary sulfides such as mackinawite and greigite (Gramp et al., 2010). An AVS determination was not possible in the spiked soils because sphalerite itself contains acid-volatile sulfide. Concurrent with the apparent formation of secondary sulfides, net (control-corrected) exchangeable (0.01 mol $CaCl_2$ L^{-1}) cadmium and zinc concentrations were considerably lower in the reduced soils, compared with their oxic equivalents (Figure 3.5 c). In addition, net EDTA-extractable cadmium (Cd_{net}) concentrations fell from 0.23 ± 0.02 μmol kg^{-1} after oxic incubation to 0.12 ± 0.02 μmol kg^{-1} after rice cultivation.

Much of the depleted soluble sulfate was not accounted for by AVS formation, suggesting that other mechanisms also contributed. There was no olfactory evidence for $H_2S_{(g)}$ evolution and sulfate adsorption is minimal in soils at neutral pH (Scherer, 2009), excluding adsorption effects. Other potential mechanisms for the observed sulfate and extractable cadmium depletion were the formation of non-acid-volatile sulfides (e.g. pyrite, greenockite) and plant uptake, respectively and these are given further consideration in section 3.3.5.2.

3.3.4 Sphalerite dissolution

3.3.4.1 Cadmium and zinc release trends

The clear distinction between cadmium concentrations obtained from control and spiked incubations (Figure 3.6) evidences the release of cadmium from sphalerite dissolution. This divergence can be seen after 7 days incubation of both the temperate and sub-tropical soils. Cadmium concentrations extracted from control

incubations were relatively constant throughout the incubation duration, which demonstrates that cadmium extractability was not affected by changes in soil pH during the oxic incubations.

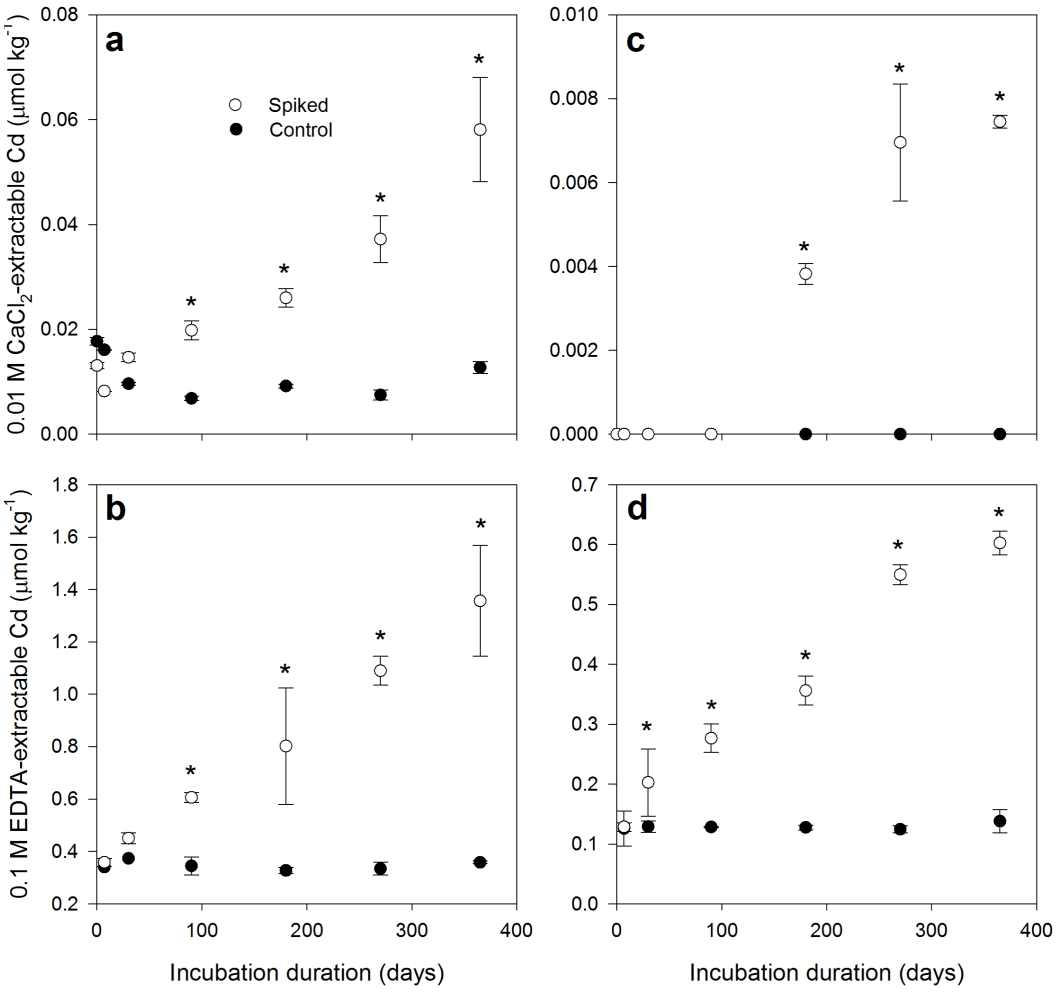

Figure 3.6: Dissolved cadmium concentrations extracted using 0.01 mol $CaCl_2$ L^{-1} and 0.1 mol EDTA L^{-1} from temperate (a & b) and sub-tropical (c & d) experimental soils. Uncertainties are reported as ± 1 standard deviation (n = 3). Note that all cadmium concentrations were below the detection limit (0.002 µmol Cd kg^{-1}) until day 180 of sub-tropical soil incubation (plot c). Asterisks denote statistically significant (p > 0.05, analysis of variance, ANOVA) differences between spiked and control soils.

Extractable zinc concentrations (Figure 3.7) were significantly higher than cadmium concentrations, reflecting the molar Zn:Cd ratio in the sphalerite. In the temperate soil (Figure 3.7 a and b), comparison with the control shows that zinc was released from sphalerite with increasing incubation time and, as with the

cadmium, the release curve did not exhibit a change in slope over the last 180 days of the experiment. Zinc concentrations released from the control soil at the beginning and the end of the experiment were not statistically different (p = 0.05).

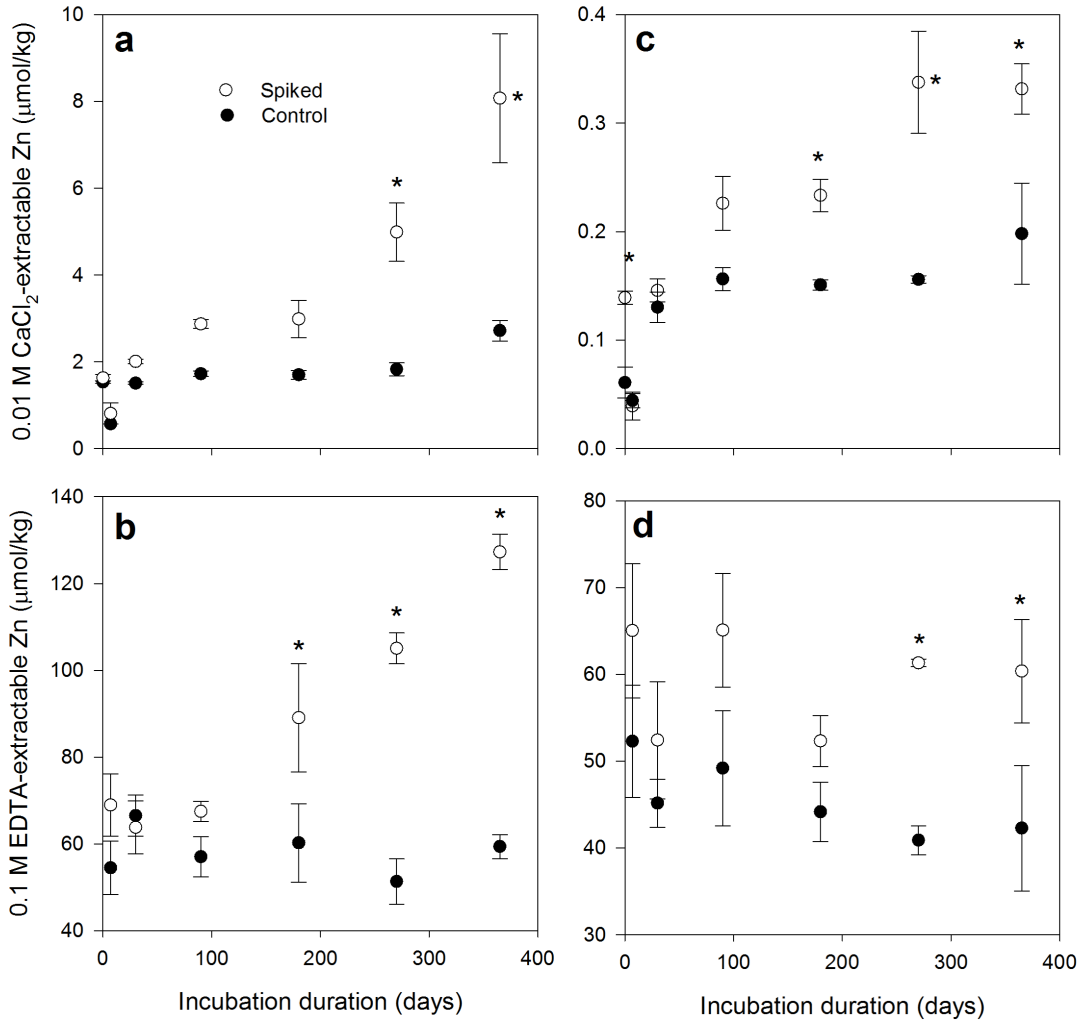

Figure 3.7: Dissolved zinc concentrations extracted using 0.01 mol L^{-1} $CaCl_2$ and 0.1 mol L^{-1} EDTA from temperate (a & b) and sub-tropical (c & d) experimental soils. Uncertainties are reported as ± 1 standard deviation (n = 3). Asterisks denote statistically significant (p < 0.05) differences between spiked and control soils.

The zinc concentrations extracted from spiked sub-tropical soils were higher than in the control soil (Figure 3.7 c and d), most notably during the last 180 days of the experiment; however the $CaCl_2$-extractable concentrations in control soils varied significantly (p < 0.05 ANOVA) during incubation. The EDTA-extractable zinc

concentrations in both spiked and control soils fluctuated throughout the incubation and there was no significant difference between concentrations at the beginning and end of the experiment ($p < 0.05$ ANOVA). Comparison of the zinc release trends with those of cadmium, which were linear with incubation time, suggest that zinc released from the sphalerite was in equilibrium with another solid phase and recalcitrant to EDTA complexation. The net release indicated by $CaCl_2$-extratcable concentrations was masked in the EDTA data, which was not sensitive to minor variations in zinc lability.

3.3.4.2 Extraction protocols

The $CaCl_2$ extraction represents the cation exchangeable fraction of cadmium and zinc and provides a 'snapshot' reflecting plant-available concentrations at a given time. The dilute neutral salt solution extracts at ambient soil pH, was of similar ionic strength to soil porewaters (Meers et al., 2007) and did not dissolve sphalerite on the timescale of the extraction protocol. The EDTA extraction protocol represents the total labile fraction of cadmium and zinc (at least 20 times higher than $CaCl_2$ values for Cd) and so estimates the total plant-available concentrations over a longer timescale than the $CaCl_2$ extraction. EDTA forms extremely stable complexes with Cd^{2+} (log K = 16.6) and Zn^{2+} (log K = 16.5) and is effective in scavenging these metals from soil solid phases (e.g. Fe/Mn oxyhydroxides, organic matter, clays) (Lo & Yang, 1999). As a proportion of EDTA-extractable cadmium, $CaCl_2$-extractable concentrations were 2.3 – 4.3 % and 1.1 – 1.3 % in the temperate and sub-tropical soils, respectively.

The EDTA-extractable cadmium concentrations were the most suitable indicator of the extent and rate of sphalerite dissolution, in this case meaning alteration from the original sulfide species, rather than EDTA-extractable zinc,

$CaCl_2$-extractable cadmium and zinc or soluble sulfate. For instance, soluble sulfate concentrations in spiked and control soils did not significantly differ throughout the oxic incubations (data not shown). Unlike zinc, cadmium ($CaCl_2$ and EDTA) produced clear and consistent trends (concentration vs. time) in both experimental soils. Additionally, cadmium release is directly correlated with sphalerite dissolution rates (Stanton et al., 2008) and cadmium exhibits minimal soil 'ageing', which would cause a shift in metal fractionation from labile (i.e. exchangeable) to increasingly recalcitrant (i.e. occluded in mineral phases) forms over time (Smolders & Mertens, 2013; Hamon et al., 1998). Finally, EDTA can effectively dissolve sphalerite oxidation products but not the sulfide itself (Rumball & Richmond, 1996), as confirmed by preliminary experiments with 0.1 mol EDTA L^{-1} (pH 7.5) and the experimental sphalerite.

3.3.4.3 Dissolution rate, trends and limits

The net cadmium release from the sphalerite was calculated by subtracting EDTA-extractable concentrations obtained from control incubations from values for the respective spiked incubations. The net release data (Cd_{net}) were used to estimate the percentage sphalerite dissolved at each incubation time point (Table 3.3). The relationship between Cd_{net} and incubation duration was linear ($R^2 \geq 0.96$) for both the temperate and sub-tropical soils, indicating that the rate of cadmium release, and therefore sphalerite dissolution, was constant throughout the incubation experiments.

Table 3.3: Dissolution rate (based on mass of sphalerite) and percentage sphalerite dissolution after 7, 30, 90, 180, 270 and 365 days incubation in both temperate and sub-tropical experimental soils. Dissolution data based on the net extraction of cadmium (Cd_{net}) using 0.1 mol EDTA L^{-1}. Uncertainties are reported as ± 1 standard deviation. Asterisks indicate that there was no significant difference between the spiked and control incubation values.

Days	Temperate soil		Sub-tropical soil	
	Cd_{net} (nmol Cd g^{-1} ZnS)	% dissolution	Cd_{net} (nmol Cd g^{-1} ZnS)	% dissolution
7	18.2 ± 15.4	0.02 ± 0.02	*	*
30	76.9 ± 21.1	0.09 ± 0.03	73.6 ± 57	0.09 ± 0.07
90	261 ± 38	0.32 ± 0.05	148 ± 24	0.18 ± 0.03
180	475 ± 223	0.58 ± 0.27	228 ± 24	0.28 ± 0.03
270	756 ± 60	0.93 ± 0.07	425 ± 18	0.52 ± 0.02
365	998 ± 212	1.23 ± 0.26	464 ± 27	0.57 ± 0.03

Several studies on sphalerite dissolution in aqueous solution show that dissolution rates decline during initial exposure (i.e. in the initial few hundred hours), after which they attain an apparent steady state (Stanton et al., 2008; Acero et al., 2007; Weisener et al., 2003). It has been proposed that this change is concurrent with the formation of zinc-deficient, polysulfide and elemental sulfur product layers on sphalerite particles, and a shift from reaction rate-limited dissolution to dissolution limited by reagent diffusion (i.e. H_3O^+, O_2, Zn^{2+}, Cd^{2+} and/or S) through those product layers (Weisener et al., 2003). Acero et al. (2007) observed the product layers but argued that, because steady state was attained, the layers were not passivating and initially high dissolution rates probably resulted from micro-crystals and oxidised phases on the pre-exposed sphalerite surfaces. The slower dissolution rate remained constant over long durations (hundreds of days) regardless of whether these product layers are porous, and therefore not diffusion limiting, or whether they are in equilibrium with bulk solution, and therefore do not accumulate.

The data from this study (Table 3.3) are consistent with slow steady-state dissolution. The constant cadmium release excludes the significant formation of stable secondary zinc (cadmium) phases, for example goslarite ($ZnSO_4 \cdot 7H_2O$), hemimorphite ($Zn_4Si_2O_7(OH)_2 \cdot H_2O$), hydrozincite ($Zn_5(CO_3)_2(OH)_6$) and smithsonite ($ZnCO_3$) (King, 1988), which would have produced declining labile cadmium concentrations with increasing incubation duration by sequestering Cd^{2+} from the porewater. This finding is also supported by SEM-EDXS examination of sphalerite platelets from the field weathering experiment (section 3.2.3) and grains from the laboratory incubation experiment (section 2.8), which presented no evidence for the formation of secondary phases rich in zinc or sulfur (cadmium was below detection limit) (Figure 3.8). Elemental distributions indicate aluminosilicates were dominant at the mineral-soil interfaces, where secondary phases may be expected to form concurrently with sphalerite dissolution. The only zinc-rich phases detected in the samples (field and laboratory) were sphalerite.

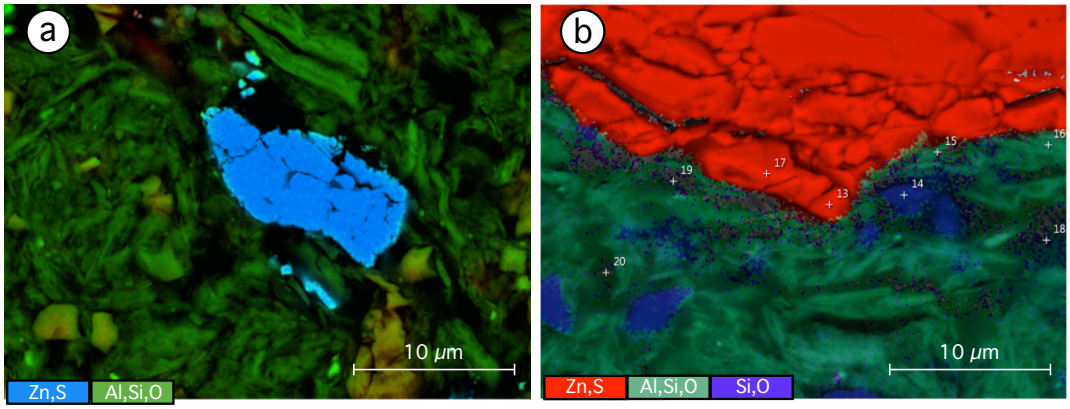

Figure 3.8: Exemplary false coloured electron micrographs produced using a combination of electron-backscatter detector data and EDXS. Elemental phase associations are colour coded. (a) sphalerite grain after incubation in oxic temperate experimental soil for 180 days; (b) mineral-soil interface showing the edge of a sphalerite platelet exposed to field conditions for 24 months.

Dissolution rates observed at 365 days are indicative of the annual average, approximately 1 μmol Cd g^{-1} ZnS and 0.5 μmol Cd g^{-1} ZnS for the temperate and sub-tropical soils, respectively. Taking account of the reducing surface area of the given mass of sphalerite during particle dissolution, and the dissolution rate being proportional to surface area (shrinking particle model) (Safari et al., 2009; Pradhan et al., 2010), the half-life of the sphalerite can be estimated to be 50 and 94 years in the temperate and sub-tropical soils, respectively.

The slower dissolution rates observed in the sub-tropical, compared with the temperate, soil can be attributed to the prevailing soil pH. Kinetic data for sphalerite dissolution in literature, derived from flow-through reactor experiments, provide a basis for estimating the effect of variable soil porewater pH on sphalerite dissolution rates. Based on data from Acero et al. (2007), a change in porewater pH from 5.53 (temperate soil) to 6.40 (sub-tropical soil) would result in dissolution rates being reduced by 66 %; therefore pH is likely to be the most significant factor affecting sphalerite dissolution in oxic soils.

The dissolution rates determined in this study are far lower than those estimated for the pyrite slurry (containing 1 – 2 % sphalerite) that contaminated ~ 40 km^2 of farmland soils, following a major tailings dam failure at Aznaćollar (southern Spain) in 1998 (Alastuey et al., 1999). It was estimated that 20 – 65 % of the sphalerite was oxidised within 25 days of the spillage (Simón et al., 2001), rising up to 70 % after 3 years (Hita & Torrent, 2005). This discrepancy can be explained by the specific nature of the incident. The slurry consisted mostly (~ 80 %) of fine-grained (< 50 μm) pyrite particles, which underwent rapid oxidation as the 'sludge-layer' sitting upon the soils dried and was exposed to oxygen, driving the pH down to ~ 2.5 (Simón et al., 2001). Not only would pyrite oxidation have enhanced sphalerite oxidation by releasing Fe^{3+} (Eqn. 3.2) and by providing the

conditions for acid-promoted dissolution (Eqn. 3.3), but sphalerite oxidation has also been found to be greatly be enhanced by a galvanic reaction with the pyrite matrix (Hita et al., 2006).

Voegelin et al. (2011) used extended X-ray absorption fine structure (EXAFS) analysis to estimate sphalerite half-lives of 1 – 3 years, based on static batch incubation (≤ 1400 d) of sphalerite-spiked soils (2000 mg Zn kg^{-1} equivalent) under very similar conditions to those applied in this study. The key differentiator of that study and the current one is the nature of the experimental sphalerite. Voegelin et al. (2011) used synthetic (high purity, > 99.9 % metals basis) zinc sulfide, with uniformly small (< 10 μm) particle size (i.e. greater surface area). As previously discussed (section 3.1), sphalerite dissolution rates from aqueous dissolution experiments range over two orders of magnitude under similar pH and temperature conditions (Table 3.1), and may depend on the guest element impurities. It can also be speculated that chemically synthesised zinc sulfide may not behave identically to geogenic sphalerite. The authors did not measure cadmium release or metal bioavailability.

3.3.5 Plant uptake of Cadmium

3.3.5.1 Uptake by wheat grown in temperate soil

Grain and stem cadmium concentrations in the spring wheat grown in the sphalerite-spiked temperate soil were considerably higher (by a factor of ≥ 75) than in plants grown in the control soil (Figure 3.9). The international food safety limit for cadmium concentration in wheat grains is 3.6 μmol kg^{-1} (WHO/FAO, 2006), making the cadmium in wheat grain from this study around 8 times higher (29.0 ± 3.3 μmol Cd kg^{-1}) than the limit value.

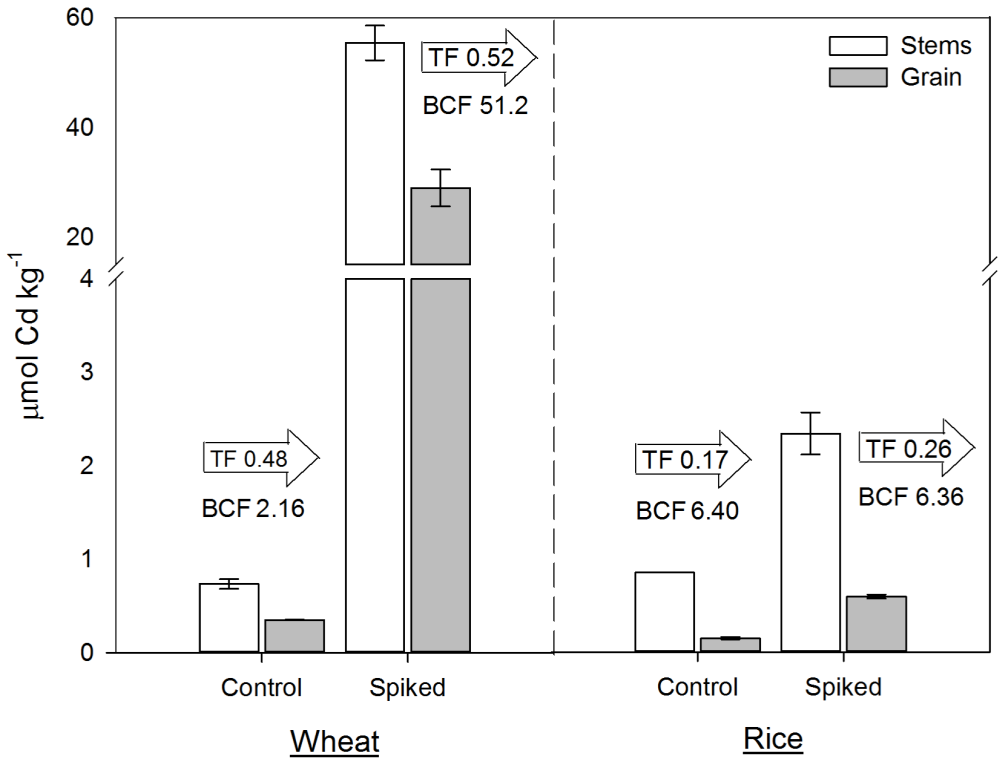

Figure 3.9: Total cadmium tissue concentrations, stem bioconcentration factors (BCF) based upon Cd_{net} concentrations and stem-to-grain transfer factors (TF) for spring wheat grown in the temperate experimental soil and rice in the flooded sub-tropical experimental soil (control and spiked). Uncertainties based on ± 1 standard deviation.

The data suggest that high cadmium concentrations in grain produced from the spiked soil relate to the magnitude and phytoaccessibility of the cadmium pools in that soil as opposed to a difference in the translocation rate to the grain grown in the control. Stem-to-grain transfer factors (TF)[7] were the same for plants grown in spiked and control soil; therefore cadmium translocation from the stem to seed was independent of the phytoaccessible cadmium concentration in the soil and the stem cadmium concentration (Figure 3.9).

Stem bioconcentration factors (BCF)[8], based on Cd_{net} values, for plants grown in spiked soils were 25 times higher than those grown in control soils. By

[7] Ratio of PTE concentration in plant grains, relative to stems.

[8] Ratio of PTE concentration in plant stems, relative to soil.

accounting for the magnitude of the available cadmium pool, these data demonstrate that cadmium released during sphalerite dissolution was significantly more bioavailable than the background soil cadmium in the temperate soil. One explanation for this observation is soil 'ageing'. Cadmium is generally regarded as exhibiting minimal ageing effect (Smolders & Mertens, 2013) but Hamon et al. (1998) demonstrated that around 1% of soil cadmium can be rendered unavailable for plant uptake per year of soil residence time. Ageing may have rendered the 'old' background cadmium in the experimental soils far less phytoavailable than the cadmium recently introduced by sphalerite dissolution.

3.3.5.2 Uptake by paddy rice grown in sub-tropical soil

Rice stem and grain cadmium concentrations of plants grown in spiked soils were 3 – 4 times higher than in control soil plants (Figure 3.9). Although this shows that the plants were contaminated by the sphalerite, the edible tissue concentration (0.597 ± 0.019 μmol Cd kg^{-1}) was well below applicable Chinese (1.78 μmol Cd kg^{-1}) and international (3.56 μmol Cd kg^{-1}) food safety limits for rice grain (USDA Foreign Agriculture Service, 2010; WHO/FAO, 2006). For comparison, cadmium concentrations in the wheat (spiked soil) were higher than those for rice by a factor of 49 in seeds and 24 in stems. Given that the rate of sphalerite dissolution in the experimental soils only varied by a factor of 2, the rice and wheat tissue concentrations illustrate significant differences in the cadmium bioavailability and/or uptake behaviour in the rice and wheat soil-plant systems.

Although rice tissue concentrations were low the data suggest that, all other factors being equal, the rice had a propensity for cadmium uptake similar to or greater than the wheat. In control soils, the wheat and rice stem concentrations were similar (0.74 – 0.85 μmol kg^{-1} Cd) and the rice stem BCF was much higher

than for the wheat (Figure 3.9). Also, the rice TF increased in spiked soils (+53 %), indicating that the plants enhanced stem-to-grain translocation in response to increased cadmium availability (section 3.3.5.2). In light of this apparent propensity for uptake, the relatively low rice tissue cadmium concentrations suggest that uptake was limited by decreased cadmium availability in the paddy soil porewater. This proposition is supported by exchangeable cadmium concentrations that were below the detection limit (Figure 3.5 c), Cd_{net} concentrations that were reduced by 49 % (versus oxic incubation) and stem BCF values that were the same (6.36 – 6.40) in spiked and control soils (i.e. equal bioavailability).

Soil-to-rice cadmium transfer was examined to determine if this could explain the decreased extractable cadmium concentrations. The plant roots were not analysed but their biomass is always much smaller than the stem biomass and therefore assuming equal contribution by the root and stems provided a conservative estimate (Kibria & Ahmed, 2006). Although the neutral soil pH and plant uptake might explain the depletion of exchangeable cadmium, these factors cannot entirely explain the decreased Cd_{net}. Firstly the EDTA extraction, from which Cd_{net} is derived, would not have been sensitive to the shift towards neutral soil pH. Secondly, after considering the estimated total cadmium uptake by rice, a 33 % decrease in Cd_{net} still remained unaccounted for. Therefore it is likely that the formation of non-acid-volatile secondary sulfide phases (section 3.3.5.2) contributed to the low bioavailability and rice uptake of cadmium in this study (de Livera et al., 2011).

Lowland rice is traditionally grown under near-constant standing water; however increasing global population and freshwater demand have catalysed the adoption of new agricultural practises, such as 'system of rice intensification' (SRI),

a set of management principles that discourage flooded agriculture (Africare et al., 2010; Zhao et al., 2010b). A shift towards more oxic soil management will remove the protective biogeochemical conditions afforded by soil flooding and enhance the bioavailability of cadmium in soils.

3.3.6 Inputs and outputs of bioavailable cadmium

Apart from plant uptake, deep soil percolation is the primary export route for bioavailable soil cadmium from the plough layer. The relative contribution of this process was considered when assessing the long-term impact of sphalerite dissolution on bioavailable cadmium concentrations in affected soils. Percentage annual losses via leaching (AL) were estimated using a simple flux model (Eqn. 3.4) after Holm et al. (1998).

$$AL = \frac{PC}{10000DBS} \times 100 \qquad \textbf{(Eqn. 3.4)}$$

where P is the annual net percolation (L ha^{-1} y^{-1}), C is the porewater cadmium concentration (mol L^{-1}), D is the plough layer depth (m), B is the soil bulk density (tonnes m^{-3}) and sulfur is total bioavailable soil cadmium (mmol Cd kg^{-1}). Temperate soil porewater cadmium concentrations (Cd_S) were estimated from both exchangeable concentrations and an empirical multivariate regression model (McBride et al., 1997) that relates soil pH, percentage organic matter (OM) and total soil cadmium (Cd_T) concentrations (Eqn. 3.5).

$$\log [Cd]_S = 3.62 - 0.50\ pH + 0.96 \log Cd_T - 0.45 \log OM \qquad \textbf{(Eqn. 3.5)}$$

Net percolation (2×10^6 L ha^{-1} y^{-1}) and bulk density (1.6 t m^{-3}) were based on estimates for temperate regions (European Commission, 2007). An estimated porewater concentration of 5.34×10^{-8} mol Cd L^{-1} yielded annual losses of 107 mmol ha^{-1} y^{-1}, which accounts for 0.03 % of the total cadmium and 2.5 % of the annual Cd_{net}, an insignificant efflux compared with wheat uptake (38 % of Cd_{net} in stems and grain).

Maintaining a saturated plough layer and surface ponding in irrigated lowland rice production may lead to significant net excess percolation of between 600 mm and 3600 mm per 120 day growing season (Bouman et al., 2007). Although cadmium leaching could be significant in this context, paddy soil porewater cadmium concentrations vary according to redox status and pH. In this study, exchangeable cadmium concentrations in the flooded soils were below the limit of detection (< 0.4 nmol L^{-1}), suggesting negligible porewater cadmium and leaching potential caused by the prevailing reducing conditions (see section 3.3.3).

3.3.7 Human health risk assessment

The human health risk associated with the consumption of the wheat and rice flour produced in contaminated soils in this study was evaluated by estimating cadmium ingestion rates for consumers and comparing these with current health protection guideline values. The most recent international intake guidelines were set in 2010 by the Joint FAO/WHO Expert Committee on Food Additives (FAO/WHO, 2011). It is important to note that laboratory experimental data cannot exactly replicate conditions in the field (Conesa et al., 2007) and that the plant tissue concentrations obtained in this study relate specifically to the chosen experimental conditions. As such, the intention of this exercise is to place those

tissue concentrations into context, not to make quantitative predictions about uptake in the field.

Cadmium ingestion rates for consumers of the grains produced in this study were estimated, assuming cereal consumption rate (3.54 kg $month^{-1}$) (European Food Safety Authority, 2011) and body weight (70 kg). Estimates were made for a worst-case scenario, in which the flours constitute the entire cereal product portion of the model consumers' diet, that they are consumed over a long timescale and that no cadmium is lost during food preparation. Consumption of the wheat flour would result in a dietary cadmium intake 6.6 times the FAO/WHO (2010) provisional monthly tolerable maximum intake (PMTMI) of 222.4 nmol kg^{-1} body weight $month^{-1}$, suggesting consumers would be at risk from chronic cadmium poisoning with the experimental sphalerite soil concentration (0.1 % m/m). Consumption of the rice flour (14 % of the PMTMI) was associated with a low risk of cadmium toxicity for regular consumers.

3.4 Conclusions

Sphalerite exhibits slow, steady dissolution behaviour in oxic agricultural soils developed under contrasting geoclimatic conditions and the primary variable affecting dissolution rate is soil pH. Sphalerite dissolution is accompanied by the release of cadmium, which often occurs as a guest element. Although dissolution is slow, the cadmium released is highly bioavailable under oxic soil conditions, as indicated by *Triticum aestivum*, and has the potential to contaminate crops and pose a human health hazard. Traditional lowland (flooded) rice growing practice can limit the impact of sphalerite contamination by providing neutral soil pH and sub-oxic conditions, which reduces the sphalerite dissolution rate and limits cadmium bioavailability, as indicated by *Oryza sativa,* possibly through the

formation of secondary sulfide phases if sulfur-reducing conditions persist. The recently publicised advantages of ending a reliance upon flooded agriculture (increased yields, reduced water consumption) suggests that growing rice under more oxic conditions will increase in popularity. A potential impact of this transition may be the removal of the protective biogeochemical conditions provided by flooding, resulting in increased risk of chronic cadmium poisoning to consumers of rice produced on sphalerite contaminated soils. At the dissolution rates observed in this study, and considering the probable residence time of cadmium in the soil, sphalerite contamination will have a long-term (decades-centuries) impact on soil quality, long after its introduction to the soil ceases.

Chapter 4

The Implications of Cinnabar Contamination in Agricultural Soils

4.1 Introduction

Mercury is regarded as a global pollutant for its atmospheric cycling (Hg^0), its environmental persistence, its ability to bioaccumulate in food chains as methylmercury (CH_3Hg) and its toxicity. Mining and the abandonment of mining wastes provide a major source of mercury in the environment. These wastes, produced from exploiting cinnabar ore (Navarro, 2008), generally consist of calcined tailings, gangue and low-grade primary ore. Several studies demonstrate that older, inefficiently processed, wastes contain very high residual mercury concentrations, compared with contemporary wastes (Gray et al., 2002; Rytuba, 2003; Biester et al., 1999) and that cinnabar and its polymorph, metacinnabar (β-HgS), are the dominant residual mercury-hosting minerals (Kim et al., 2004; Loredo, et al., 2003b).

Ore roasting/retorting (Gosar et al., 2006), processing, transportation (Higueras et al., 2006; Martínez-Coronado et al., 2011) and waste pile erosion (Loredo et al., 2003a) have been identified as the primary aeolian source-pathways for cinnabar dispersal. For example, cinnabar represented up to 40 % of the mercury content of soils sampled in proximity to the Idrija mining complex (Slovenia), which are enriched (median = 234 μmol Hg kg^{-1}) by a factor of 50 – 100 times versus the global background level (Gosar & Miler, 2011; Biester et al., 1999). Cinnabar also has been identified as the dominant (≤ 68 %) mercury-hosting (250 to 500000 μmol Hg kg^{-1}) phase found in aerosols (including PM_{10}) emanating from historic mercury mining areas (Moreno et al., 2005; Kocman et al., 2011).

Release of colloidal cinnabar and metacinnabar, resulting from infiltration and surface run-off of waste heaps and tailings, has been identified an important process (Kim et al., 2001; Lowry et al., 2004; Slowey et al., 2005). The preferential

mercury enrichment of finer particles in fluvial sediments (Lowry et al., 2004) and aerosols (Moreno et al., 2005) enhances their environmental impact because very fine particles have high reactive surface areas, are likely to be transported over greater distances by fluvial and aeolian source-pathways and are more easily re-mobilised after deposition. Streams and rivers have been reported to transport mercury waste particles over large distances (i.e. as far as 50 km) from their source (Horvat et al., 1999), producing extremely contaminated (up to 0.1 % mercury) sediments and overbank deposits (Gray et al., 2000; Rytuba, 2003), and also raising concern over the contamination of agricultural floodplain soils (Qiu et al., 2005).

The complex environmental biogeochemistry of mercury involves possible speciation modifications in all environmental compartments, affecting the transport, fate and toxicity of this element (Figure 4.1). Cinnabar has low water-solubility and can precipitate authigenically under moderately reducing conditions (Figure 4.1); therefore it is often regarded as a mercury sink, not a source of bioavailable mercury in the surficial environment (Schuster, 1991). However, there is growing evidence that cinnabar dissolution is enhanced by abiotic oxidation (Barnett et al., 2001; Holley et al., 2007), complexation with dissolved organic matter at the mineral surface (Ravichandran et al., 1998; Waples et al., 2005; Slowey, 2010) and through oxidation by sulfur-oxidising bacteria (Vazquez-Rodriguez et al., 2012; Vazquez-Rodriguez et al., 2013). Through these processes, mercury could be released from cinnabar into soil porewater and become available for plant uptake.

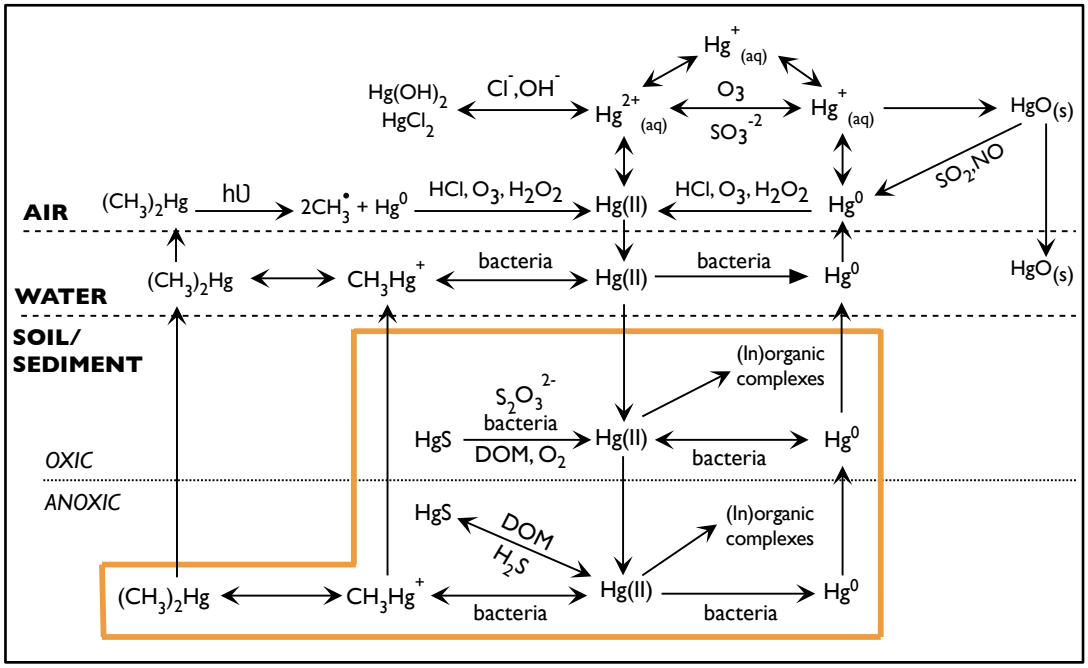

Figure 4.1 Overview of the dominant mercury species and species conversions known to occur in environmental compartments, modified after Stein et al. (1996) to include recent discoveries relating to cinnabar dissolution and precipitation in soils and sediments. The transformations and compartments most relevant to this study are highlighted (orange box).

The mobility of mercury in soils is strongly influenced by its ability to form complexes. The most important mobile species, uncharged complexes formed by Hg(II) and chloride or hydroxyl ligands, are weakly adsorbed by charged colloidal soil constituents, such as clays (Steinnes, 2013). At pH ≥ 4 the dominant soluble species is $Hg(OH)_2^0$, the precipitation of which limits Hg solubility at pH ≥ 7 (Fergusson, 1990). This species is specifically adsorbed by soil constituents, such as metal oxyhydroxide mineral surfaces, showing higher affinity with increasing pH (3.5 – 7.0). The influence of sparingly adsorbed chloromercury complexes (i.e. $HgCl_2$) is strongest at low pH, when hydroxyl groups have lower activity. Hence, under acid conditions (< pH 4.5) complexation by humic matter (solid phase) is the most important process limiting Hg(II) solubility (Schuster, 1991). The importance of humic matter binding is also evidenced by reports that mercury, deposited from

the atmosphere, preferentially accumulates in the organic surface soil horizon (Han et al., 2006). Low estimated losses from soils due to leaching (< 1 % y^{-1}) have also been attributed to humic matter binding (Steinnes, 2013).

The sulfide ligand becomes more influential under mildly to strongly reducing conditions (Figure 4.1). Mildly reducing conditions promote authigenic cinnabar precipitation (Barnett et al., 1997), whilst very strongly reducing conditions may promote mercury solubility due to the reduction of mercuric ion to the elemental form (Schuster, 1991) or the presence of bidentate polysulfide ligands in solution, which have been shown to enhance cinnabar solubility (Paquette & Helz, 1997). Sulfur reducing organisms, which are active in reducing soil environments, such as flooded paddy soils, are also associated with mercury methylation (Meng et al., 2011; Ullrich et al., 2001; Paquette & Helz, 1997).

Excluding occupational vapour exposure, diet and dental amalgam constitute most of people's mercury intake, with fish consumption as the key dietary contributor (methylmercury – see Figure 4.1) for most populations (Horvat et al., 2003). However, recent studies suggest that crops may be the dominant vector of potentially harmful levels of mercury to inland communities living near abandoned mercury mines (Feng et al., 2008; Rothenberg et al., 2011; Zhang et al., 2010). For example, Qiu et al. (2006) found an average of 1.3 μmol Hg kg^{-1} in rice, corn and brassicas in the Wuchuan mining area, China, one order of magnitude higher than the Chinese food safety limit of 0.1 μmol Hg kg^{-1}.

The central nervous system is the most sensitive organ in respect to chronic mercury exposure (Holmes et al., 2009; Tchounwou et al., 2003) and children are the most sensitive receptors due to greater intestinal absorption, bodily retention and rapidly developing brain/nervous system compared with adults (ATSDR, 1999). As such, relationships between prenatal methylmercury exposure and

developmental neurotoxicity have been used to derive the most stringent human health protection limits (WHO/FAO, 2003). Both elemental (Hg^0) and organic (CH_3Hg, $(CH_3)_2Hg$) mercury are lipophilic, allowing for their widespread bodily distribution and passage through the blood-brain barrier, placenta and into breast milk (Ullrich et al., 2001). Unlike these species, lipophobic inorganic mercury(II) compounds tend to accumulate in the kidneys; however exposure is still associated with permanent damage to the central nervous system (Tchounwou et al., 2003). Elemental mercury is sparingly absorbed via the intestines (< 0.01 %) compared with methylmercury (95 %) and inorganic mercury(II) (2 – 38 %), which are the dominant forms found in foodstuffs (WHO, 2003) and therefore represent the primary hazard via dietary intake. Debate lingers regarding the health effects from low-level environmental mercury exposure, leading health regulators to call for mercury use to be minimised wherever possible (Holmes et al., 2009).

Discoveries, concerning DOM-induced dissolution (Waples et al., 2005), abiotic oxidation (Holley et al., 2007) and biotic oxidation (Vazquez-Rodriguez et al., 2013) of cinnabar, suggest that this mineral is not as inert as previously thought and may behave as a source of bioavailable mercury. These discoveries, combined with evidence showing that cinnabar behaves as a vector for mercury contamination and the human health risks associated with living in areas impacted by mercury mining, demonstrate the importance of understanding the stability of cinnabar in soils.

4.2 Experimental

The overall investigative strategy and experiments are summarised in this section, with reference to relevant sub-sections in Chapter 2, where the applied methods are described in full detail.

4.2.1 Investigative approach

This study comprised three strands of investigation (Figure 4.2):

(1) A field weathering experiment to investigate secondary mineral phase formation associated with long-term exposure of cinnabar within soils under environmental conditions.

(2) Laboratory batch incubations of soils spiked with cinnabar (0.1 % HgS m/m) to determine the dissolution behaviour of cinnabar in soils under controlled conditions. Addition incubations, with a high cinnabar concentration (10 % HgS m/m), were performed with the aim of identifying secondary alteration phases.

(3) Phytoavailability experiments where *Triticum aestivum* and *Oryza sativa* were grown in samples of the temperate and flooded sub-tropical soils, respectively, to evaluate the bioavailability of mercury released from cinnabar under oxic and sub-oxic conditions.

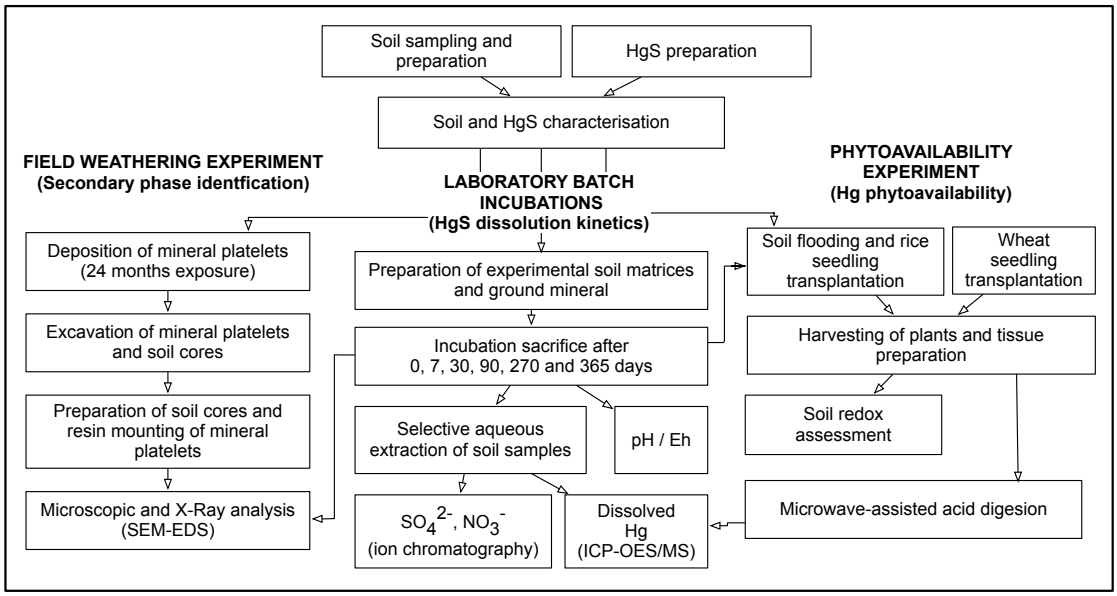

Figure 4.2: Schematic summarising the experimental approaches taken in this study.

4.2.2 Soil and mineral sampling, preparation and characterisation

Soils of temperate and sub-tropical provenance were collected on the basis of their contrasting geological and climatic character (section 2.3.1). The fine soil fraction (< 2 mm) was carefully homogenised to produce what will hereafter be referred to as the temperate and sub-tropical *experimental soils* (section 2.3.2) and these were characterised by determining their physical and chemical features (section 2.3.3).

Small platelets (~ 2 cm^2 × 0.3 cm) and a fine powder (< 63 μm) were prepared from specimen cinnabar. The cinnabar was characterised by examining its mineralogy and elemental composition as described in section 2.4.

4.2.3 Field weathering experiment

Cinnabar platelets were deposited approximately 0.1 m below ground level within a 0.1 m × 0.1 m horizontal grid and then remained *in situ* for 24 months at the sampling location for the temperate experimental soil. The platelets were

excavated in cores and prepared as polished epoxy resin sections prior to examination for secondary phase formation using SEM-EDXS (section 2.5).

4.2.4 Laboratory batch incubation experiments

Temperate and sub-tropical soils were spiked with cinnabar at concentrations of 0.05 % m/m for aliquots used for day 7 to day 90 sacrifice and 0.1 % m/m for all other aliquots (all < 63 μm). The different concentrations were logistically necessary because the amount of available cinnabar was limited and additional experiments (requiring cinnabar) were planned after elements of the batch incubation experiment had begun. Experimental and control (not spiked) soils were incubated under laboratory conditions for durations ranging 0 to 365 days as described in section 2.6. After incubation, the samples were analysed for water-soluble major anions (NO_3^-, SO_4^{2-}) and cation-exchangeable mercury (0.01 mol $CaCl_2$ L^{-1} extract). The samples were also sequentially extracted to determine (i) the non-cinnabar mercury fraction (i.e. total liberated mercury) using 14 mol HNO_3 L^{-1} and (ii) the residual cinnabar fraction using 2.3 mol Na_2S L^{-1} and microwave-assisted acid digestion. The resulting data were used to determine the release trends and geochemical associations of the cinnabar constituents as weathering progressed during the experiment (section 2.6.3.3).

In addition, soils spiked with a higher concentration of cinnabar (10 % m/m) were incubated for 180 days with the aim of detecting secondary phase formation using XRD, and examination using SEM-EDXS (section 2.8).

4.2.5 Phytoavailability experiments

Large (4 L) analogues of the laboratory batch incubation experiments were incubated for 180 days before *Triticum aestivum* or *Oryza sativa* were transplanted

into the temperate and sub-tropical experimental soils, respectively (section 2.9). The total mercury concentration of the stems and grains was determined to evaluate the bioavailability of mercury released during cinnabar weathering and the hazard posed to human health via the crop contamination pathway. In addition, the biogeochemical conditions prevailing in the flooded sub-tropical soils after rice cultivation were determined to examine relationships between soil conditions and the plant uptake and geochemical associations of mercury liberated during cinnabar weathering (section 2.9.4).

4.3 Results and discussion

4.3.1 Experimental soil and cinnabar characterisation

A general discussion and data summary of the chemical, physical and mineralogical compositions of the experimental soils is given in section 3.3.1. The temperate and sub-tropical experimental soils had background total mercury concentrations of 1.30 ± 0.26 and 0.78 ± 0.22 μmol Hg kg^{-1} (n = 5), respectively. A survey of the literature (Steinnes, 2013) suggests that, globally, agricultural soils contain 0.5 μmol Hg kg^{-1} but concentrations range widely from 4.9 × 10^{-3} to 5.9 μmol Hg kg^{-1}. The background mercury concentration in both soils fell within 1 μmol kg^{-1} of the global average for agricultural soils, indicating they were not exposed to anthropogenic point-source contamination prior to this study.

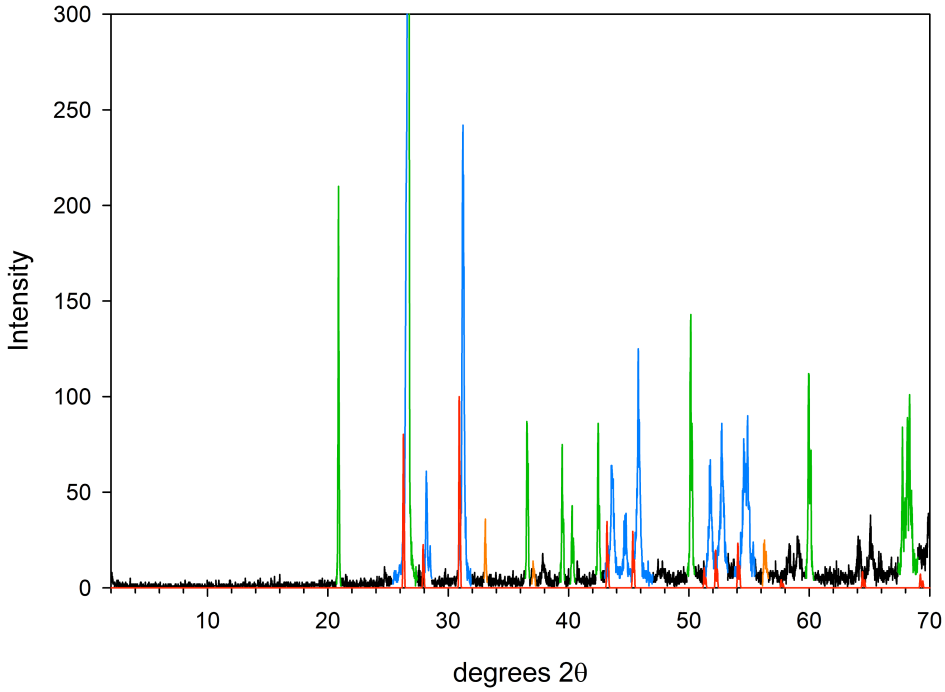

Figure 4.3 X-ray diffractogram for the experimental cinnabar (< 63 µm) showing peaks for the two dominant phases: cinnabar (blue), quartz (green) and pyrite (orange).

Solid-phase characterisation (Figure 4.3 and Figure 4.4) indicated that the 'experimental cinnabar', which was obtained as a specimen with granular crystal habit (Almadén, Spain), consisted of veins of pure $Hg_{1.05}S_{0.95}$ in a quartz matrix with minor inclusions of pyrite. Wet chemical and gravimetric analyses of the bulk material indicated a percentage (mass) constitution of 43.3 ± 0.5 Hg, 10.3 ± 0.3 S and 50.8 ± 7.0 % quartz. It is important to note that the volume of material occupied by quartz is disproportionate to the percentage mass, owing to considerable differences in relative mass (i.e. Hg vs. Si/O) and mineral density. A comparison of the XRD spectra obtained from the material (Figure 4.3) with mineral databases demonstrated the crystalline structure of cinnabar (α-HgS) and not the polymorph, metacinnabar (β-HgS), which has previously been observed to form from cinnabar during grinding, weathering and exposure to radiation, including sunlight (Bearat et al., 2005; King, 2002).

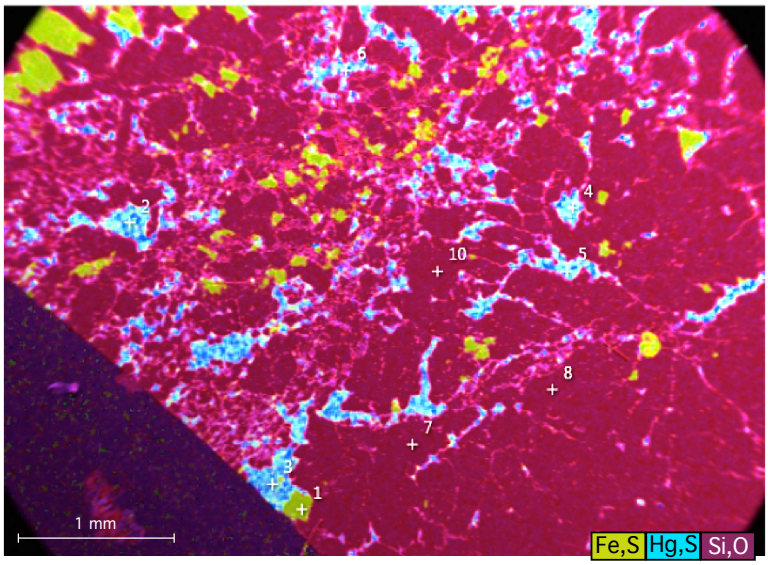

Figure 4.4 False coloured electron micrograph produced using a combination of electron-backscatter detector data and EDXS. Elemental phase associations are colour coded.

4.3.2 Biogeochemical conditions in experimental soils

4.3.2.1 Oxic incubations

As the pH was not controlled during the oxic incubation experiment, notable pH decreases occurred in both temperate (- 0.88 pH units) and sub-tropical (- 0.30 pH units) experimental soils during the initial 30 days of incubation (Figure 4.5). After 30 days, the temperate and sub-tropical soils fluctuated around pH 5.45 ± 0.20 and pH 6.31 ± 0.11, respectively. The decline can be attributed to the activity of sulfur and ammonium oxidising bacteria and pH differences between the soils reflect their respective pH buffering capacity, as previously discussed (section 3.3.2). The soils were periodically checked for redox potential, which indicated consistently oxic conditions (Eh 350 – 400 mV) throughout the incubations.

4.3.2.2 Flooded sub-tropical 'paddy' soils

After rice cultivation, during which time (152 days) the sub-tropical soils were constantly flooded, soils had attained neutral pH (6.95) and moderately reducing conditions (Eh = - 26 ± 11 mV), as would be expected for flooded paddy soils (Ponnamperuma, 1972). Nitrate and iron reducing conditions were indicated by the depletion of soluble nitrate (> 99 %), compared with the soils incubated under oxic conditions (180 – 365 days), and the majority of the acid-extractable iron obtained from the flooded soils (86 ± 3 %) was found as Fe(II). In addition, sulfate-reducing conditions were evidenced by the depletion of the soluble sulfate (≥ 96 %) and the detection of AVS (200 ± 16 μmol S^{2-} kg^{-1}). The resulting availability of dissolved sulfide is conducive to authigenic cinnabar precipitation (Barnett et al., 1997). However, there is no evidence that precipitation of reduced mercury species occurred, as the concentrations of exchangeable (17.7 ± 8.4 nmol Hg kg^{-1}) and total liberated (130 ± 13 μmol Hg kg^{-1}) mercury determined in the flooded soils were within the experimental uncertainty of those obtained from oxic incubations of the same soil.

4.3.3 Cinnabar alteration

4.3.3.1 Sulfate liberation

Water-extractable sulfate concentrations were monitored as an indicator for the oxidative dissolution of cinnabar in the oxic incubation experiments (Figure 4.5). The overall trend for water-extractable sulfate in both experimental soils was a rapid increase during the initial 90 days of incubation, followed by a plateau and then relatively stable concentrations for the remainder of the experiment. Apart from the 365 day incubation time-point of the temperate soil ($p < 0.01$, Holm-Sidak

T-test), no significant differences were found when comparing sulfate data from spiked and control soils.

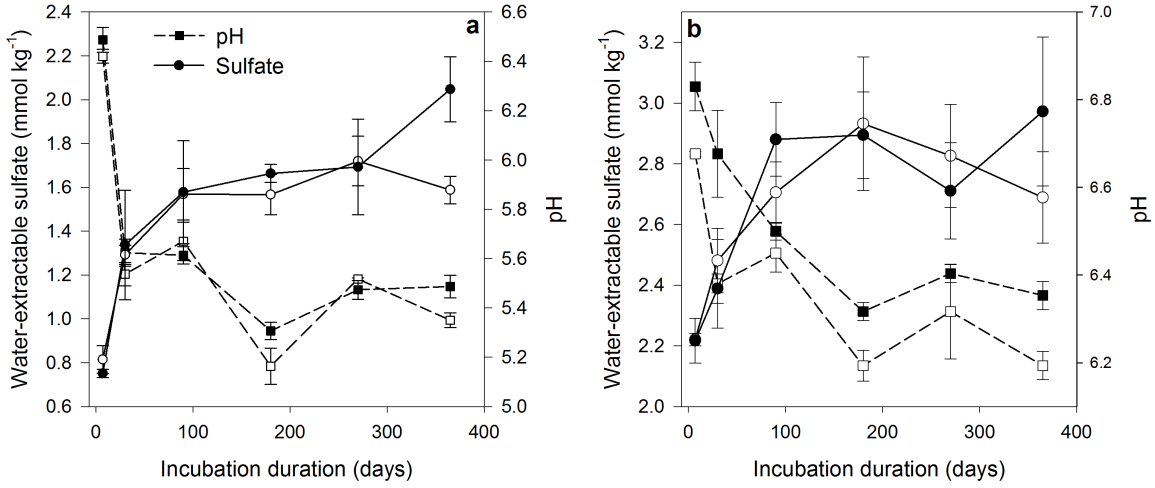

Figure 4.5 Water-extractable sulfate concentrations and soil pH plotted against incubation durations for both the temperate (a) and sub-tropical (b) soils. Filled and unfilled data markers represent spiked and control soils, respectively. Lines connecting data points are presented for the sake of clarity. Error bars are reported as ± 1 standard deviation (n = 3).

Previous laboratory dissolution studies in aqueous media (Holley et al., 2007; Barnett et al., 2001) suggest that oxidative dissolution of cinnabar by dissolved oxygen in soil porewater (Eqn. 4.1) would produce an excess of sulfate in the spiked soil, relative to the control.

$$HgS_{(s)} + 2O_{2(aq)} + 2H_2O \leftrightarrow Hg(OH)_2^0 + SO_4^{2-} + 2H^+ \quad \textbf{(Eqn. 4.1)}$$

The sensitivity of the obtained sulfate data as an oxidation indicator can be evaluated by analysing data uncertainty. The uncertainty of the control soil data (σ = 0.01 – 0.22 mmol S kg^{-1}, n=3) indicate that, assuming equal variance in both data sets, a minimum excess sulfate concentration of > 0.2 mmol S kg^{-1} was required to produce statistically significant differences between spiked and control soils. This

concentration equates to ~10 % cinnabar oxidation at any point during the experiments and marks the minimum extent of oxidation that can be detected using sulfate concentrations. The variation between water-soluble sulfate concentrations in spiked and control soils, was independent of incubation time despite the cinnabar concentration in spiked soils varying between 0.1 and 0.05 % at various incubation time-points (section 4.2.4). This strongly suggests that the extracted sulfate originated from pre-existing sources, not from the cinnabar.

4.3.3.2 Mercury liberation

Mercury concentrations extractable by cation-exchange (0.01 mol $CaCl_2$ L^{-1}) obtained from the cinnabar-spiked and control experimental soils in the oxic incubation experiment are presented in Figure 4.6 for temperate (a) and sub-tropical soils (c). The percentage of the total sequentially extracted mercury attributed to non-cinnabar forms (14 mol HNO_3 L^{-1} extraction) is shown as 'percentage mercury liberation' in Figure 4.6 (b) and cinnabar, extracted using microwave-assisted acid digestion, is given as 'percentage HgS' in Figure 4.6 (d).

Significantly and consistently higher exchangeable (plots a + c) concentrations obtained from spiked soils vs. controls confirm that the alteration of cinnabar contributed to the labile mercury reservoir of both experimental soils during the course of the incubation experiments (365 days). The exchangeable concentration plots (a + c) show similarities in the first 180 days of incubation: a sharp decline between 0 and 7 days incubation and resurgence at 30 days incubation. In the sub-tropical soil, the concentrations declined after 30 days and remained stable, whereas the data continued to fluctuate in the temperate soil.

The exchangeable concentrations were very low as a proportion of total liberated mercury: around 0.3 % and 0.6 % in the temperate and sub-tropical soils,

respectively. At the prevailing pH (5.4 – 6.8) and redox (> 350 mV) conditions, mercury is likely to bind to metal (Fe, Al, Mn) oxyhydroxides and organic matter (Schuster, 1991) and this may explain the low exchangeable mercury fraction. Whilst concentrations in the most bioavailable and environmentally labile fraction were low in both soils, those obtained from the temperate soil were consistently higher (by factors ranging 1.8 – 16.7) than those from the sub-tropical soil.

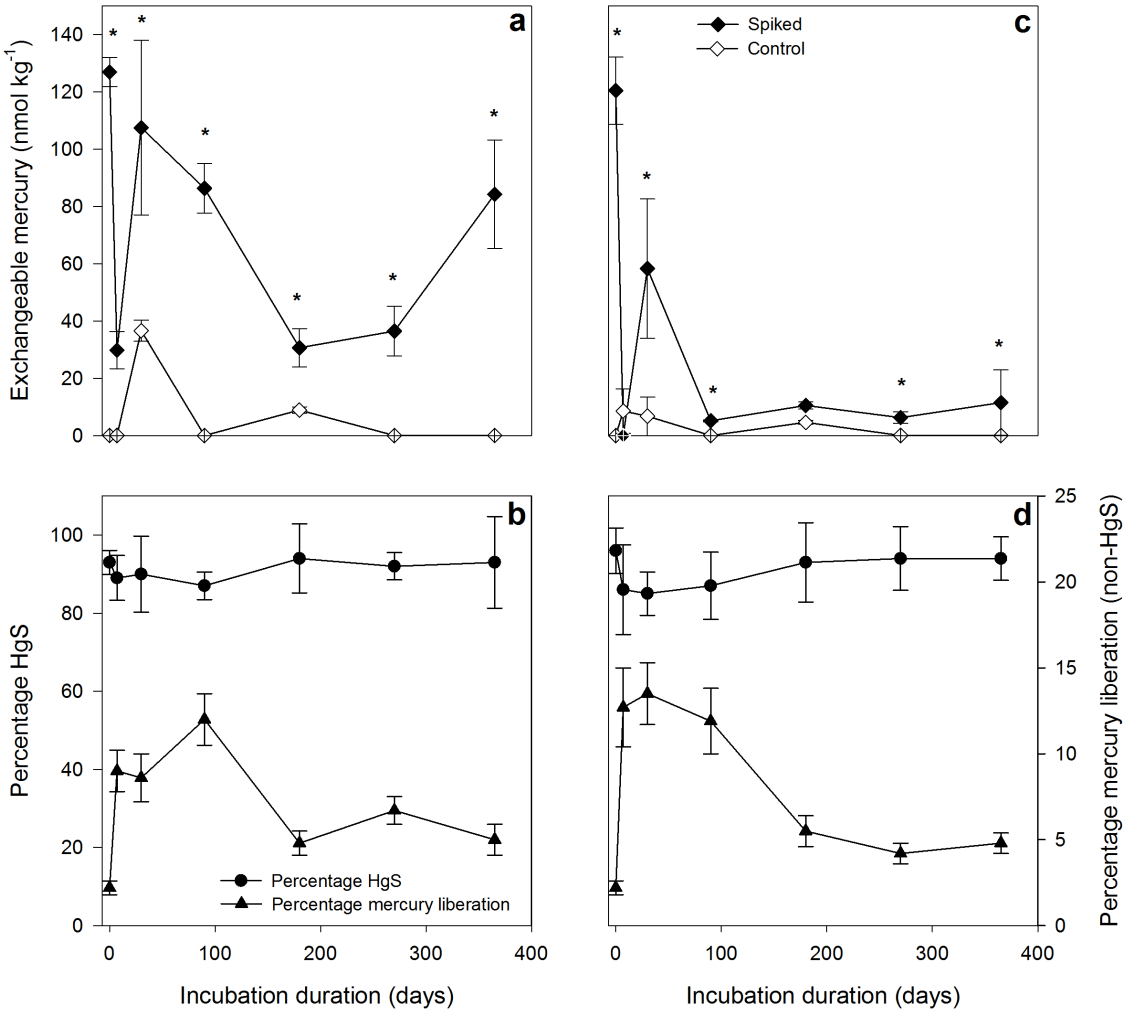

Figure 4.6 Plots a + c: Exchangeable mercury concentrations obtained from temperate (a) and sub-tropical (c) experimental soils incubated for 0 – 365 days under oxic conditions. Asterisks denote significant ($p < 0.01$) differences (spiked vs. control) and crossed diamonds denote values below the detection limit (2.5 nmol Hg kg^{-1}). Plots b + d: Percentage mercury determined as cinnabar and non-cinnabar forms (percentage mercury liberation) in temperate (b) and sub-tropical (d) experimental soils. All plots: Error bars are reported as ± standard deviation (n = 3). Lines connecting data points are displayed for clarity.

Several studies have quantified the cinnabar content of soils by selective sequential aqueous extraction. Investigators employed 14 mol HNO_3 L^{-1} to extract mercury from soils in all forms excluding cinnabar (Revis et al., 1989; Bloom et al., 2003), followed by extraction of the cinnabar-bound fraction using either acid digestion (microwave-assisted, aqua regia,) to dissolve the residue, which is attributed to cinnabar (Fernández-Martínez & Rucandio, 2005; Mikac et al., 2003), or saturated Na_2S, which selectively dissolves cinnabar (Revis et al., 1989). These approaches were validated in previous work (Han et al., 2003; Fernández-Martínez & Rucandio, 2005) demonstrating that 14 mol HNO_3 L^{-1} extraction at room temperature completely dissolves most mercury species commonly found in soils ($HgCl_2$, HgO, $HgSO_4$, $Hg(NO_3)_2$, MeHgCl, EtHgCl, Hg^0), other than cinnabar.

During this study, both Na_2S extraction and microwave-assisted acid digestion were performed in addition to the initial HNO_3 step. Both approaches proffered very similar mercury partitioning trends, however the Na_2S data demonstrated a lesser degree of analytical control and, therefore, the microwave-assisted *aqua regia* digestion (section 4.2.4) data were selected for further interpretation.

After a small reduction within the first 7 – 30 days of the experiment, the proportion of cinnabar-bound mercury recovered from minima of 85 – 87% to around 96%, and remained relatively consistent for both soils throughout the experiment (Figure 4.6 b + d). As the percentage mercury liberation curves illustrate more clearly, these data indicate that no more than 15 % of cinnabar in the experimental soils was altered during the course of the experiment.

Both experimental soils yielded very similar trends for percentage mercury liberation (non-HgS) throughout the experiment (Figure 4.6 b & d), starting with an increase by a factor of 2 – 4 in the first 7 days. The percentage peaked at 12.0 ± 1.5 % (90 days) and 13.5 ± 1.8 % (30 days) in the temperate and sub-tropical soils,

respectively, followed by a decline to a steady level in both soils (5.2 ± 0.9 %) between 180 and 365 days. In comparison, the total liberated mercury concentrations in control soils (below the working scale of Figure 4.6) were 30 – 200 times lower than those obtained for the spiked equivalents. Again, this confirms that the total liberated mercury obtained from spiked soils originated from the cinnabar.

4.3.3.3 Mechanisms of mercury release

Cinnabar is considered practically insoluble in water (standard conditions) and its weathering by simple dissolution (Eqn. 4.2) is thermodynamically ($K = 10^{-38}$) limited (Barnett et al., 1997).

$$HgS_{(s)} + 2H_2O \leftrightarrow Hg(OH)_2^0 + H_2S \qquad \textbf{(Eqn. 4.2)}$$

As previously stated, abiotic and biologically enhanced oxidative dissolution and dissolved organo-mercury complex formation are the reported mechanisms by which cinnabar can be chemically weathered under surficial environmental conditions. The sulfate release data (section 4.3.3.1) are inconsistent with oxidative dissolution as the dominant mechanism for the mercury release found in this study, suggesting DOM-induced (dissolved organic matter) dissolution is the more probable explanation for the findings.

The proposed mechanism for DOM-induced cinnabar dissolution involves adsorption of organic ligands to the mineral surface and the detachment of stable mercury-organic complexes (e.g. $Hg(OH)_2$-fulvic acid complex) (Reddy & Aiken, 2001) into solution (Ravichandran et al., 1998; Ravichandran, 2004). Such complex formation was also attributed to the inhibition of metacinnabar precipitation

under reducing conditions (Ravichandran et al., 1999). Experimental data show that DOM-induced dissolution requires direct contact between DOM and the mineral surface and that DOM saturation of cinnabar surfaces is rate-limiting (Waples et al., 2005; Ravichandran et al., 1998). This limiting mechanism is consistent with the mercury liberation trends (Figure 4.6 b + d) which suggest that, in terms of mercury release, cinnabar equilibrated with the soils in no more than 180 days and that the chemical weathering was not a continuous process but rather one occurring in the first weeks of soil exposure.

An alternative potential mechanism involves the direct release of elemental mercury from the cinnabar into the soil. That assertion is supported by observations that the specimen experimental cinnabar 'bled' mercury droplets before its preparation into platelets or powder, and this behaviour is also implied by reports of large pools of elemental mercury being found at the base of cinnabar-rich tailings (Biester et al., 1999) and droplets in tailings and contaminated soils in association with cinnabar (Higueras et al., 2006; Moreno et al., 2005; King, 2002; Gray et al., 2000). This mechanism is also consistent with a relatively large mercury release in a short period (≤ 7 days).

An evaluation of the selectivity of the sequential extraction procedure on the experimental cinnabar (10 mg HgS) demonstrated minimal mercury extraction (1.50 ± 0.18 %) by 14 mol HNO_3 L^{-1} (i.e. non-cinnabar mercury forms), which is consistent with previous work demonstrating that cinnabar is resistant to concentrated HNO_3. Interestingly, when the cinnabar was combined with soil (10 mg HgS and 1 ± 0.01 g soil), extraction significantly increased (3.65 ± 0.58 to 3.78 ± 0.59) despite < 3 h having passed between preparing the cinnabar/soil mixture and performing the extraction. This agrees with observations by Han et al. (2008), who reported 2.5 % extractability (HNO_3) after 5 h of soil exposure. Whilst this can

be attributed to rapid cinnabar-soil interactions, it can also be speculated that the presence of soil increased the wettability of the cinnabar and some evidence indicates that the chloride content of soils (Fernández-Martínez & Rucandio, 2005; Mikac et al., 2003) enhances cinnabar solubility in concentrated HNO_3 solution, but the mechanism remains unclear.

4.3.3.4 Stabilisation of liberated mercury

The decline in percentage mercury liberation observed in both experimental soils after 90 days incubation suggests that the mercury liberated from the cinnabar matrix became less soluble and less potentially bioavailable with increasing exposure time. One potential explanation for the apparent declining percentage liberation is mercury loss from the experimental system. Since the incubations were performed without drainage (i.e. water was only lost by evaporation) and no material was removed during the experiment, the only plausible route by which mercury could have escaped from the soils was via the air, having a more pronounced effect on samples incubated for longer durations (> 90 days). Several key mercury species are volatile (elemental mercury and dimethylmercury, Figure 4.1) and atmospheric loss from contaminated soils is a well-documented phenomenon (Kocman et al., 2011; Li et al., 2012; Martínez-Coronado et al., 2011). Cinnabar is considered non-volatile at ambient temperatures (Han et al., 2006) and so it stands to reason that the liberated mercury fraction, which may include volatile species (Schlüter, 2000), would be disproportionately affected by volatilisation compared with the cinnabar fraction, reducing the proportion of mercury determined in non-cinnabar forms in the experimental soils. Atmospheric losses would be evident from the total mercury recovery obtained from soils after the experiment, which were 93.7 ± 7.4 % and

92.0 ± 8.7 % for the temperate and sub-tropical soils, respectively. The uncertainty in the data and the trend in recoveries (Table 4.1) do not clearly reflect atmospheric loss from the later samples, which casts doubt upon this explanation for declining percentage mercury liberation Figure 4.6 (b + d).

Table 4.1 Total mercury recovery obtained using microwave-assisted acid digestion, based on the nominal contribution made by cinnabar to the spiked soils. Uncertainties are reported as ± 1 σ (n=3).

Days	Temperate soil Total recovery (%)	Sub-tropical soil Total recovery (%)
0	96.1 ± 5.3	91.7 ± 4.7
7	101 ± 3	89.8 ± 2.5
30	96.5 ± 4.9	80.5 ± 3.6
90	90.5 ± 1.0	90.0 ± 1.9
180	93.6 ± 2.7	85.3 ± 3.8
270	78.9 ± 1.4	104 ± 2
365	99.8 ± 5.0	102 ± 4

The samples at incubation time-points with the highest percentage mercury liberation (7 – 90 days) were also the samples with the lower (i.e. 0.05 % HgS) cinnabar concentration, which suggests that cinnabar concentration may have influenced its HNO_3-extractabilty. Fernández-Martínez and Rucandio (2005) specifically tested for this effect and found no significant difference in the relative extractability (HNO_3) of soils spiked with cinnabar at concentrations ranging over two orders of magnitude.

On the basis that only cinnabar is recalcitrant to the HNO_3 extraction, the reduced percentage liberation (Figure 4.6 b and d) indicates secondary cinnabar or metacinnabar precipitation in the experimental soils. Some evidence for secondary cinnabar formation exists in the form of significantly ($p < 0.05$, ANOVA) higher

mercury concentrations attributed to cinnabar (Na_2S extraction) in temperate soils incubated for ≥ 270 days, compared with the unincubated samples (Figure 4.7).

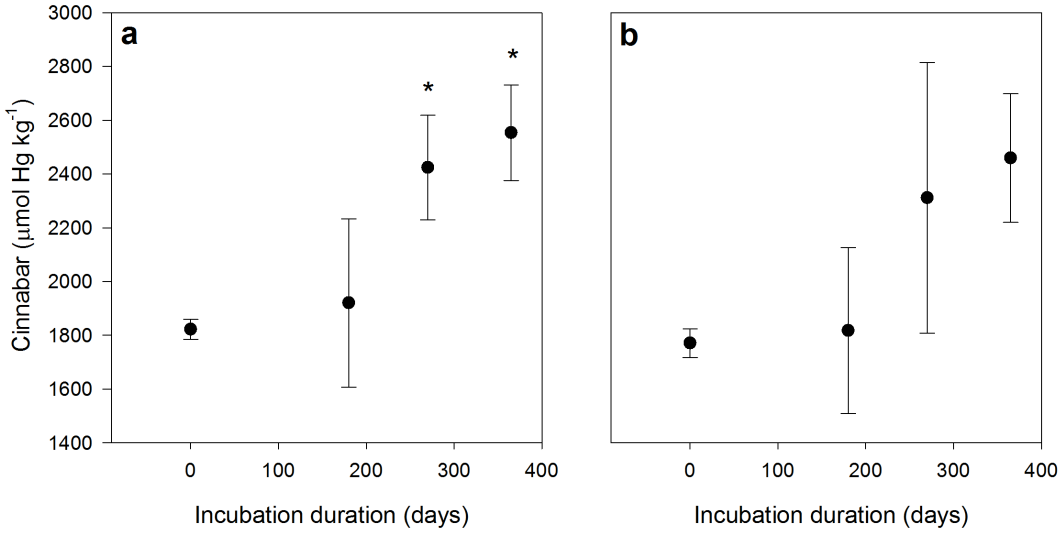

Figure 4.7 Comparison of cinnabar-bound mercury concentrations (Na_2S extraction) obtained from soils after 0 days (unincubated) and 180 – 365 days incubation in the temperate (a) and sub-tropical (b) cinnabar-spiked experimental soils. Asterisks denote statistically significant ($p < 0.05$) differences between unincubated and incubated samples. Uncertainties are reported as ± 1σ (n = 3).

Authigenic cinnabar precipitation has been reported in soils and sediments. For example, soils affected by the Oak Ridge National Security Facility in Tennessee USA, which were severely contaminated with elemental mercury in the 1950s – 1960s, now feature cinnabar (or metacinnabar) as the dominant mercury phase, suggesting that elemental mercury is transformed to cinnabar or metacinnabar over the course of decades (Han et al., 2006; Revis et al., 1989). However, the process requires an abundance of dissolved sulfide only likely to be found under sulfur-reducing conditions (Barnett et al., 1997). Consistently oxic bulk soil conditions were maintained in the incubated soils and there was no evidence for sulfate-reduction in those samples (section 4.3.2.1), unlike the flooded soils used to grow *Oryza sativa* (section 4.3.2.2). Although soil microenvironments may

exhibit contrasting properties from the bulk conditions that may be conducive to secondary cinnabar precipitation, apart from the sequential extraction, the data obtained in this study do not support this as a mechanism by which the mercury was 'stabilised' after 180 days incubation in these experiments.

Other secondary phases that have been reported in association with cinnabar in mining wastes include montroydite (HgO), calomel (Hg_2Cl_2) and, rarely, other chlorine-rich phases, such as corderoite ($Hg_3S_2Cl_2$), eglestonite ($Hg_6Cl_3O(OH)$) and kuzminite ($Hg_2(Br,Cl)_2$) (Navarro et al., 2009; King, 2002; Moreno et al., 2005; Foord et al., 1974). Of these, montroydite and calomel have been tested for solubility in HNO_3, showing complete and partial (0.6 – 11 %) dissolution, respectively. The present evidence suggests that the formation of secondary phases, possibly calomel, could act to sequester environmentally and biologically available mercury after its release from cinnabar in soils.

4.3.3.5 Examination of spiked soils for secondary phase formation

Experimental soils spiked with 10 % cinnabar were analysed using XRD both before and after 180 days incubation under laboratory conditions. The composite spectra (example shown in Figure 4.8), which were normalised by the intensity of peaks for an internal standard (corundum), revealed an extremely similar peak distribution for the incubated and unincubated samples. A slight decrease in the intensity of some peaks related to cinnabar (marked) was evident, which is consistent with the weathering data already presented. However, no new peaks, which could identify secondary phases formed during the incubation time, were identified in either experimental soil. It is important to recognise that XRD has a relatively high detection limit (1 – 3 %) and therefore, only significant secondary phase formation would be apparent.

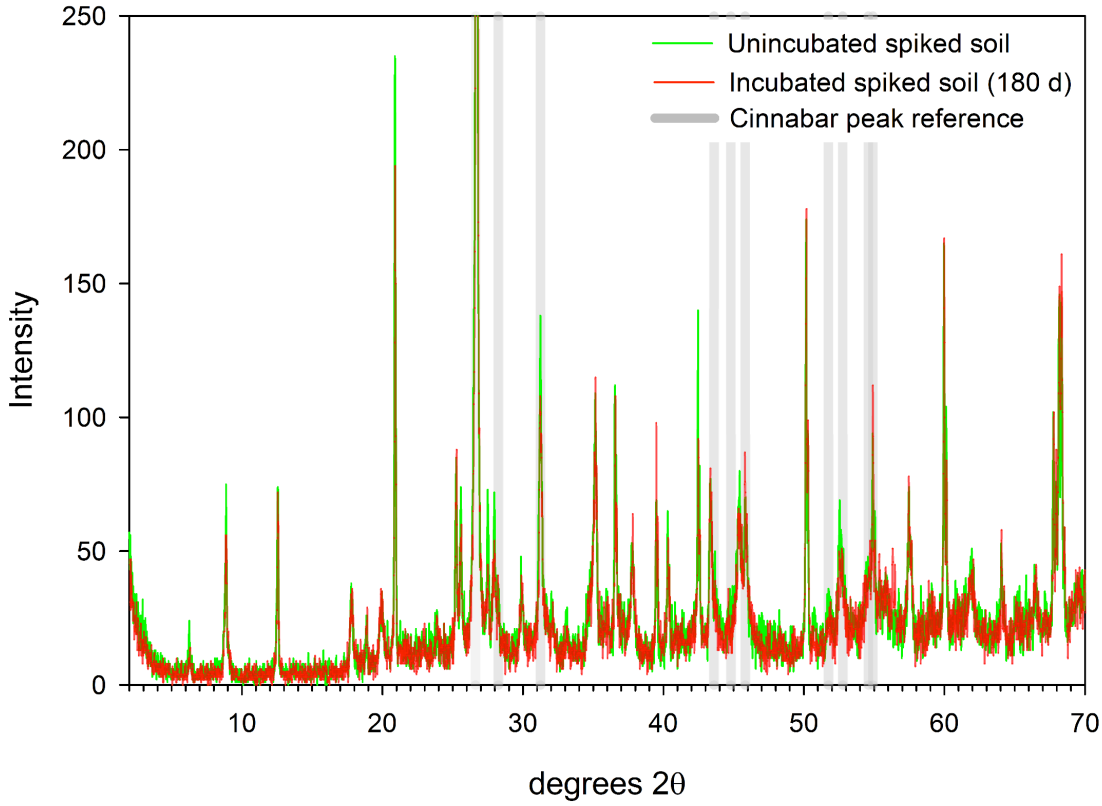

Figure 4.8 Composite of XRD spectra for temperate experimental soil spiked with cinnabar (10 %) and either not incubated (green spectra) or incubated for 180 days (red spectra). Intensity was normalised using an internal standard (Al_2O_3). Grey vertical lines show the position of diffraction peaks associated with cinnabar.

Polished sections of the incubated (180 days) cinnabar-spiked (10 %) experimental soils (section 4.2.4) were also examined using SEM-EDXS. Mercury-rich phases, which were first identified with an electron backscatter detector, were examined in detail using EDXS to determine their elemental composition and associations (Figure 4.9). Mercury-rich areas of the polished surfaces were only found as discrete phases in association with sulfur, with the composition of those phases corresponding to cinnabar.

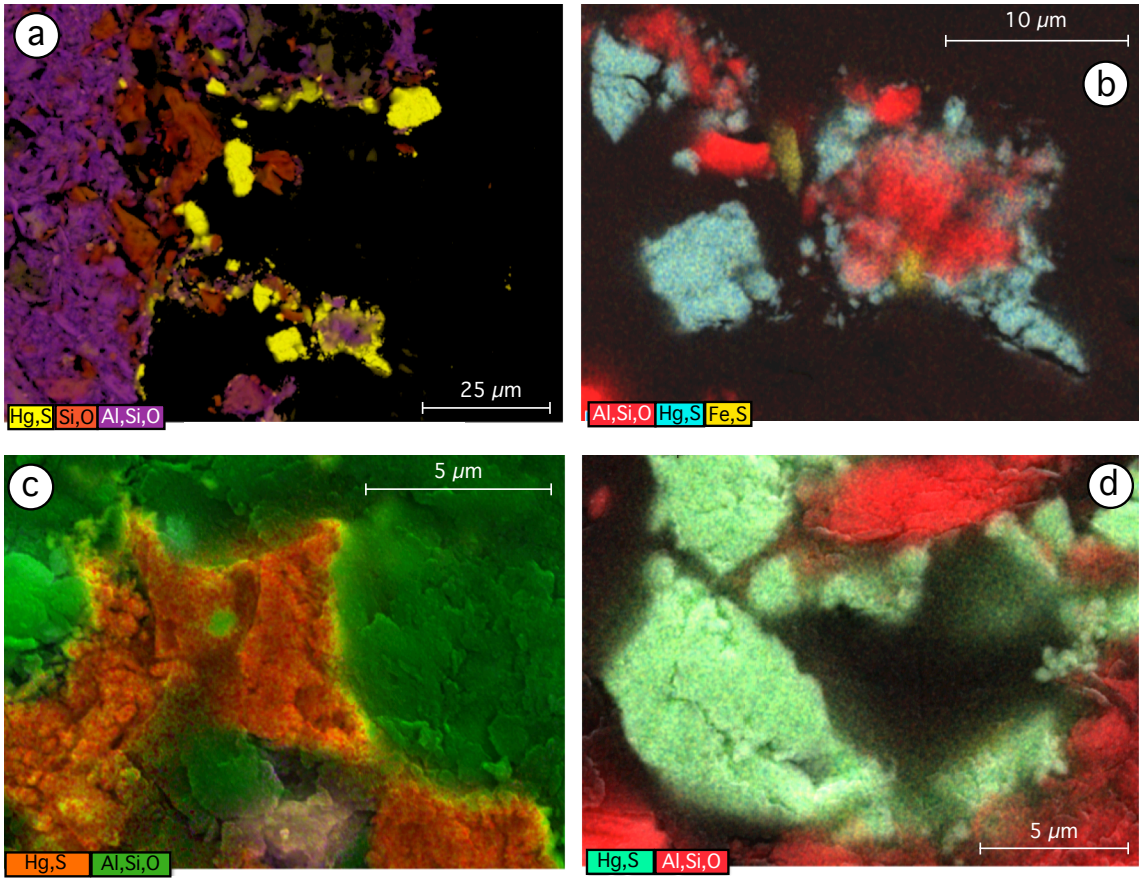

Figure 4.9 A selection of false-colour images derived using backscattered electron micrographs and elemental distribution data from EDXS analyses. Images show the morphology and elemental distribution observed in association with mercury-rich phases in cinnabar-spiked temperate (a,b,d) and sub-tropical (c) soils incubated for 180 days under laboratory conditions.

The cinnabar grains were observed in association with aluminosilicates and fragments of pyrite (Figure 4.9 b + d), which were previously identified in the experimental mineral matrix (section 4.3.1). No evidence of secondary phase rims was found on the cinnabar particles, nor were any phases rich in mercury and chlorine (i.e. previously reported secondary phases) detected. An equivalent examination of cinnabar platelets, which were exposed to the soil under environmental conditions (see 3.2.3), produced the same findings. As such, the mineralogical data do not directly support the formation of secondary phases suggested by the declining percentage mercury liberation observed in the batch incubation experiments (Figure 4.6).

4.3.4 Phytoavailability of liberated mercury

4.3.4.1 Mercury uptake by Oryza sativa

Concentrations of mercury in grains (0.959 ± 0.053 µmol Hg kg^{-1}) obtained from rice plants grown in spiked sub-tropical soil were 7 times higher than those determined for plants grown in control soils (0.135 ± 0.022 µmol Hg kg^{-1}) (Figure 4.10). Grain produced in this study exceeded the Chinese standard for mercury in cereals (0.1 µmol Hg kg^{-1}) (USDA Foreign Agriculture Service, 2010) by a factor of 10 (spiked soils), while plants grown in control soil produced grains that slightly exceeded this limit. There are currently no international (i.e. WHO/FAO) safety limits for cereal grain mercury concentrations.

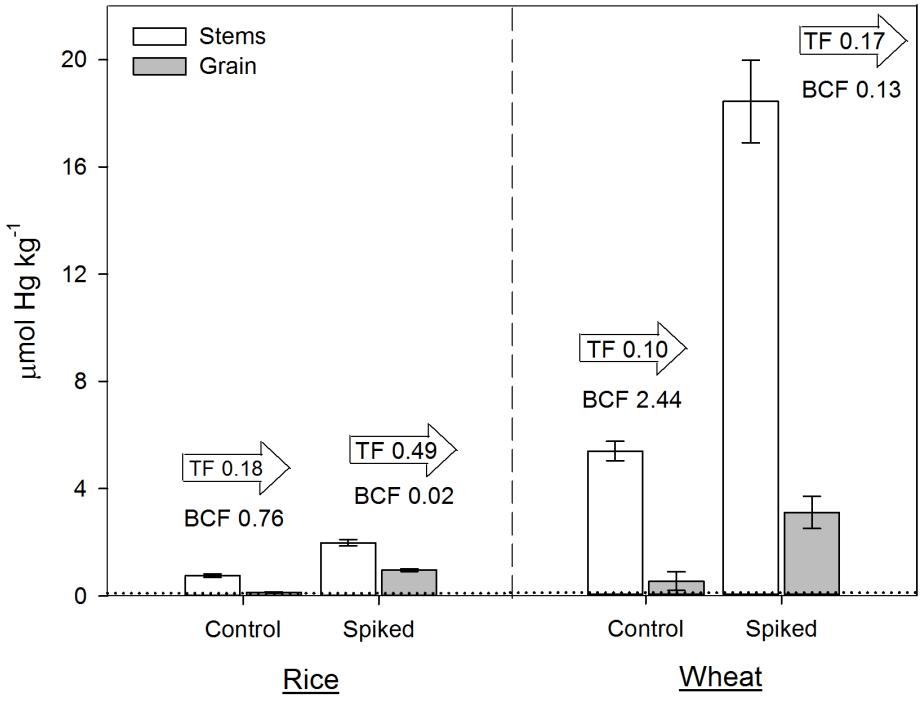

Figure 4.10 Total mercury tissue concentrations, stem bioconcentration factors (BCF) based upon total liberated mercury concentrations and stem-to-grain transfer factors (TF) for spring wheat grown in the temperate experimental soil and rice grown in the flooded sub-tropical experimental soil (control and spiked). Uncertainties based on ± 1 standard deviation.

The mercury tissue concentrations reported in the literature follow the trend: grains < stems < roots (Liu et al., 2007), which can be viewed as indicative of physiological limits on upward mercury translocation. A study on *Zhea mays* showed that inorganic mercury is effectively sequestered in the apoplastic space of the root epidermis, limiting transport to the upper parts of the plant (Debeljak et al., 2013). Evidence from *Oryza sativa* and the mercury hyperaccumulator, *Marrubium vulgare*, also demonstrated that phytochelatin complexes retard the translocation of inorganic mercury from the roots to the upper plant tissues (Krupp et al., 2009). The higher stem-to-grain transfer factors (TF) obtained for both species grown in spiked soils compared with the controls (Figure 4.10), implies that those translocation limits were overcome by increased bioavailable mercury activity liberated from cinnabar.

Direct adsorption of mercury vapour has been reported in stems and foliage of *Triticum aestivum* and *Oryza sativa* (Niu et al., 2011; Meng et al., 2012). It should be noted that plants were not grown in sealed chambers with gaseous mercury monitoring during this study and therefore, the impact of gaseous adsorption cannot be quantified or excluded. However, gaseous mercury absorption can most likely be excluded as a contributor to mercury concentrations in grains because the husks were removed from grains prior to analyses, removing any absorbed mercury. Vapour adsorption by the stems appears unlikely since, having excluded the same effect for gains, stem adsorption would result in *lower* grain:stem ratio (i.e. the TF value) for plants grown in the presence of mercury contamination (i.e. spiked soils).

The TF for *Oryza sativa* grown in spiked soil (TF = 0.49) was considerably higher than the other plant/soil combinations (< 0.2) and the literature provides the most evidence for an explanation involving methylmercury; The proportion of

mercury reported to be present in rice grains as methylmercury ranges widely (1 – 99 %) but is usually substantial (30 – 50 %) (Li et al., 2013; Qiu et al., 2006) because the majority of the plant methylmercury burden is translocated to the grains during the filling stage (Li et al., 2013; Meng et al., 2011), likely assisted by complexation to CH_3Hg-cysteinate (Li et al., 2010). This is significant because the aforementioned phytochelatins are largely ineffective against methylmercury translocation from the roots to stems (Krupp et al., 2009) and because the reducing conditions in which rice grows (section 4.3.2.2) promote the methylation of inorganic mercury (Meng et al., 2011).

4.3.4.2 Mercury uptake by Triticum aestivum

As observed for *Oryza sativa*, the incubated cinnabar contributed markedly to the bioavailable mercury reservoir in the temperate soil (Figure 4.10), yielding grain concentrations for plants grown in spiked soil (3.09 ± 0.60 μmol Hg kg^{-1}) that were around six times higher than those grown in control soil (0.53 ± 0.35 μmol Hg kg^{-1}) and 30 times the Chinese safety standard.

In addition, the wheat tissue concentrations were consistently higher than those of the rice, grown in both control and spiked soils (factors of 3 – 4 for seeds and 7 – 10 for stems). It has been shown that mercury concentrations in the most labile forms (extractable by 0.01 M $CaCl_2$) were significantly higher in the temperate soil (section 4.3.3.2) than the sub-tropical soil, which explains, at least partially, the difference. Uptake data for *Triticum aestivum* grown in soils with such relatively high mercury concentrations are not reported elsewhere in the literature and therefore, the extent to which species (genotypic) differences and metal tolerance affects accumulation and translocation is unknown.

Some investigators have reported that methylmercury represents a much smaller proportion of the total mercury concentration in crops like *Zhea mays* (< 1 %), which are grown in well-drained soils like *Triticum aestivum*, compared with *Oryza sativa* (Qiu et al., 2006; Colombo et al., 2013). This is primarily attributed to the biogeochemical soil conditions under which rice is normally cultivated. As a result, the absorption and relative toxicity of the mercury in wheat tissue will be lower than for rice.

4.3.5 Human health risk assessment

The human health risk associated with the consumption of the wheat and rice flour produced in contaminated soils in this study was evaluated by estimating total mercury ingestion rates for consumers and comparing these with current health protection guideline values. As previously discussed (section 3.3.7), this exercise is intended to provide a human health context for the grain concentrations reported in this chapter, and not to make quantitative predictions of mercury concentrations for crops grown in the field.

The most recent international intake guideline for total mercury (provisional maximum tolerable weekly intake, PMTWI = 20 nmol kg^{-1} body weight $week^{-1}$) were established in 2011 by the Joint FAO/WHO Expert Committee on Food Additives (FAO/WHO, 2010). This is complemented by a separate guideline (WHO/FAO, 2003) for methyl mercury (8 nmol kg^{-1} body weight $week^{-1}$).

Total mercury ingestion rates for consumers of the grains produced in this study were estimated (probable weekly intake), assuming a cereal consumption rate of 3.54 kg $month^{-1}$ (European Food Safety Authority, 2011) and a body weight of 70 kg for the wheat consumers. Estimates for rice consumption were based on Chinese data (60 kg body weight, 550 g day^{-1} rice consumption (Zhang et al., 2010;

Feng et al., 2008) and an assumed 65 % water content in cooked rice (Dibba et al., 1991). Estimates were made for a worst-case scenario, in which the foods constitute the entire cereal product portion of the model consumers' diet, that they are consumed regularly and over a long timescale and that no mercury is lost during food preparation. Consumption of the rice and wheat flour would result in a dietary total mercury intake exceeding the PMTWI by 8 % and 83 %, respectively. This suggests that, with the cinnabar concentration (0.1 % m/m) and conditions selected for this study, consumers of the grains would have a level of mercury in their diets above what is considered protective for human health. Mercury speciation was not determined in the plant tissues, but 50 % methylmercury represents a conservative estimate for rice (section 4.3.4.1) and, on that basis, the model consumer of the rice grown in this study would exceed the PMTWI for methylmercury by 35 %. It is important to note that a safety factor (e.g. 10) is used when formulating toxicological guidelines and so the health effects associated with up to twice the guideline level are still likely to result in minimal harm.

Grazing cattle on contaminated fodder represents another potential human health hazard because, if methylated, the much higher mercury concentrations found in the stems (i.e. animal feed) may result in bioaccumulation in livestock, indirectly introducing mercury to the human diet (Loredo et al., 2003b).

4.4 Conclusions

Cinnabar weathering occurs rapidly (< 7 days) after introduction to oxic soils of contrasting climatic and geological provenance. Weathering, as indicated by the proportion of cinnabar-bound mercury liberated from the mineral matrix, peaks (12.0 – 13.5 %) within 90 days exposure, after which a significant proportion of the released mercury is sequestered in biogeochemically unavailable forms. The

aqueous extraction data suggest the formation of recalcitrant secondary phases, possibly secondary cinnabar, although examination of cinnabar grains exposed to the soil environment (180 days) did not present any phases previously reported as alteration products of cinnabar weathering. Further investigation using complementary analytical approaches, for example thermal desorption atomic absorption spectrometry, is required to further elucidate this effect. The lack of detectable sulfate release (indicative of oxidative dissolution) and apparent equilibration between the cinnabar and the experimental soils suggests that DOM-mercury complex induced dissolution, which is limited by DOM saturation of the mineral surfaces, could be the mechanism of release. This equilibration effect indicates that cinnabar weathering in soils occurs over a limited timeframe so long as the prevailing biogeochemical conditions are maintained. This discontinuous weathering is consistent with previous work showing the redistribution of bioavailable mercury species with more recalcitrant phases over the course of decades of soil residence.

The weathering process contributes to the bioavailable mercury reservoir of the contaminated soils, resulting in the accumulation of potentially hazardous mercury concentrations in the grains of important cereal species.

Chapter 5

The Implications of Arsenopyrite Contamination in Agricultural Soils

5.1 Introduction

Arsenic contamination is of global importance due to its chronic toxicity at low concentrations and environmental ubiquity (Wenzel, 2013). Food and beverage consumption are primary arsenic intake routes for humans (Huang et al., 2006), provoking the establishment of health protection guidelines for drinking water (133 nmol L^{-1}) and overall intake (26.7 nmol kg^{-1} BW day^{-1}) (WHO/FAO, 1989; WHO, 1993). The documented health effects related to chronic inorganic arsenic exposure include dermal (hyperkeratinisation, hyperpigmentation) and circularity (cyanosis, gangrene) issues, as well as peripheral neuropathy, gastrointestinal inflammation, and carcinogenicity (skin, bladder, lung). Less toxicological information is available for organic arsenic species (e.g. arsenobetaine, commonly found in fish), but there is a consensus that these species are less harmful than inorganic species. Both inorganic and organic species are considered highly absorbable via oral intake; intestinal absorption has been reported in the range 80 – 95 % of the oral dose. Evidence from humans chronically exposed to inorganic and organic arsenic species suggest the element is, for the most part, evenly distributed across the body, potentially affecting all bodily systems (ATSDR, 2007 and references therein).

The dominant arsenic species found in soil porewaters are inorganic As(V) acids ($H_2AsO_4^-$, $HAsO_4^{2-}$, and AsO_4^{3-}) under oxic conditions and As(III) arsenous acids ($HAsO_3^{2-}$, $H_2AsO_3^-$ and H_3AsO_3) under reducing conditions (Luong et al., 2007), although minor proportions of organic species (i.e. monomethylarsonic acid, dimethylarsenic acid, arsenobetaine) have also been reported (Xu et al., 2008; Geiszinger et al., 2002) and arsenic may also exist in association with dissolved organic matter (Wenzel, 2013). The solubility of arsenates (AsO_4^{3-}), the most stable form in oxic soils, is thought to be predominantly controlled by forming bidentate

inner-sphere complexes (O'Reilly et al., 2001) with surfaces of amorphous and crystalline iron oxyhydroxides such as ferrihyrite and goethite, as evidenced both indirectly (Jiang et al., 2005) and directly, using X-ray absorption near-edge structure (XANES) analysis (Takahashi et al., 2004). As a consequence of the abundance and adsorption capacity of these phases and other solid-phase interactions, the soluble-exchangeable (most bioavailable) fractions typically account for < 2 % of the total arsenic in soils (Huang et al., 2006). Tight associations of soil arsenic and iron oxyhydroxides have also been used to explain increased arsenic solubility in increasingly reducing soils, resulting from reductive dissolution of the host phases (Bennett & Dudas, 2003; Erbs et al., 2010), particularly ferrihydrite, and from the biotic reduction of As(V) to As(III), which has a lower affinity for those phases (Takahashi et al., 2004). Although pH-dependent adsorption/desorption behaviour has been reported in pure mineral experimental systems, numerous soil surveys indicate that pH plays a minor role in arsenic solubility (i.e. bioavailability, environmental mobility) (Wenzel, 2013 and references therin).

Arsenopyrite is the primary source of arsenic, and has been identified as an important arsenic-hosting phase (0.1 – 30 %) in mining wastes associated with zinc, lead and copper (Antosiewicz et al., 2008; la Campa et al., 2011; Castillo et al., 2013), tin and tungsten (Fordyce et al., 2003; García-Sánchez et al., 2010), gold and silver (Foster et al., 2011; Chon et al., 2005) and mercury (Loredo et al., 2006). Arsenopyrite transport has been reported through wind-blown dust dispersion, both directly (Corriveau et al., 2011) and indirectly from the distribution and geochemical signatures observed in contaminated soils (la Campa et al., 2011; Razo et al., 2004; Rytuba et al., 2007). In addition, arsenopyrite transport has been reported in surface waters (Craw et al., 2003; Rytuba et al., 2007) and floodplains

(Fordyce et al., 2003; Zarcinas et al., 2004), tailings run-off (Lee et al., 2008) and tailings dam failure (Hita et al., 2006; Simón et al., 2001). Declining arsenic production (i.e. demand) since the 1960s (WHO, 2000) is likely to have stimulated arsenopyrite disposal as an uneconomic guest mineral (i.e. from gold exploitation) (Corkhill & Vaughan, 2009; Fordyce et al., 2003).

Arsenopyrite is vulnerable to oxidative dissolution in the surface environment, raising concerns that it may release inorganic arsenic species into soils, groundwater and surface waters. The dissolution rates reported for arsenopyrite range from 2.75×10^{-5} to 2.08×10^{-4} mol m^{-2} s^{-1} within the pH range 5.5 to 6.4 and dissolved oxygen concentrations between 5.52 and 44.6 mmol L^{-1} (Asta et al., 2010; Walker et al., 2006; Yu et al., 2007). The reaction rate appears to be limited by dissolved oxygen concentrations and, while Fe(III) may also act as oxidant, this is not favoured under circum-neutral conditions, where Fe(III) hydrolyses and precipitates. Secondary phase coatings may also protect arsenopyrite surfaces from continuous oxidation. This 'encapsulation effect' was observed in weathered tailings, as arsenopyrite grains occluded within scorodite ($FeAsO_4.2H_2O$) (Salzsauler et al., 2005) or unidentified Fe-As-O phases (Parviainen et al., 2012b).

In recent years, health concerns over arsenic-contaminated groundwater in Asia have received much attention (Pal et al., 2009) and there has also been interest in the contamination of important crops by inorganic arsenic contamination (Williams et al., 2005; Duxbury et al., 2003) and the associated risk posed to populations subsisting in mining-impacted areas (Lee et al., 2008; Liu et al., 2010). However, less is understood about the risk of human exposure to arsenic from the dissemination of arsenic-bearing mineral particles. Recent reviews on the oxidation-dissolution of arsenic-bearing sulfides (Corkhill & Vaughan, 2009;

Lengke et al., 2009) highlight that, with the exception of the Mihaljevič et al. (2010) *in situ* study on arsenopyrite alteration under acid forest soils, arsenopyrite oxidation has not been studied directly in anthropogenically contaminated soils. In addition, to the knowledge of the author, there have been no studies on the weathering behaviour of this mineral in soils under agriculturally relevant conditions, and of the bioavailability of the weathering products to important human food crops.

5.2 Methods

The overall investigative strategy and experiments are summarised in this section, which reference to relevant sub-sections in Chapter 2, where the applied methods are described in detail.

5.2.1 Investigative approach

This study comprised three strands of investigation (Figure 5.1):

(1) A field weathering experiment to investigate secondary mineral phase formation associated with long-term arsenopyrite soil exposure under environmental conditions.

(2) Laboratory batch incubations of arsenopyrite-spiked (0.1 % FeAsS m/m) soils to determine arsenopyrite dissolution behaviour in soils under controlled conditions and the potential for secondary phase formation. Additional incubations, with a higher arsenopyrite concentration (10 % FeAsS m/m), were performed with the aim of identifying secondary alteration phases.

(3) Phytoavailability experiments where *Triticum aestivum* and *Oryza sativa* were grown in samples of the temperate and flooded sub-tropical soils,

respectively, to evaluate the bioavailability of arsenic released from arsenopyrite under oxic and sub-oxic conditions.

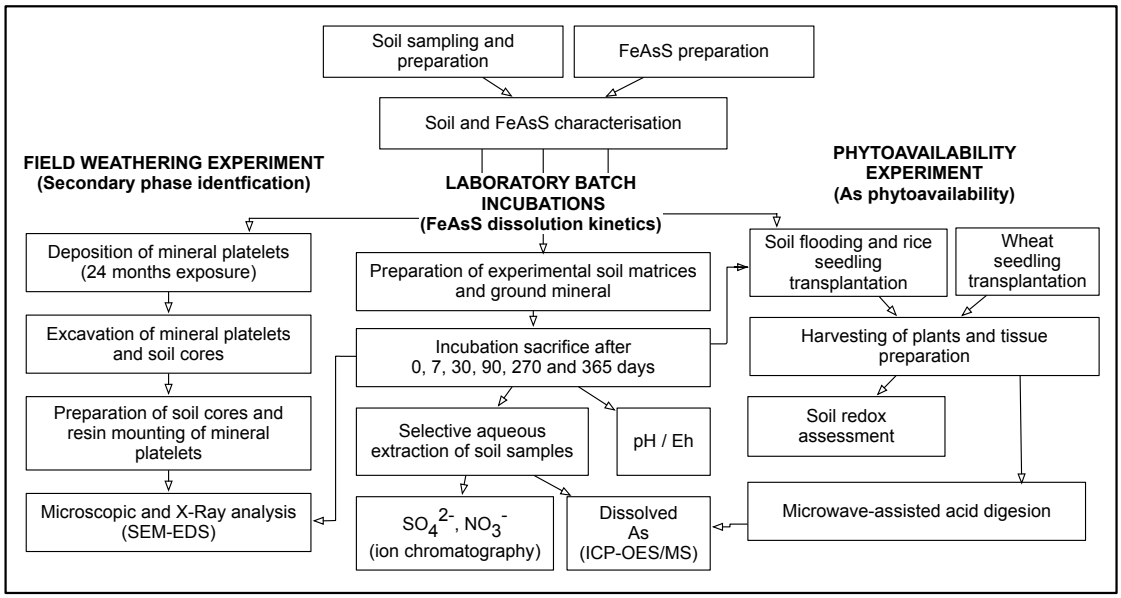

Figure 5.1: Schematic summarising the experimental approaches taken in this study.

5.2.2 Soil and mineral sampling, preparation and characterisation

Soils of temperate and sub-tropical provenance were collected on the basis of their contrasting geological and climatic character (section 2.3.1). The fine soil fraction (< 2 mm) was carefully homogenised to produce what will hereafter be referred to as the temperate and sub-tropical *experimental soils* (section 2.3.2) and these were characterised by determining their physical and chemical features (section 2.3.3).

Small platelets (~ 2 cm^2 × 0.3 cm) and a fine powder (< 63 μm) were prepared from specimen arsenopyrite (FeAsS). The arsenopyrite was characterised by examining its mineralogy and elemental composition as described in section 2.4.

5.2.3 Field weathering experiment

Arsenopyrite platelets were deposited approximately 0.1 m below ground level within a 0.1 m × 0.1 m horizontal grid and then remained *in situ* for 24 months at the sampling location for the temperate experimental soil. The platelets were excavated in cores and prepared as polished epoxy resin sections prior to examination for secondary phase formation using SEM-EDXS (section 2.5).

5.2.4 Laboratory batch incubation experiments

Arsenopyrite-spiked (0.1 % m/m, < 63 μm) and control (not spiked) temperate and sub-tropical experimental soils were incubated under laboratory conditions for durations ranging 0 to 365 days as described in section 2.6. After incubation, the samples were analysed for water-soluble major ions (NO_3^-, SO_4^{2-}) and anion-exchangeable arsenic (0.1 mol L^{-1} potassium phosphate extract) to determine the release trends and geochemical associations of the arsenopyrite constituents as weathering progressed during the experiment (section 2.6.3.1).

In response to an unexpected decline in soil pH observed during the initial 30 days of incubation, an abiotic control incubation was conducted to replicate that incubation period under sterile conditions (section 2.7). That experiment was designed to test a hypothesis: the activity of ammonium and sulfur oxidising bacteria produced an excess of protons that were not lost by percolation (impossible) and so acidified the soils.

Additional highly concentrated arsenopyrite-spiked (10 % m/m) soils were also incubated for 180 days with the aim of detecting secondary phase formation using XRD, although these samples were also examined using SEM-EDXS (section 2.8).

5.2.5 Phytoavailability experiments

Large (4 L) analogues of the laboratory batch incubation samples were incubated for 180 days before *Triticum aestivum* (spring wheat) or *Oryza sativa* (lowland rice) were transplanted into the temperate and sub-tropical experimental soils, respectively (section 2.9). The total arsenic concentration of the stems and grains was determined to evaluate the bioavailability of arsenic released during arsenopyrite weathering and the hazard posed to human health via the crop contamination pathway. In addition, the biogeochemical conditions prevailing in the flooded sub-tropical soils after rice cultivation were determined to examine relationships between soil conditions and the plant uptake and geochemical associations of arsenic liberated during arsenopyrite weathering (section 2.9.4).

5.3 Results and discussion

5.3.1 Soil and arsenopyrite characterisation

A full summary of the chemical and mineralogical character of the experimental soils is given in section 3.3.1. Both soils had similar natural sulfur concentrations (17.0 – 17.1 mmol S kg^{-1}) and the background arsenic concentrations (0.292 – 0.579 mmol As kg^{-1}) of both soils were approximately one order of magnitude below the arsenopyrite spike (which was 4.93 mmol kg^{-1} As).

Elemental analysis (ICP-OES, CHNS), SEM-EDXS and powder XRD (Figure 5.2) showed that the specimen arsenopyrite matrix consisted of $Fe_{1.02}As_{1.00}S_{0.98}$ with inclusions of galena (PbS) and pyrite (FeS_2), and a bulk purity of 85 % m/m based on total iron, arsenic and sulfur concentrations.

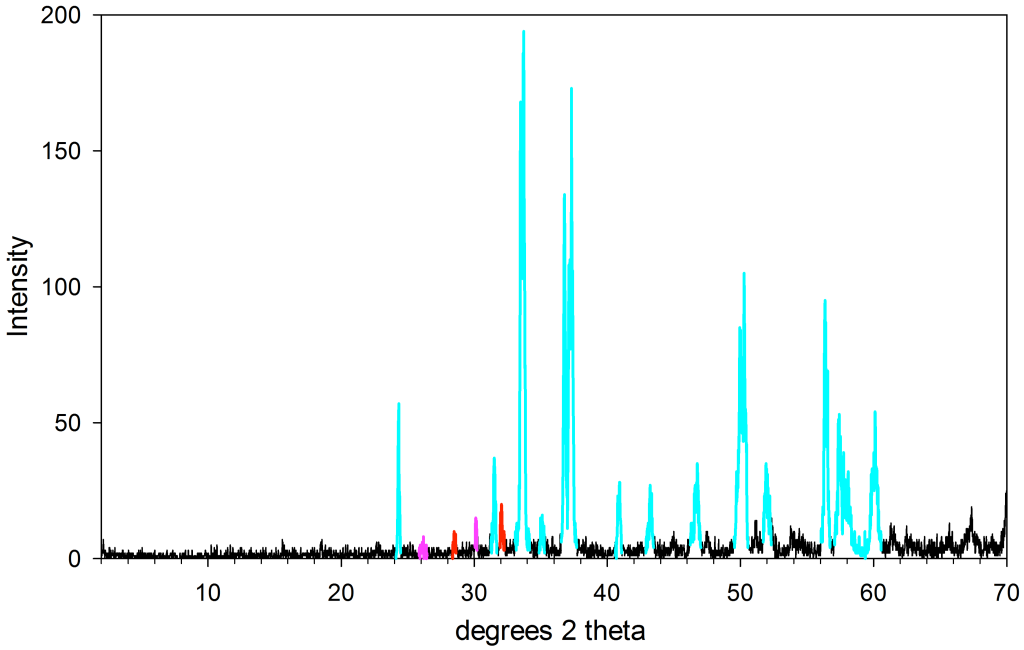

Figure 5.2 XRD spectrum of ground (< 63 µm) arsenopyrite used throughout the study. Peaks are colour-coded by phase: arsenopyrite (light blue), galena (pink) and pyrite (red).

5.3.2 Arsenopyrite alteration

5.3.2.1 Secondary phase formation during arsenopyrite alteration

Secondary Fe-O-As phases were observed (SEM-EDXS) at the soil-mineral interface in samples deposited in temperate soil under field conditions for 24 months (Figure 5.3). These phases, which were present as agglomerates and rims, were broadly categorised as Fe-arsenate (Fe:As < 1.5) and oxyhydroxides co-precipitated with arsenic (Fe:As > 1.5 < 5) or with arsenic adsorbed post-precipitation (Fe:As > 5) (Paktunc & Bruggeman, 2010) (Table 5.1).

Table 5.1 Summary of compositional data (elemental %) for Fe-O-As phases identified at the soil-mineral interface of FeAsS samples deposited in temperate soil under field conditions for 24 months. Fe-ox co-precipitated = phases with arsenic likely associated with iron oxyhydroxides by co-precipitation. Fe-ox adsorbed = phases with arsenic likely associated with iron oxyhydroxides by adsorption (i.e. after iron precipitation). Uncertainties are reported as ± 1 standard deviation.

	O (%)	Fe (%)	As (%)	Fe:As	Fe:O
Fe-arsenate	64 ± 4.6	19 ± 1.3	15 ± 0.8	1.2 ± 0.07	0.28 ± 0.04
Fe-ox co-precipitated	55 ± 5.7	19 ± 6.0	9.5 ± 4.2	2.2 ± 0.63	0.34 ± 0.13
Fe-ox adsorbed	59 ± 0.3	6.3 ± 0.33	0.9 ± 0.2	7.0 ± 1.8	0.11 ± 0.01

The chemical composition of the Fe-arsenate (up to 4.68 mol kg^{-1} As) does not conform to any specific IMA-defined (International Minerals Association) arsenate mineral and therefore, could be composed of several different minerals. The SEM-EDXS technique cannot facilitate the unequivocal identification of the mineral phases, but Fe:O ratios for some of the observed phases suggest the presence of As-hosting ferrihydrite and goethite. SEM-EDXS elemental distribution mapping suggests that iron and arsenic released from the bulk mineral (FeAsS) formed secondary phases devoid of sulfur at the mineral-soil interface, and that any sulfate produced by arsenopyrite oxidation was leached from the interfacial soil.

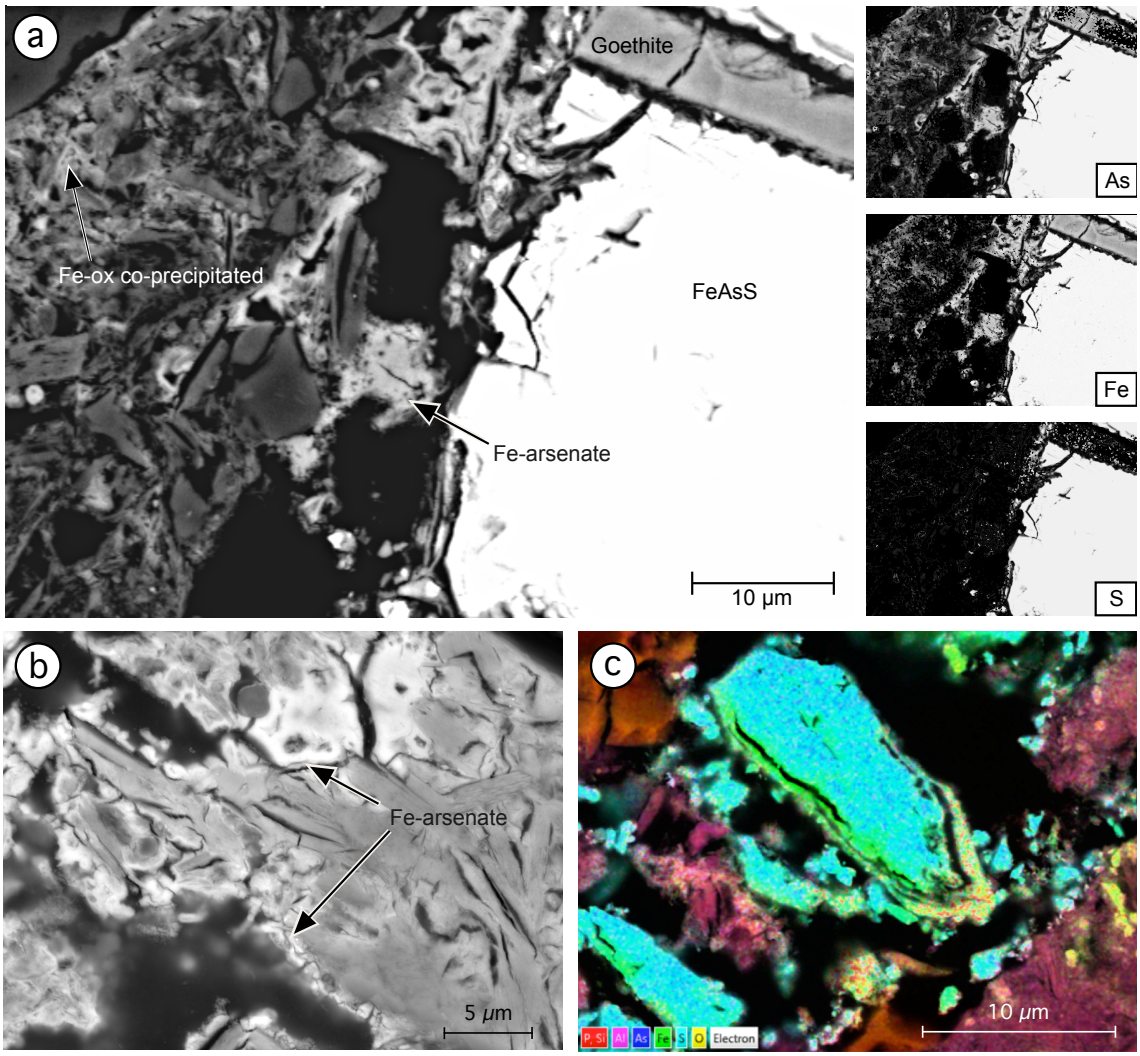

Figure 5.3 (a) Backscattered electron micrograph (left) and EDXS-derived element maps showing arsenic, iron and sulfur distribution and relative abundance (right). The un-altered FeAsS is shown on the right-hand side of the images. Fe-arsenate, iron oxyhydroxide co-precipitated with arsenic (Fe-ox co-precipitated) and As-hosting ferrihydrite (As + ferrihydrite) secondary phases are indicated at the soil/mineral interface (arrows). Element maps (right) have been manipulated to show areas of greatest abundance of arsenic, iron and sulfur, respectively. (b) Secondary arsenate phases precipitated on soil mineral surfaces. (c) Artificially coloured element map image showing fragment of weathered arsenopyrite (light blue) encapsulated in secondary arsenate (green-yellow).

5.3.2.2 Changes in soil pH during oxic soil incubation

The pH was not controlled during the experiment and within the first 30 days of incubation, a reduction in pH was observed for both soil types (Table 5.2). The oxidation of arsenous acid (As (III)), the immediate product of arsenopyrite

oxidation-dissolution, to arsenate (As (V)) (Eqn. 5.2 pg 131) is net proton producing. However, sulfide oxidation cannot explain the pH shift, since pH values from the control incubations closely match those for spiked soils. Concurrent with the pH decrease, soluble nitrate and sulfate concentrations increased by a factor of 6.6 – 7.8 and 1.4 – 2.1, respectively, in both temperate and sub-tropical control soil incubations (0 – 90 days). It is suggested that the activity of ammonium and sulfur oxidizing bacteria is connected with the observed pH decline, through their production of nitrite (subsequently oxidised to nitrate) (Brady & Weil, 2003) and sulfate (sulfuric acid) (Yang et al., 2007). An abiotic control experiment (section 2.7) was performed to test this hypothesis, as discussed in section 3.3.2.

Table 5.2 Soil pH determined in arsenopyrite-spiked (spiked) and un-spiked (control) temperate and sub-tropical soils, after 7, 30, 90, 180, 270 and 365 days of incubation. Uncertainties reported as ± 1 standard deviation (n = 3).

	Temperate soil		Sub-tropical soil	
Days	pH		pH	
	Spiked	Control	Spiked	Control
0	-	6.6 ± 0.1	-	6.8 ± 0.1
7	6.3 ± 0.1	6.4 ± 0.1	6.7 ± 0.1	6.7 ± 0.1
30	5.6 ± 0.1	5.5 ± 0.1	6.4 ± 0.1	6.4 ± 0.1
90	5.5 ± 0.1	5.7 ± 0.1	6.4 ± 0.1	6.5 ± 0.1
180	5.1 ± 0.1	5.2 ± 0.1	6.1 ± 0. 1	6.2 ± 0.1
270	5.4 ± 0.1	5.5 ± 0.1	6.3 ± 0.1	6.3 ± 0.1
365	5.4 ± 0.1	5.4 ± 0.1	6.1 ± 0.1	6.2 ± 0.1

The pH change observed during the incubations is unlikely to have affected the arsenopyrite dissolution rate. Measuring the dependence of the arsenopyrite dissolution rate upon pH is confounded by the precipitation of ferrihydrite and concurrent sorption of arsenic at pH ≥ 5.5, which may produce an apparent rate reduction under circum-neutral conditions (Yu et al., 2007). However, several

authors have reported a minimal hydrogen ion effect on steady-state dissolution rates (based on iron or arsenic) at pH 1 – 6 (Asta et al., 2010; Lengke et al., 2009; Yu et al., 2007). This suggests that the effect of pH change on the dissolution rate in this experiment would be negligible. Furthermore, the most significant pH shift occurred during the first 30 days of incubation, after which the pH was relatively stable.

5.3.2.3 Geochemical conditions under sub-oxic (reducing conditions) in sub-tropical experimental soil

After rice cultivation, during which time (152 days) the sub-tropical soils were constantly flooded, those soils had attained neutral pH (6.98 ± 0.06) and were approaching reducing conditions (Eh = 7 ± 2 mV) as would be expected for flooded paddy soils (Ponnamperuma, 1972). Biotic nitrate and iron-reducing conditions were indicated by the depletion of soluble nitrate (> 99 %) compared with the soils incubated under oxic conditions (180 – 365 days) and the majority of the acid-extractable iron obtained from the flooded soils (86 ± 3 %) was found as Fe(II). In addition, sulfate-reducing conditions were evidenced by the depletion of the soluble sulfate (≥ 96 %) and the detection of AVS (200 ± 16 μmol S^{2-} kg^{-1}).

5.3.2.4 Rate and extent of arsenopyrite alteration

Exchangeable arsenic and soluble sulfate concentrations broadly followed the same trend over the incubation period in both the temperate (Figure 5.4 a) and sub-tropical (Figure 5.4 b) soils.

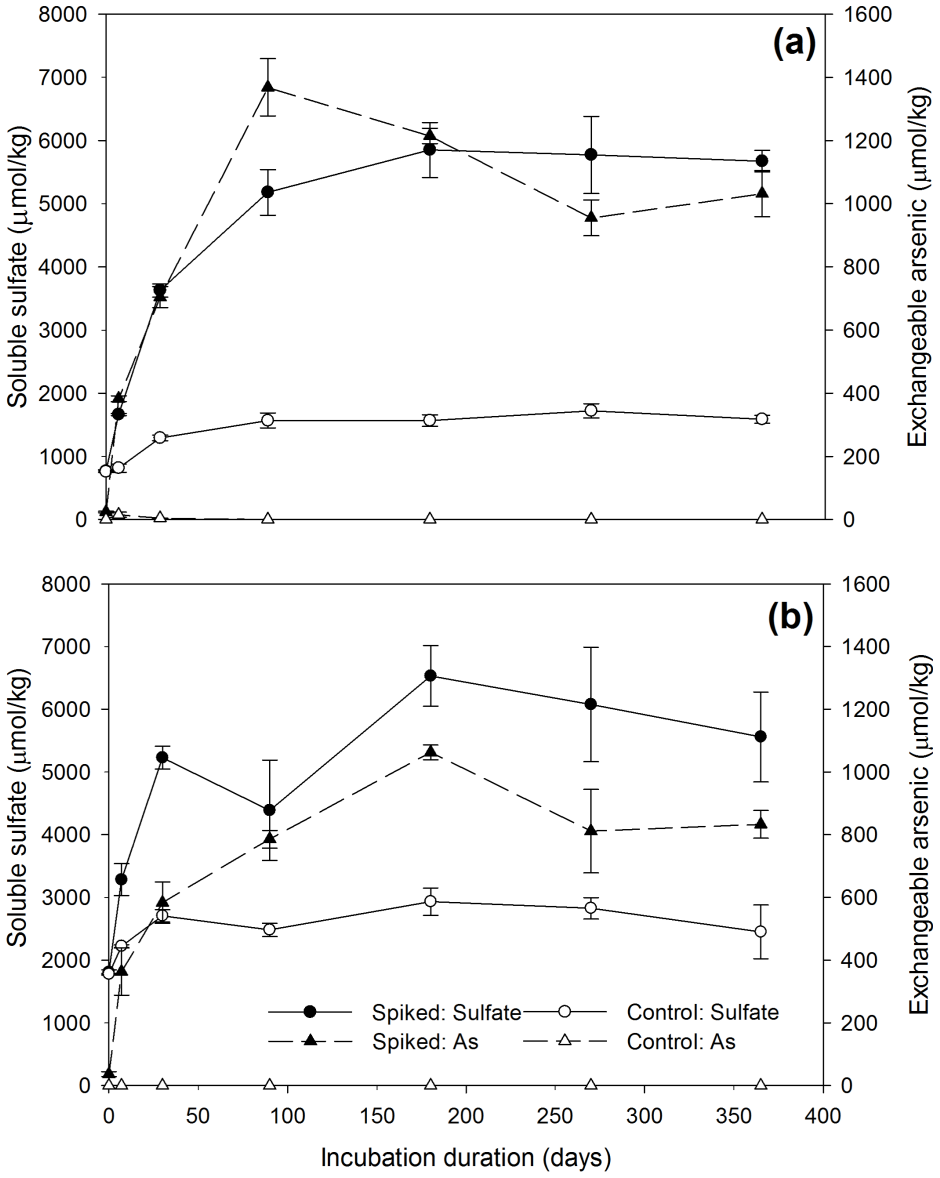

Figure 5.4 Time series showing exchangeable arsenic and soluble sulfate concentrations from (a) temperate and (b) sub-tropical soil after 0, 7, 30, 90, 180, 270 and 365 days incubation. Data are shown for both arsenopyrite-spiked soils and the controls. Arsenic concentrations were below the detection limit (23 µmol kg^{-1} As) in the un-spiked samples. Uncertainties reported as ± 1 standard deviation (n = 3). Data markers are connected for the sake of clarity.

Arsenic and sulfate concentrations obtained from spiked samples diverged from those of control samples after 7 days of incubation, indicating that the extracted arsenic and sulfur (sulfate) originated from the arsenopyrite in the spiked soil. The data are consistent with the extensive oxidative dissolution of arsenopyrite (Eqn. 5.1), yielding sulfate, arsenous acid (Eqn. 5.2), which oxidises to arsenate (Eqn.

5.3), and Fe^{2+}, which subsequently undergoes hydrolysis to yield iron oxyhydroxide (Eqn. 5.4) under surface soil conditions (Walker et al., 2006). Based on pKA values, Eqn. 5.2 (pKa = 6.77) is favoured over Eqn. 5.3 (pKa = 2.25), assuming the soil at the mineral interface had a similar pH to the bulk material.

$$4FeAsS + 11O_2 + 6H_2O \rightarrow 4Fe^{2+} + 4H_3AsO_3 + 4SO_4^{2-} \quad \textbf{(Eqn. 5.1)}$$

$$2H_3AsO_3 + O_2 \rightarrow 2HAsO_4^{2-} + 4H^+ \quad \textbf{(Eqn. 5.2)}$$

$$2H_3AsO_3 + O_2 \rightarrow 2H_2AsO_4^{-} + 2H^+ \quad \textbf{(Eqn. 5.3)}$$

$$4Fe^{2+} + O_2 + 10H_2O \rightarrow 4Fe(OH)_3 + 8H^+ \quad \textbf{(Eqn. 5.4)}$$

The percentage of extractable arsenic and sulfur originating from the arsenopyrite spike were calculated by subtracting the exchangeable arsenic or soluble sulfate concentrations in controls from those in spiked soils, respectively (Table 5.3). The results show that up to 28 % of the total arsenopyrite-bound arsenic was mobilised and present in a phosphate-exchangeable form. Sulfur release values were 40 – 70 % higher than those obtained for arsenic. Furthermore, the percentage of exchangeable arsenic decreases towards the end of the experiment, indicating processes that attenuate arsenic, but not sulfur, occurred.

Table 5.3 Percentage of total arsenic (exchangeable arsenic) and sulfur (soluble sulfate) added to the soil as arsenopyrite, extracted after 0, 7, 30, 90, 180 and 270 days incubation. Uncertainties are ± 1 standard deviation (n = 3). The sulfur values were derived by subtracting the respective control soil concentrations from those for spiked soils (combined uncertainty given for those data). Exchangeable arsenic concentrations in the controls were below the detection limit.

Days	Temperate soil		Sub-tropical soil	
	Arsenic (%)	Sulfur (%)	Arsenic (%)	Sulfur (%)
0	0.48 ± 0.05	0.17 ± 0.40	0.73 ± 0.16	0.45 ± 0.67
7	7.8 ± 0.2	13 ± 1	7.4 ± 1.5	16 ± 4
30	14 ± 1	36 ± 2	12 ± 1	39 ± 3
90	28 ± 2	56 ± 6	16 ± 1	30 ± 13
180	25 ± 1	66 ± 7	22 ± 1	56 ± 8
270	19 ± 1	63 ± 10	16 ± 3	50 ± 14
365	21 ± 2	63 ± 3	17 ± 1	48 ± 13

Molar concentrations of exchangeable arsenic and water extractable sulfur may be utilised to estimate the rate and extent of arsenopyrite alteration during the incubation experiment. However, arsenic that has been incorporated into, as opposed to adsorbed on, iron phases is recalcitrant to extraction by ligand exchange processes, such as the phosphate extraction applied in this study (Alam et al., 2001). Even at lower pH values than those used in this study (2.8 – 5.3), phosphate extraction does not dissolve either poorly-ordered or crystalline iron oxyhydroxides (Jackson & Miller, 2000). Therefore, exchangeable arsenic concentrations are likely to underestimate the full extent of arsenopyrite alteration. The apparent depletion of sulfur from the interfacial soil (Figure 5.3) and minimal sorption of sulfate (i.e. to aluminosilicates) at pH ≥ 6 (Scherer, 2009) attest to the usefulness of excess sulfate concentrations to estimate the overall degree of arsenopyrite alteration in this system. The inclusion of sulfate-S in organic substances (Scherer, 2009) has been accounted for by the control incubations, assuming these were analogous to spiked samples in all respects, other than their arsenopyrite content.

Sulfate release indicates that arsenopyrite alteration proceeded most rapidly for the first 30 days of incubation in both soil types and continued for up to 90 days in the temperate soil and 180 days in the sub-tropical soil, after which excess sulfate concentrations plateau or slightly decline (Figure 5.4 a and Figure 5.4 b). A maximum alteration of between 56 % (sub-tropical soil) and 66 % (temperate soil) occurred during the equivalent of a growing season.

Sulfur release rates declined pseudo-exponentially with increasing incubation duration (temperate soil: 120 ± 9.1 to 21.2 ± 2.8 μmol kg^{-1} day^{-1} S; sub-tropical soil: 147 ± 2.9 to 18.8 ± 2.9 μmol kg^{-1} day^{-1} S), indicating a slowing of arsenopyrite alteration over time. Such rapidly declining (order of 10 – 1000s of h) arsenopyrite dissolution rates have previously been attributed to the reduction in available surface area and the formation of passivation layers (Asta et al., 2010; Walker et al., 2006). Following the logic of passivation layer formation and the micro-analytical data (Figure 5.3) obtained, the sulfur release data can be described by the steady formation of relatively insoluble secondary Fe-bearing phases that eventually completely encapsulated the arsenopyrite particle remnants.

Data from the abiotic incubation of arsenopyrite-spiked temperate soil (section 2.7) offer a suggestion that the oxidation discussed in this study was biotically enhanced (Corkhill et al., 2008). Excess soluble sulfate data indicate that 9.3 ± 1.9 % of the arsenopyrite was weathered after 30 days abiotic incubation, around four times lower than the level found under biotic incubation conditions (36 ± 2 %). It should be noted that this result is preliminary and that, although the evidence for a pH effect on arsenopyrite dissolution is scant, the biotic incubations had a considerably lower pH (5.6 ± 0.1) than the abiotic equivalents (pH 6.8 ± 0.1).

Other factors may also be important; therefore further investigation would be necessary to elucidate the proposed effect.

5.3.2.5 Ageing and stability of secondary phases

Unlike the sulfate concentrations, which plateaued, the exchangeable arsenic concentrations decreased after their maxima by up to 30 % (Figure 5.4), indicating the sequestration of previously labile arsenic due to mineralogical change. The adsorption of arsenate to variable-charge oxyhydroxide/clay exchange sites, which usually decreases above pH 7 (Cheng et al., 2009), cannot explain this apparent sequestration, because the experimental soils remained below pH 7. Several authors have reported soil ageing effects, whereby the geochemical partitioning of arsenic species shifts during soil residence time and the arsenic becomes increasingly recalcitrant to aqueous extraction (Quazi et al., 2011). One explanation for this is the incorporation of surface adsorbed arsenate into oxide structures, e.g. during the dissolution of ferrihydrite and recrystallization as more crystalline phases, such as goethite (Pedersen et al., 2006; Schwertmann & Murad, 1983), or via the physical entrapment of adsorbed arsenate by oxide agglomeration (Arai & Sparks, 2002). This is consistent with the secondary phases observed at the soil-mineral interface in samples deposited under field conditions for 24 months (Figure 5.3), implying that the long-term evolution of the system being investigated is dominated by iron mineralogy.

Fe oxyhydroxides are generally stable under pH (6 – 8) and oxic conditions prevailing in temperate agricultural systems (Al-Abed et al., 2007). Fe-arsenates commonly found in arsenic contaminated systems, such as mine waste (e.g. scorodite), typically exhibit minimum solubility at low pH (< 4) (Drahota & Filippi, 2009; Langmuir et al., 2006), indicating that the (mineralogically unidentified) Fe-

arsenate phases observed in this study (Figure 5.3) may be of a transient nature. The prevailing pH of the experimental soils may promote the transformation of those Fe-arsenates to As-hosting ferrihydrite (Langmuir et al., 2006).

5.3.3 Phytoavailability of arsenopyrite alteration products and risk to human health

5.3.3.1 Uptake of arsenic by wheat grown in temperate soil

The grain of spring wheat grown in the arsenopyrite-spiked soils contained an arsenic concentration over one order of magnitude higher (21.2 µmol As kg^{-1}) than that of plants grown in the control soils (1.88 µmol As kg^{-1}, Figure 5.5), demonstrating that the alteration products of arsenopyrite are phytoavailable. Published edible tissue concentrations of wheat range from 0.187 – 1.15 µmol As kg^{-1} (Huang et al., 2008; Wojciechowska-Mazurek et al., 2006) in uncontaminated soils and 11.2 – 25.2 µmol As kg^{-1} in heavily contaminated soils (1.33 mmol As kg^{-1} in soil) (Zhang et al., 2009). This places the tissue concentrations obtained in this study (with 4.93 mmol As kg^{-1} in soil) with those of plants grown in heavily contaminated soils. There are currently no active international (FAO & WHO) safety limits for arsenic concentrations in foods, but China has adopted a standard (2.7 µmol As kg^{-1}) for total arsenic in cereals (inorganic arsenic in paddy rice) (USDA Foreign Agriculture Service, 2010), which was exceeded by a factor of almost 8 in the wheat grains grown in arsenopyrite-spiked soils during this study. An international (WHO/FAO) limit of 2.7 µmol kg^{-1} inorganic arsenic in polished rice has also been proposed (FAO/WHO, 2013).

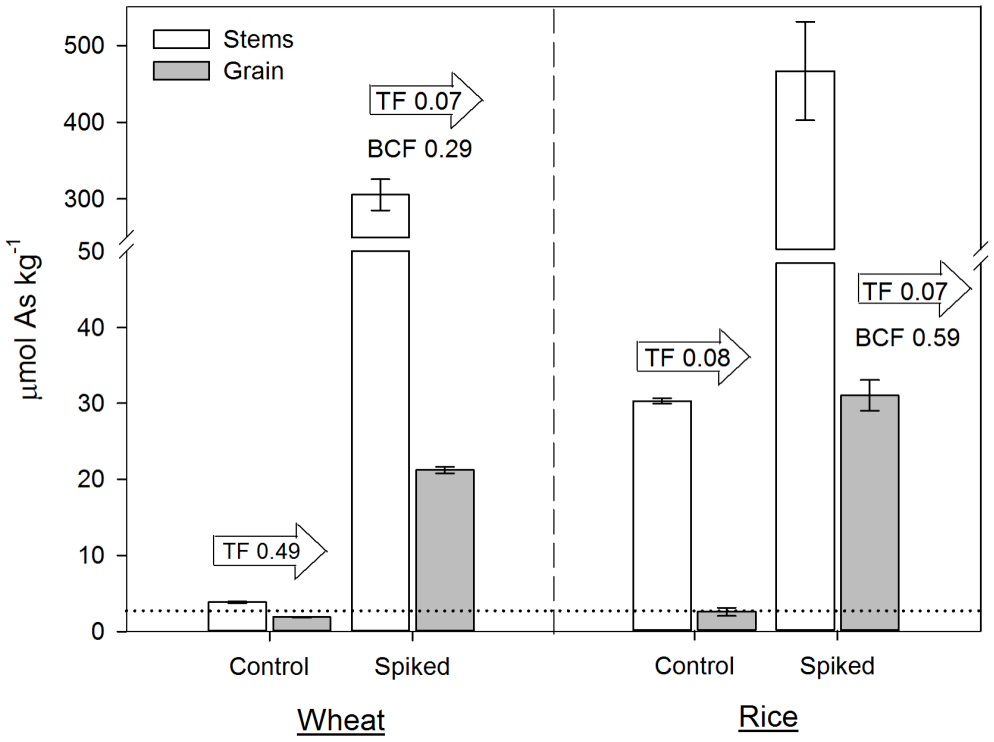

Figure 5.5 Total arsenic tissue concentrations, stem bioconcentration factors (BCF) based upon exchangeable arsenic concentrations and stem-to-grain transfer factors (TF) for spring wheat grown in the temperate experimental soil and rice grown in the flooded sub-tropical experimental soil (control and spiked). BCF values are not reported for plants from control soils as exchangeable arsenic concentrations were below the detection limit (< 23 µmol kg^{-1}). Uncertainties are reported as ± 1 standard deviation. Horizontal dotted line indicates relevant Chinese food safety standard concentration.

The soil > stem bioconcentration factors (BCF) show that arsenic uptake into the stem tissue depends on its speciation in the soil. The BCF, based on total arsenic, was approximately one order of magnitude higher for the spiked soil (BCF_{total} = 6.2 × 10^{-2}) compared with the control soil (BCF_{total} = 6.7 × 10^{-3}), showing that the sulfide-derived arsenic was more bioavailable than the background soil content. Although the BCF, based upon exchangeable arsenic concentrations (0.29), confirmed that the sulfide-derived arsenic was readily taken up into the stems of spring wheat, the stem > grain transfer factor (TF) was much more limited in the plants grown in the spiked soil (TF = 0.07) than in the control (TF = 0.49). This suggests that the plants responded to arsenic stress by limiting its translocation.

5.3.3.2 Uptake of arsenic by rice grown in flooded sub-tropical soil

Rice plants grown in arsenopyrite-spiked soils accumulated grain (32.0 ± 2.1 μmol As kg^{-1}) and stem (470 ± 61 μmol As kg^{-1}) arsenic concentrations 12 – 15 times higher than the grains (2.57 ± 0.54 μmol As kg^{-1}) and stems (31.2 ± 0.3 μmol As kg^{-1}) of plants grown in the control soil. These tissue concentrations indicate that arsenopyrite alteration products are bioavailable to rice in the sub-tropical soil and also, in comparison with the wheat (section 5.3.3.1), rice grain and stem arsenic concentrations were ~ 50 % higher and the BCF value (based on exchangeable As) was ~ 100 % higher (Figure 5.5).

The comparatively higher stem and grain concentration in the rice are in agreement with the literature (Yu-Hong et al., 2010; Williams et al., 2007; Norton et al., 2013). Rice has been shown to accumulate higher arsenic concentrations than other cereals (wheat and barley) both due to physiological differences between plant species and the waterlogged (anoxic-reducing) conditions under which rice is often grown. Reducing conditions (Eh < 100) result in the reduction of arsenate, which dominates in oxic soils, to arsenite (Li et al., 2009). Under reducing conditions, the greater solubility of arsenite, which exists as uncharged undissociated arsenous acid (H_3AsO_3), is attributed to less efficient adsorption by iron oxyhydroxide minerals and the reductive dissolution of those phases also releases arsenate into soil solution (Xu et al., 2008), followed by reduction to arsenite (Abedin et al., 2002). The efficiency with which rice takes up arsenite is attributed to the high expression of silicon transporter proteins (Lsi1 and Lsi2) that also mediate arsenite transport (Yu-Hong et al., 2010). Also, unlike arsenate uptake, arsenite uptake is uninhibited by the competitive effects of phosphate in soil solution (Abedin et al., 2002). The greater arsenic uptake potential of the rice is also evidenced by the rice stem concentration (31.2 ± 0.3 μmol As kg^{-1}), which

was eight times higher than that of the wheat (3.83 ± 0.13 μmol As kg^{-1}) grown in soils with equal total arsenic content.

The exchangeable, and therefore potentially bioavailable, arsenic concentration in the sub-tropical soil after rice cultivation (332 days, 791 ± 21 μmol As kg^{-1}) was at least 20 % lower than in the temperate soil after wheat cultivation (365 days, 1032 ± 73 μmol As kg^{-1}). The apparent conflict between these values and the greater arsenic uptake determined in the rice can be arrested by considering that phosphate buffer extracts both arsenate and arsenite (Georgiadis et al., 2006); this corroborates the findings of studies that suggest arsenite, the dominant arsenic species found in paddy soil conditions (Takahashi et al., 2004; Ma et al., 2008), represents a greater proportion of the exchangeable arsenic in the flooded sub-tropical soil extracts.

Unlike the wheat, the rice TF values were constant (0.08 ± 0.02 – 0.07 ± 0.01) for plants grown in both spiked and control soil. Williams *et al.* (2007) found that TF decreased exponentially with increasing stem concentration in several rice varieties, in the range 10 μmol As kg^{-1} to 2.7 mmol As kg^{-1}, and that TF values were consistently < 0.1 when stem concentrations exceeded 60 μmol As kg^{-1} (i.e. this study), reflecting tight physiological control on stem > grain arsenic translocation.

The exchangeable arsenic concentrations determined in the sub-tropical soil under oxic (365 days, 833 ± 44 μmol As kg^{-1}) and reducing (332 days, 791 ± 21 μmol As kg^{-1}) conditions did not significantly differ. Higher exchangeable concentrations were anticipated in the flooded soil because the presence of extractable Fe(II) (section 5.3.2.3) is indicative of the reductive dissolution of iron oxyhydroxide phases, a process that releases co-precipitated arsenic (such as the phases discussed in section 5.3.2.1) in flooded paddy soils (Takahashi et al., 2004). The proportion of the exchangeable arsenic taken up by the plants was negligible

(< 0.5 %) so the remaining concentrations are not an artefact of uptake. Importantly, exchangeable arsenic peaked at 180 days in the incubation experiment (the same time as the soils were flooded) and so the effect of reduced dissolved oxygen in the soils can be discounted (i.e. the oxidative dissolution had already ceased). Some potential explanations are the sequestration of arsenic during formation of secondary arsenic-bearing sulfide phases, owing to the sulfate-reducing conditions prevailing in the flooded soils (section 5.3.2.3), or during iron plaque formation (arsenate) in rice roots resulting from rhizosphere oxidation (Xu et al., 2008).

5.3.3.3 Human health risk assessment

Estimated arsenic ingestion rates for each crop were compared with health protection guidelines to place the tissue concentrations obtained during this study in a human health risk context (see section 3.3.7). Ingestion rates were estimated by assuming a typical cereal consumption rate of 118 g day^{-1} (European Food Safety Authority, 2011) and body weight (70 kg). Estimates were made for a worst-case scenario, in which the flours constitute the entire cereal product portion of the model consumers' diet, that they are consumed over a long timescale and that no arsenic is lost during food preparation (Duxbury et al., 2003).

The most recent international tolerable weekly intake value was 200 nmol kg^{-1} body weight $week^{-1}$ (WHO/FAO, 1989), although this value was withdrawn in 2010 and the expert committee could not reach agreement on a new value (WHO/FAO, 2010). Consumption of the wheat flour would result in a dietary arsenic intake (250 nmol kg^{-1} body weight $week^{-1}$), that is 25 % higher than the weekly intake guideline. The same assumptions, applied to the rice grains,

produced an estimated consumption rate of 378 nmol kg^{-1} body weight $week^{-1}$, which is 89 % higher than the guideline. These values suggest that, with the experimental arsenopyrite soil concentration (0.1 % m/m), contaminated staple crops could contribute a significant and hazardous amount of arsenic to the diets of communities farming on impacted soils. This contribution would be more significant in regions that are also affected by arsenic-contaminated water supplies.

The data from this study (section 5.3.3.2) suggest that a shift from lowland rice cultivation under near-constant standing water towards more intense, aerobic (Africare et al., 2010; Zhao et al., 2010b) rice production would have a strong influence on the hazard posed by arsenopyrite contamination. Our current understanding of arsenic redox chemistry and the uptake data from this study indicate that inorganic arsenates, which are less soluble and less bioavailable to rice than arsenite, would dominate in oxic soils. As such, oxic rice cultivation would be conducive to reduced arsenic uptake by rice. Conversely, oxic soils would provide the molecular oxygen that results in arsenopyrite oxidation and the subsequent release of arsenic into porewaters. Further investigation is required to better predict the influence of these combined, opposing factors.

It is well established that inorganic arsenic, particularly As(III) species, are considerably more toxic to humans than organic arsenic species (e.g. dimethylarsinic acid, monomethylarsonic acid, arsenobetaine) (Table 5.4), which warrants some consideration of the speciation of arsenic in plant grains (ATSDR, 2007).

Table 5.4 Summary of toxicological data (rat) for various environmentally important arsenic species.

Arsenic species	LD_{50} dose	Reference
As^{+3}	20 µmol kg^{-1}	(Vela & Caruso, 1993)
As^{+5}	67 µmol kg^{-1}	
Monomethylarsonic acid	667 µmol kg^{-1}	
Dimethylarsenic acid	8 mmol kg^{-1}	
Arsenobetaine	> 133 mmol kg^{-1} (not LD_{50})	(Shiomi, 1994)

Recent research has demonstrated that plants are incapable of methylating arsenic themselves (Lomax et al., 2011) but that they do take up dimethylarsinic acid and monomethylarsonic acid from soil solution after biotic methylation by soil biota. Although there have been reports of significant proportions of dimethylarsinic acid in rice grains of certain cultivars (Xu et al., 2008; Williams et al., 2005), inorganic As(III) and As(V) are generally reported as the dominant species (64 – 100 %) (Yu-Hong et al., 2010; Williams et al., 2005; Norton et al., 2013). The limited data on arsenic speciation in wheat tissues (Yu-Hong et al., 2010; D'Amato et al., 2010; Zhao et al., 2010a) also suggests a dominance of inorganic arsenic (95 – 100 %). As such, the uptake of less toxic organic arsenic species most likely has only a minor impact of the toxicity of arsenic in these food crops.

5.4 Conclusions

Arsenopyrite oxidation-dissolution was extensive and rapid (56 ± 8 to 66 ± 7 % after 180 days) in both the temperate and sub-tropical soils, and the exchangeable arsenic in the alteration products was also notably phytoavailable to spring wheat and lowland rice. This demonstrates that the contamination of agricultural soils with arsenopyrite particles presents a serious hazard in soils formed under a

range of geological and climatic settings. The key processes that controlled the availability of arsenic for plant uptake (i.e. risk) under the experimental conditions were: (1) Passivation layer formation on the weathering arsenopyrite surfaces effectively halted oxidation-dissolution after 180 days exposure to the soil environment; (2) Secondary phase formation (including the passivating layers) efficiently sequestered arsenic from soil solution upon release from the arsenopyrite, reducing its mobility and therefore phytoavailability. Secondary phase 'ageing' appeared to sequester the arsenic into increasingly recalcitrant forms over time; (3) Spring wheat and lowland rice both appeared to actively limit the translocation of arsenic to the edible tissues (grains).

Under a situation with constant arsenopyrite particle deposition, the labile arsenic reservoir would be continually refreshed. However, upon cessation of the deposition, the associated risk would decline over time, as the oxidation-dissolution stops and the arsenic is taken up by plants (i.e. removed from the soil) and/or incorporated into more recalcitrant phases.

The secondary Fe-arsenates and As-hosting Fe oxyhydroxides, which control the mobility of arsenic after arsenopyrite oxidation-dissolution, are generally regarded as pH and redox sensitive (i.e. unstable under reducing conditions). Most cultivated plant species require oxic soils at pH 6 – 7.5, therefore properly managed soils should also maintain the conditions under which these phases have maximum stability. While flooded agricultural regimes (i.e. paddy) with reducing soil conditions would limit the oxidative processes prerequisite for arsenopyrite dissolution, these conditions may also promote the abundance of exceptionally bioavailable (to rice) arsenic species (i.e. arsenite). As such, periodically dry and flooded regimes would provide both the conditions for arsenopyrite oxidative dissolution and, subsequently, those encouraging plant

uptake of the liberated arsenic. In addition, the re-working of productive soils could also enhance arsenopyrite oxidation by mechanically abrading passivation layers from previously oxidised arsenopyrite grains.

Chapter 6
Conclusions and future work

6.1 Conclusions

The exploitation of sulfide ores for valuable metals and metalloids has, since ancient times, produced vast quantities of fine-grained wastes, which present a major environmental source of PTEs. There are concerns that these waste particles can behave as vectors, facilitating the transport of PTEs into the soils and surface waters in mining regions, and contaminating soils used to support human populations. This kind of contamination is most likely to affect poor communities practicing subsistence agriculture who, due to inadequate or poorly enforced legislation, are not sufficiently protected from the environmental impacts of mining.

The overall project aim was to investigate the potential impacts of mining on agricultural soils through the contamination of soils with mineral waste particles. The primary objective was to investigate the chemical weathering of several sulfide ores in soils and the geochemical associations and bioavailability of toxic metals, liberated during weathering, to crops under conditions relevant to agriculture. This work has shown that sulfide ore grains (< 63 μm) introduced to oxic agricultural soils undergo chemical weathering (oxidative, acid-promoted and DOM-promoted) and, consequently, release nonessential PTEs into the soil matrix in forms that are taken up and accumulated in the edible grains of important food crops (rice and wheat). In addition, the primary constraints on the rate of weathering and the bioavailability of liberated metals and metalloids have been identified. As such, the main aim of this study has been achieved.

6.1.1 Ore weathering, PTE liberation and crop contamination

All three of the ores studied during this project (sphalerite, cinnabar and arsenopyrite) exhibited metastability when exposed to oxic agricultural soils of

both temperate and sub-tropical provenance, and released nonessential PTEs (cadmium, mercury, arsenic) in forms that were bioavailable to important food crops, namely *Triticum aestivum* and *Oryza sativa*. Importantly, the ores underwent chemical weathering at rates that are relevant to agricultural cycles (i.e. crop production), which demonstrates that the weathering of the mineral grains in soils, subsequent metal release and plant uptake can occur concurrently. For instance, sphalerite weathered at 0.6 to 1.2 % a^{-1} (Cd basis) in the experimental soils, releasing 0.5 to 1 μmol Cd g^{-1} ZnS a^{-1} into the soil matrix. The bioavailability of the cadmium resulted in wheat grains exceeding food safety limits by a factor of 8 and rice grain cadmium concentrations that were 3 – 4 times higher than plants grown in uncontaminated soil. Cinnabar weathering reached a maximum of 12.0 – 13.5 % (Hg basis) after 90 days exposure in oxic soils, resulting in rice and wheat grain mercury concentrations that exceeded food safety guidelines by a factor of 10 and 30, respectively. Arsenopyrite weathering was rapid and extensive, reaching 56 to 66 % (S basis) after 180 days soil exposure. Consequently, the wheat and rice plants grown in the arsenopyrite-contaminated soils accumulated grain arsenic concentrations that exceeded food safety limits by a factor of 8 – 12. These marked differences in weathering rates of each ore demonstrate the need for mineral-specific investigations when considering the influence of mining-derived particulate contaminants on the supply and biogeochemical cycling of potentially toxic elements in environmental systems.

6.1.2 Factors affecting PTE liberation and bioavailability

While the weathering rate of each ore depends on the stability of the crystal lattice and weathering mechanisms under the exposure conditions (Figure 6.1 pathway 1), the accumulation of PTEs in plant tissues is also controlled by the solid-phase

associations of liberated PTEs, which reduce the bioavailable reservoir, and the metal homeostatic responses of crop plants.

Solid phase associations (i.e. surface complexes) between liberated PTEs and soil constituents, such as clays, metal oxyhydroxides and organic matter strongly regulated the solubility of those PTEs in the experimental soils (Figure 6.1 pathway 2). Consequently, the proportion of PTEs, liberated during sphalerite and cinnabar weathering, which were found in the 'soluble-exchangeable' fraction (i.e. using 0.01 M $CaCl_2$ extraction), was consistently low (< 5 %).

In addition, secondary phase formation was identified as a mechanism limiting the release and/or bioavailability of released PTEs with respect to all three of the ores under study (Figure 6.1 pathway 3). Arsenopyrite weathering was, after 180 days exposure in oxic soils, halted by secondary iron-arsenate formation that passivated the unaltered grains from further oxidative attack and also acted to sequester the liberated arsenic by co-precipitation, both of which processes acted to reduce the bioavailability of the arsenopyrite-hosted arsenic. Secondary phase formation was identified as the cause of decreasing HNO_3-extractable mercury (liberated from cinnabar) after mercury release from cinnabar in oxic soils peaked (≤ 90 days exposure), although the identity and formation mechanism of the secondary phase(s) responsible for this effect could not be confirmed. For sphalerite, the evidence indicates that secondary sulfide phases formed under the sulfate-reducing soil conditions produced for rice cultivation, limiting the availability of cadmium previously liberated under oxic conditions, to rice plants.

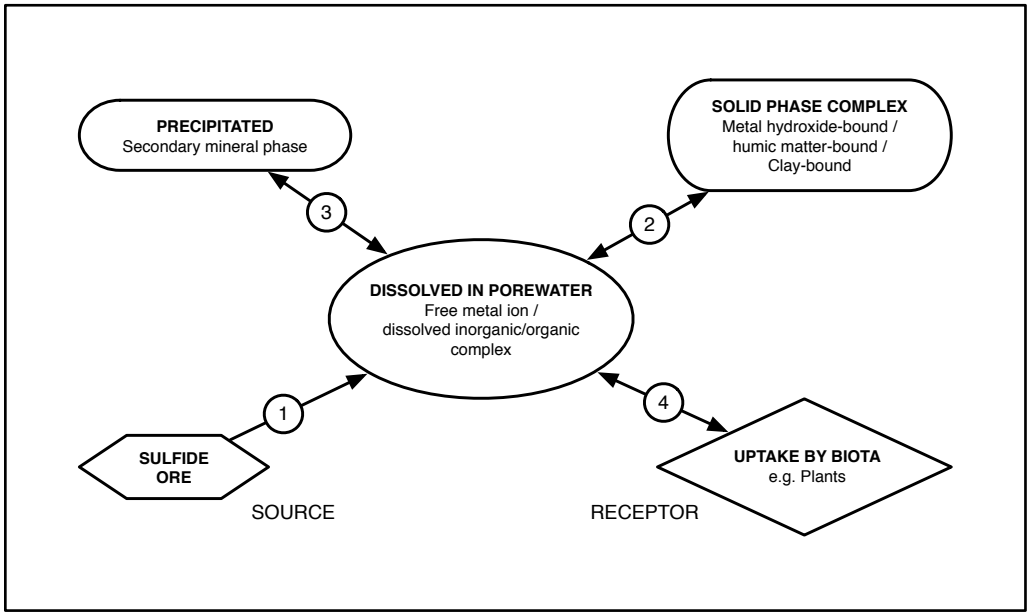

Figure 6.1 Partial conceptual model of a soil – sulfide – plant system. Please refer to Figure 1.4 for the full proposed conceptual model. Biogeochemical processes represented by each pathway are discussed by number in the text.

The third important factor influencing the concentration of PTEs in crop grains was plant uptake and translocation behaviour. In addition to the magnitude and speciation of PTEs in the rhizosphere, accumulation depends on the rate of root uptake and translocation from root > stem > grains (Figure 6.1 pathway 4). Physiological limitations, inhibiting PTE translocation from stems to grains, were apparent in both plant species grown in soils contaminated with each of the three ore minerals studied, respectively. This was evident from consistently and significantly lower PTE concentrations determined in plant grains, compared with stems (transfer factors ranging 0.07 - 0.52). Distinctions between each plant's responses to growing in soils contaminated with the different ore minerals were also evident, based on comparisons of PTE accumulation in the stems and translocation to the grains in contaminated and uncontaminated (control) soils. Cadmium accumulation, relative to the available soil reservoir, in the stems of wheat was drastically increased in sphalerite-contaminated soils (BCF = 51.2)

compared with plants in control soils (BCF = 2.16). The stem-to-grain transfer factors (TF), which were equal or greater for plants grown in contaminated soils compared with those grown in control soils, demonstrated that translocation was not down-regulated in response to increased cadmium uptake. Also, the sphalerite-derived cadmium was the only PTE studied to be hyperaccumulated (BCF > 1) by the crops grown in this study.

The uptake and translocation behaviour also differed between plant species exposed to the same ore mineral. For instance, the wheat responded to increased arsenic availability (from arsenopyrite) by down-regulating translocation (TF from 0.49 to 0.29) while the rice, grown in control and spiked soils, exhibited relatively limited translocation regardless of arsenic availability (0.07 to 0.08). Both plant species accumulated drastically lower proportions (from 0.76 to 0.02 rice; from 2.44 to 0.13 wheat) of the available mercury (from cinnabar), compared with the native mercury content of the soil. Conversely, the plants growing in cinnabar-contaminated soils up-regulated translocation (from 0.18 to 0.49 for rice; 0.10 to 0.17 for wheat).

These observations highlight the complexity of soil-mineral-PTE-plant relationships and the need to consider the physiology and uptake response of each plant species, in addition to the magnitude and speciation of the potentially bioavailable reservoir of PTEs in the soils.

6.1.3 Long-term impacts on soil quality and influences of agricultural practice

The long-term impacts of the studied ore mineral upon soil quality are determined primarily by the formation and stability of the aforementioned secondary phases and the redox conditions of the host soils. Sphalerite contamination is likely to

have a long-term, deleterious influence in productive soils by slowly but continuously releasing cadmium on a timescale of decades, regardless of a continuous supply of this mineral to soils. No secondary phase formation was observed to impede weathering or sequester the liberated cadmium under oxic conditions, which was also readily taken up by crops and accumulated in their edible grains. In contrast, arsenopyrite and cinnabar exhibited a limited phase of PTE liberation when exposed to oxic soils. For these ore minerals, the potentially bioavailable PTE concentrations decreased after peaking, an effect attributed to secondary phase formation. These findings predict that, upon introduction to soils, arsenic and mercury liberation would be short-lived, and that the solid-phase associations and 'ageing effects' would reduce the bioavailability of those liberated PTEs over time, assuming stable biogeochemical conditions.

Soil redox status was found to be an important factor affecting the bioavailability of cadmium and arsenic in soils contaminated by sphalerite and arsenopyrite, respectively. Flooded, reducing soil conditions controls cadmium bioavailability to rice, by providing a neutral soil pH and encouraging the formation on secondary cadmium sulfide phases. In contrast, those same conditions (Eh < 100 mV) encourage arsenic bioavailability to rice through a speciation shift to arsenite (i.e. arsenous acid), which is less efficiently adsorbed by iron oxyhydroxide minerals and more effectively taken up and translocated by rice plants.

Increasing global population and freshwater demand have catalysed the adoption of new agricultural practices such as 'system of rice intensification', a set of management principles that discourage flooded agriculture. A shift towards more oxic soil management would remove the protective biogeochemical conditions afforded by soil flooding and enhance the bioavailability of cadmium in

soils. The situation is more complicated for arsenopyrite because, although oxic conditions would reduce arsenic bioavailability, they also provide the oxygen responsible for the oxidative dissolution of this mineral.

6.2 Project evaluation and future work

The key findings of this project demonstrate a potential human health hazard relating to the dispersal of PTE-hosting sulfide ore particles produced by mining activities into soils supporting human populations. This work also highlights the wider importance of mineral waste particles as environmental vectors for PTEs and may be of interest to environmental scientists, environmental health specialists and regulators. The envisaged applications of this work are to support further research on the human health and ecotoxicological impacts of mining activities on soils.

The findings of this project were obtained through the application of laboratory-based static soil incubations, coupled with various selective aqueous extractions, and X-ray based spectroscopic techniques, and plant uptake experiments. Selective aqueous extractions provided information on the PTE release kinetics and solid-phase associations, whilst SEM-EDXS analyses enabled the coupling of those data with mineralogical evolution of the systems. Plant uptake experiments provided direct indications of PTE bioavailability within the soil-ore mineral-plant systems being studied. This combination, and the corroborative evidence provided by each approach, allowed for a stronger interpretation of the processes being studied than afforded by either approach in isolation. Future studies would benefit from the more powerful, synchrotron-based, spectroscopic techniques that provide data on the molecular environment of PTEs in the soils (e.g. XANES, NEXAFS), allowing for greater detection and

certainty of solid-phase speciation in the experimental systems. In addition, spatially resolved techniques (e.g. μXRD, μXRF) can overcome the high detection limits associated with their 'bulk analysis' counterparts by allowing for the analysis of very small regions of a heterogeneous sample.

Whilst laboratory-based experiments provided controlled conditions, they cannot completely replicate environmental conditions, and are best suited for elucidating processes and building the theoretical framework, upon which field investigations can be designed and against which field data are interpreted. Three important sulfide minerals were chosen for this project, but many other primary (i.e. sulfide) and secondary (alteration phases) minerals also present in mining wastes that deserve attention in future studies.

With the limitations of laboratory-based experiments in mind, the next phase of this research should focus on field-scale case studies. Reports in the literature, identifying populations affected by mining and inappropriate management of the environmental and human health impacts of mining, focus on Asian countries, notably Peoples Republic of China, South Korea and Thailand. Therefore, the field investigation phase should be targeted on these localities in the first instance. Whilst several studies report the distribution and concentration of PTEs in areas affected by mining, and supporting human populations, there is a paucity of contemporary quantitative mineralogical data in these settings. This prevents a full evaluation of the magnitude and significance of the potential human hazard identified from this project. In addition, there are numerous local factors (e.g. farming practices, contaminant source and character, climate) that can only be accounted for by conducting field investigations. Therefore, the primary aim of the next phase of works should be to address these data requirements, enabling a comprehensive risk assessment. The key components envisaged for this work are:

- Detailed mineralogical profile of the probable contamination source and of soils used to produce crops. Mineralogical data and PTE speciation would be determined using techniques such as XRD, SEM-EDX, μXRD and XANES.
- Identification of the dominant pathways connecting mines with productive soils. Active air quality sampling and passive sediment/irrigation water sampling would be combined with elemental and speciation analyses, using techniques such as μXRD, μXRF and XANES.
- Regional (targeted) vegetation sampling and analyses. Speciation analysis would be performed using a combination of high-performance separation (i.e. chromatography) coupled with ICP-MS or atomic fluorescence spectometry (Hg).

In addition to field investigations, the following laboratory-based investigations are suggested to augment the current findings:

- Chemical speciation of PTEs in soil porewater and accumulated in edible plant tissues to refine the toxicological risk associated with PTE accumulation in crops, and to potentially yield new insights into soil-plant interactions and uptake mechanisms.
- Column experiments to provide a dynamic simulation of the mineral weathering under controlled conditions, the stability of secondary phases and the environmental mobility of PTEs liberated from mineral matrices in soils.
- Work with a greater focus on the potential ecotoxicological effects of particulate contamination from mining.

References

Abedin, M.J., Feldmann, J. & Meharg, A.A. (2002) Uptake kinetics of arsenic species in rice plants. *Plant Physiology*, 128 (3), pp.1120–1128.

Acero, P., Cama, J. & Ayora, C. (2007) Sphalerite dissolution kinetics in acidic environment. *Applied Geochemistry*, 22 (9), pp.1872–1883.

Africare, Oxfam AmericaWWF-ICRISAT Project (2010) *More Rice for People, More Water for the Planet*. Hyderabad, India, WWF-ICRISAT Project.

Al-Abed, S.R., Jegadeesan, G., Purandare, J. & Allen, D. (2007) Arsenic release from iron rich mineral processing waste: Influence of pH and redox potential. *Chemosphere*, 66 (4), pp.775–782.

Alam, M.G.M., Tokunaga, S. & Maekawa, T. (2001) Extraction of arsenic in a synthetic arsenic contaminated soil using phosphate. *Chemosphere*, 44, pp.1035–1041.

Alastuey, A., Garcıa-Sánchez, A., López, F. & Querol, X. (1999) Evolution of pyrite mud weathering and mobility of heavy metals in the Guadiamar valley after the Aznalcóllar spill, south-west Spain. *Science of The Total Environment*, 242 (1), pp.41–55.

Albering, H.J., van Leusen, S.M., Moonen, E.J., Hoogewerff, J.A. & Kleinjans, J.C. (1999) Human health risk assessment: A case study involving heavy metal soil contamination after the flooding of the river Meuse during the winter of 1993-1994. *Environmental Health Perspectives*, 107 (1), p.37.

Allen, H.E., Fu, G. & Deng, B. (1993) Analysis of acid-volatile sulfide (AVS) and simultaneously extracted metals (SEM) for the estimation of potential toxicity in aquatic sediments. *Environmental Toxicology and Chemistry*, 12 (8), pp.1441–1453.

Anthony, J.W., Bideaux, R.A., Bladh, K.W. & Nichols, M.C. (1990) *Handbook of Mineralogy*. Tucson Arizona, USA, Mineral Data Publishing.

Antosiewicz, D.M., Escudě-Duran, C., Wierzbowska, E. & Skłodowska, A. (2008) Indigenous plant species with the potential for the phytoremediation of arsenic and metals contaminated soil. *Water, Air & Soil Pollution*, 193 (1-4), pp.197–210.

Arai, Y. & Sparks, D.L. (2002) Residence time effects on arsenate surface speciation at the aluminum oxide-water interface. *Soil Science*, 167 (2), pp.303–314.

Arbestain, M.C., Rodríguez-Lado, L., Bao, M. & Macías, F. (2009) Assessment of mercury-polluted soils adjacent to an old mercury-fulminate production plant. *Applied and Environmental Soil Science*, 2009, pp.1–9.

Asta, M.P., Cama, J., Ayora, C., Acero, P. & De Giudici, G. (2010) Arsenopyrite dissolution rates in O_2-bearing solutions. *Chemical Geology*, 273 (3-4), pp.272–

285.

ASTM International (2012) *ASTM D5744-12: Standard Test Method for Laboratory Weathering of Solid Materials Using a Humidity Cell*. West Conshohocken, PA, USA, ASTM International.

ATSDR (2007) *Toxicological profile for arsenic*. Atlanta, GA, US, Agency for Toxic Substances and Disease Registry.

ATSDR (1999) *Toxicological profile for mercury*. Atlanta, Georgia, USA, Agency for Toxic Substances and Disease Registry.

Bagnold, R.A. (1941) *The Physics of Blown Sands and Desert Dunes*. London, UK, Methuen.

Barnett, M.O., Harris, L.A., Turner, R.R., Stevenson, R.J., Henson, T.J., Melton, R.C. & Hoffman, D.P. (1997) Formation of mercuric sulfide in soil. *Environmental Science & Technology*, 31 (11), pp.3037–3043.

Barnett, M.O., Turner, R.R. & Singer, P.C. (2001) Oxidative dissolution of metacinnabar (b-HgS) by dissolved oxygen. *Applied Geochemistry*, 16, pp.1499–1512.

Bearat, H., Chizmeshya, A., Sharma, R., Barbet, A. & Fuchs, M. (2005) *Mechanistic and computational study of cinnabar phase transformation: Applications and implications to the preservation of this pigment in historical painting*. Natchitoches, LA, USA, National Center for Preservation Technology and Training. Available from: http://ncptt.nps.gov/wp-content/uploads/Final-report.pdf [Accessed July 2013].

Beesley, L., Moreno-Jimenez, E., Clemente, R., Lepp, N. & Dickinson, N. (2010) Mobility of arsenic, cadmium and zinc in a multi-element contaminated soil profile assessed by in-situ soil pore water sampling, column leaching and sequential extraction. *Environmental Pollution*, 158 (1), pp.155–160.

Bennett, B. & Dudas, M.J. (2003) Release of arsenic and molybdenum by reductive dissolution of iron oxides in a soil with enriched levels of native arsenic. *Journal of Environmental Engineering and Science*, 2 (4), pp.265–272.

Biester, H., Gosar, M. & Müller, G. (1999) Mercury speciation in tailings of the Idrija mercury mine. *Journal of Geochemical Exploration*, 65 (3), pp.195–204.

Blight, G.E. & Da Costa, F.A. (2001) On the mechanics of wind erosion from tailings dams. In: Proceedings of the eighth international conference on tailings and mine waste, Fort Collins, Colorado, USA, pp.189–196. Rotterdam, Nederlands, Balkema.

Bloom, N.S., Preus, E., Katon, J. & Hiltner, M. (2003) Selective extractions to assess the biogeochemically relevant fractionation of inorganic mercury in sediments and soils. *Analytica Chimica Acta*, 479 (2), pp.233–248.

Bouman, B.A.M., Lampayan, R.M. & Tuong, T.P. (2007) *Water Management in Irrigated Rice: Coping with Water Scarcity*. Los Baños, Philippines, International

Rice Research Institute.

Brady, N.C. & Weil, R.R. (2003) *Elements of the Nature and Properties of Soils*. 2nd ed. New Jersey, USA, Prentice Hall.

Butler, L.C. (2003) *Mercury preservation techniques*. [online], US Environmental Protection Agency. Available from: <http://www.epa.gov/esd/factsheets/mpt.pdf>. [Accessed October 2012].

Candeias, C., da Silva, E.F., Salgueiro, A.R., Pereira, H.G., Reis, A.P., Patinha, C., Matos, J.X. & Avila, P.H. (2010) Assessment of soil contamination by potentially toxic elements in the Aljustrel mining area in order to implement soil reclamation strategies. *Land Degradation & Development*, 22 (6), pp.565–585.

Carter, M.R. & Gregorich, E.G. (2007) *Soil Sampling and Methods of Analysis*. 2nd ed. Boca Raton, USA, CRC Press.

Castillo, S., de la Rosa, J.D., de la Campa, A.M.S., González-Castanedo, Y., Fernández-Caliani, J.C., Gonzalez, I. & Romero, A. (2013) Contribution of mine wastes to atmospheric metal deposition in the surrounding area of an abandoned heavily polluted mining district (Rio Tinto Mines, Spain). *Science of The Total Environment*, 449, pp.363–372.

Chamon, A.S., Gerzabek, M.H., Mondol, M.N., Ullah, S.M., Rahman, M. & Blum, W.E.H. (2005) Influence of cereal varieties and site conditions on heavy metal accumulations in cereal crops on polluted soils of Bangladesh. *Communications in Soil Science and Plant Analysis*, 36 (7/8), pp.889–906.

Cheng, H., Hu, Y., Luo, J., Xu, B. & Zhao, J. (2009) Geochemical processes controlling fate and transport of arsenic in acid mine drainage (AMD) and natural systems. *Journal of Hazardous Materials*, 165 (1-3), pp.13–26.

Chon, H., Ahn, J.S. & Jung, M.C. (2005) Heavy metal contamination around the abandoned Au-Ag and base metal mine sites of Korea. *International Journal of Economic and Environmental Geology*, 38 (2), pp.101–111.

Chopin, E.I.B. & Alloway, B.J. (2007) Distribution and mobility of trace elements in soils and vegetation around the mining and smelting areas of Tharsis, Ríotinto and Huelva, Iberian Pyrite Belt, SW Spain. *Water, Air & Soil Pollution*, 182, pp.245–261.

Clark, M.W., Walsh, S.R. & Smith, J.V. (2001) The distribution of heavy metals in an abandoned mining area; a case study of Strauss Pit, the Drake mining area, Australia: implications for the environmental management of mine sites. *Environmental Geology*, 40 (6), pp.655–663.

Clemens, S., Aarts, M.G.M., Thomine, S. & Verbruggen, N. (2013) Plant science: the key to preventing slow cadmium poisoning. *Trends in Plant Science*, 18 (2), pp.92–99.

Clemens, S., Palmgren, M.G. & Krämer, U. (2002) A long way ahead: understanding and engineering plant metal accumulation. *Trends in Plant Science*, 7 (7), pp.309–315.

Cline, J.D. (1969) Spectrophotometric determination of hydrogen sulfide in natural waters. *Limnology & Oceanography*, 14 (3), pp.454–458.

Colombo, M.J., Ha, J., Reinfelder, J.R., Barkay, T. & Yee, N. (2013) Anaerobic oxidation of Hg(0) and methylmercury formation by *Desulfovibrio desulfuricans* ND132. *Geochimica et Cosmochimica Acta*, 112, pp.166–177.

Concas, A., Ardau, C., Cristini, A., Zuddas, P. & Cao, G. (2006) Mobility of heavy metals from tailings to stream waters in a mining activity contaminated site. *Chemosphere*, 63 (2), pp.244–253.

Conesa, H.M., Faz, A. & Arnaldos, R. (2006) Heavy metal accumulation and tolerance in plants from mine tailings of the semiarid Cartagena–La Unión mining district (SE Spain). *Science of The Total Environment*, 366 (1), pp.1–11.

Conesa, H.M., Schulin, R. & Nowack, B. (2007) A laboratory study on revegetation and metal uptake in native plant species from neutral mine tailings. *Water, Air & Soil Pollution*, 183 (1), pp.201–213.

Cook, N.J., Ciobanu, C.L., Pring, A., Skinner, W., Shimizu, M., Danyushevsky, L., Saini-Eidukat, B. & Melcher, F. (2009) Trace and minor elements in sphalerite: A LA-ICPMS study. *Geochimica et Cosmochimica Acta*, 73 (16), pp.4761–4791.

Corkhill, C.L. & Vaughan, D.J. (2009) Arsenopyrite oxidation - a review. *Applied Geochemistry*, 24 (12), pp.2342–2361.

Corkhill, C.L., Wincott, P.L., Lloyd, J.R. & Vaughan, D.J. (2008) The oxidative dissolution of arsenopyrite (FeAsS) and enargite (Cu_3AsS_4) by *Leptospirillum ferrooxidans*. *Geochimica et Cosmochimica Acta*, 72 (23), pp.5616–5633.

Corriveau, M.C., Jamieson, H.E., Parsons, M.B., Campbell, J.L. & Lanzirotti, A. (2011) Direct characterization of airborne particles associated with arsenic-rich mine tailings: Particle size, mineralogy and texture. *Applied Geochemistry*, 26 (9-10), pp.1639–1648.

Craw, D., Falconer, D. & Youngson, J.H. (2003) Environmental arsenopyrite stability and dissolution: theory, experiment, and field observations. *Chemical Geology*, 199 (1-2), pp.71–82.

D'Amato, M., Aureli, F., Ciardullo, S., Raggi, A. & Cubadda, F. (2010) Arsenic speciation in wheat and wheat products using ultrasound- and microwave-assisted extraction and anion exchange chromatography-inductively coupled plasma mass spectrometry. *Journal of Analytical Atomic Spectrometry*, 26 (1), p.207.

de Livera, J., McLaughlin, M.J., Hettiarachchi, G.M., Kirby, J.K. & Beak, D.G. (2011) Cadmium solubility in paddy soils: effects of soil oxidation, metal sulfides and competitive ions. *Science of The Total Environment*, 409 (8), pp.1489–1497.

Debeljak, M., van Elteren, J.T. & Vogel-Mikuš, K. (2013) Development of a 2D laser ablation inductively coupled plasma mass spectrometry mapping procedure for mercury in maize (*Zea mays L.*) root cross-sections. *Analytica Chimica Acta*, 787, pp.155–162.

Dibba, D., Weaver, L.T. & Hudson, G.J. (1991) Water content of cooked rice is related to variety and cooking method. *Nutrition Research*, 12 (11), pp.1397–1402.

Dorren, D.I. & Blight, G.E. (1986) Erosion of the slopes of gold-residue dams on the Transvaal Highveld-preliminary results. *Journal of South African Institute of Mining and Metallurgy*, 86 (12), pp.475–480.

Drahota, P. & Filippi, M. (2009) Secondary arsenic minerals in the environment: A review. *Environment International*, 35, pp.1343–1255.

Dudka, S., Piotrowska, M., Chlopecka, A. & Witek, T. (1995) Trace metal contamination of soils and crop plants by the mining and smelting industry in Upper Silesia, South Poland. *Journal of Geochemical Exploration*, 52, pp.237–250.

Duxbury, J.M., Mayer, A.B., Lauren, J.G. & Hassan, N. (2003) Food chain aspects of arsenic contamination in Bangladesh: effects on quality and productivity of rice. *Journal of Environmental Science and Health, Part A*, 38 (1), pp.61–69.

Erbs, J.J., Berquó, T.S., Reinsch, B.C., Lowry, G.V., Banerjee, S.K. & Penn, R.L. (2010) Reductive dissolution of arsenic-bearing ferrihydrite. *Geochimica et Cosmochimica Acta*, 74 (12), pp.3382–3395.

European Commission (2007) *European Union risk assessment report: Cadmium oxide and cadmium metal part 1 - Environment*. Luxembourg, European Commission. Available from: <http://publications.jrc.ec.europa.eu/repository/bitstream/111111111/1032/1/reqno_jrc38226_european%20union%20risk%20assessment%20report%20-%20part%201%20-%20environment%20-%20cadmium%20oxide%20and%20cadmium%20metal%5B2%5D.pdf>. [Accessed November 2012].

European Food Safety Authority (2011) Use of the EFSA Comprehensive European Food Consumption Database in exposure assessment. *EFSA Journal*, 9, pp.2097–2131.

FAO/WHO (2013) *Joint FAO/WHO food standards programme: COXEX Committee on Contaminants in Foods seventh session provisional agenda*. Rome, Italy, World Health Organisation. Available from: <http://www.codexalimentarius.org/input/download/report/797/cf07_01e.pdf>.

FAO/WHO (2010) *Seventy-second report of the joint FAO/WHO expert committee on food additives*. Geneva, Switzerland, Food and Agriculture Organizaton of the United Nations & World Health Organization.

FAO/WHO (2011) *Summary Report of the Seventy-Third Meeting of Joint FAO/WHO Expert Committee on Food Additives*. Geneva, Switzerland, Food and Agriculture Organizaton of the United Nations & World Health Organization.

Feng, X., Li, P., Qiu, G., Wang, S., Li, G., Shang, L., Meng, B., Jiang, H., Bai, W., Li, Z. & Fu, X. (2008) Human exposure to methylmercury through rice intake in

mercury mining areas, Guizhou province, China. *Environmental Science & Technology*, 42 (1), pp.326–332.

Fergusson, J.E. (1990) *The heavy elements: Chemistry, environmental impact and health effects*. Oxford, UK, Pergamon Press.

Fernández-Martínez, R. & Rucandio, M.I. (2005) Study of the suitability of HNO_3 and HCl as extracting agents of mercury species in soils from cinnabar mines. *Analytical and Bioanalytical Chemistry*, 381 (8), pp.1499–1506.

Foord, E.E., Berendsen, P. & Storey, L.O. (1974) Corderoite, first natural occurrence of α-$Hg_3S_2Cl_2$, from the Cordero mercury deposit, Humboldt County, Nevada. *American Mineralogist*, 59, pp.652–655.

Fordyce, F.M., Williams, T.M., Paijitprapapon, A. & Charoenchaisri, P. (2003) *Hydrogeochemistry of arsenic in an area of chronic mining-related arsenism, Ron Phibum District, Nakhon Si Thammarat Provice, Thailand: Preliminary Results*. Nottingham, UK, British Geological Survey.

Foster, A.L., Ashley, R.P. & Rytuba, J.J. (2011) Arsenic species in weathering mine tailings andbiogenic solids at the Lava Cap Mine Superfund site, Nevada City, CA. *Geochemical Transactions*, 12 (1), p.1.

García-Sánchez, A., Alonso-Rojo, P. & Santos-Frances, F. (2010) Distribution and mobility of arsenic in soils of a mining area (Western Spain). *Science of The Total Environment*, 408 (19), pp.4194–4201.

Geiszinger, A., Goessler, W. & Kosmus, W. (2002) Organoarsenic compounds in plants and soil on top of an ore vein. *Applied Organometallic Chemistry*, 16 (5), pp.245–249.

Georgiadis, M., Cai, Y. & Solo-Gabriele, H.M. (2006) Extraction of arsenate and arsenite species from soils and sediments. *Environmental Pollution*, 141 (1), pp.22–29.

Gleyzes, C., Tellier, S., Sabrier, R. & Astruc, M. (2001) Arsenic characterisation in industrial soils by chemical extractions. *Environmental Technology*, 22 (1), pp.27–38.

Gosar, M. & Miler, M. (2011) Anthropogenic metal loads and their sources in stream sediments of the Meža River catchment area (NE Slovenia). *Applied Geochemistry*, 26 (11), pp.1855–1866.

Gosar, M., Šajn, R. & Biester, H. (2006) Binding of mercury in soils and attic dust in the Idrija mercury mine area (Slovenia). *Science of The Total Environment*, 369 (1-3), pp.150–162.

Gramp, J.P., Bigham, J.M., Jones, F.S. & Tuovinen, O.H. (2010) Formation of Fe-sulfides in cultures of sulfate-reducing bacteria. *Journal of Hazardous Materials*, 175 (1-3), pp.1062–1067.

Gray, J.E., Crock, J.G. & Fey, D.L. (2002) Environmental geochemistry of abandoned mercury mines in West-Central Nevada, USA. *Applied Geochemistry*, 17 (8),

pp.1069–1079.

Gray, J.E., Theodorakos, P.M., Bailey, E.A. & Turner, R.R. (2000) Distribution, speciation, and transport of mercury in stream-sediment, stream-water, and fish collected near abandoned mercury mines in southwestern Alaska, USA. *Science of The Total Environment*, 260, pp.21–33.

Greeley, R. & Iversen, J.D. (1985) *Wind as a Geological Process on Earth, Mars, Venus and Titan*. New York, USA, Cambridge University Press.

Hamon, R.E., McLaughlin, M.J., Naidu, R. & Correll, R. (1998) Long-term changes in cadmium bioavailability in soil. *Environmental Science & Technology*, 32 (23), pp.3699–3703.

Han, F.X., Safwan, S., Jian, C., Yi, S., Monts, D.L., Waggoner, C.A. & Matta, F.B. (2008) Extractability and bioavailability of mercury from a mercury sulfide contaminated soil in Oak Ridge, Tennessee, USA. *Water, Air & Soil Pollution*, 194 (1-4), pp.67–75.

Han, F.X., Su, Y., Monts, D.L., Waggoner, C.A. & Plodinec, M.J. (2006) Binding, distribution, and plant uptake of mercury in a soil from Oak Ridge, Tennessee, USA. *Science of The Total Environment*, 368 (2-3), pp.753–768.

Han, Y., Kingston, H.M., Boylan, H.M., Shah, S., Richter, R.C., Link, D.D. & Bhandari, S. (2003) Speciation of mercury in soil and sediment by selective solvent and acid extraction. *Analytical and Bioanalytical Chemistry*, 375 (3), pp.428–436.

Handley-Sidhu, S., Worsfold, P.J., Livens, F.R., Vaughan, D.J., Lloyd, J.R., Boothman, C., Sajih, M., Alvarez, R. & Keith-Roach, M.J. (2009) Biogeochemical controls on the corrosion of depleted uranium alloy in subsurface soils. *Environmental Science & Technology*, 43 (16), pp.6177–6182.

Heidel, C., Tichomirowa, M. & Breitkopf, C. (2011) Sphalerite oxidation pathways detected by oxygen and sulfur isotope studies. *Applied Geochemistry*, 26 (12), pp.2247–2259.

Henson, M.C. & Chedrese, P.J. (2004) Endocrine disruption by cadmium, a common environmental toxicant with paradoxical effects on reproduction. *Experimental Biology and Medicine*, 229 (4), pp.383–392.

Higueras, P., Oyarzun, R., Lillo, J., Sánchez-Hernández, J.C., Molina, J.A., Esbrí, J.M. & Lorenzo, S. (2006) The Almadén district (Spain): anatomy of one of the world's largest Hg-contaminated sites. *Science of The Total Environment*, 356 (1), pp.112–124.

Hita, R. & Torrent, J. (2005) Weathering of pyrite and sphalerite in soils contaminated with pyritic sludge. *Soil Science Society of America Journal*, 69 (4), p.1314.

Hita, R., Torrent, J. & Bigham, J.M. (2006) Experimental oxidative dissolution of sphalerite in the Aznalcóllar sludge and other pyritic matrices. *Journal of Environmental Quality*, 35 (4), pp.1032–1039.

Holley, E.A., McQuillan, J.A., Craw, D., Kim, J.P. & Sander, S.G. (2007) Mercury mobilization by oxidative dissolution of cinnabar (α-HgS) and metacinnabar (β-HgS). *Chemical Geology*, 240 (3-4), pp.313–325.

Holm, P.E., Christensen, T.H., Lorenz, S.E., Hamon, R.E., Domingues, H.C., Sequeira, E.M. & McGrath, S.P. (1998) Measured soil water concentrations of cadmium and zinc in plant pots and estimated leaching outflows from contaminated soils. *Water, Air & Soil Pollution*, 102 (1), pp.105–115.

Holmes, P., James, K.A.F. & Levy, L.S. (2009) Is low-level environmental mercury exposure of concern to human health? *Science of The Total Environment*, 408 (2), pp.171–182.

Horvat, M., Covelli, S., Faganeli, J., Logar, M., Mandić, V., Rajar, R., Širca, A. & Žagar, D. (1999) Mercury in contaminated coastal environments; a case study: the Gulf of Trieste. *Science of The Total Environment*, 237, pp.43–56.

Horvat, M., Nolde, N., Fajon, V., Jereb, V., Logar, M., Lojen, S., Jacimovic, R., Falnog, I., Liya, Q., Faganeli, J. & Drobne, D. (2003) Total mercury, methylmercury and selenium in mercury polluted areas in the province Guizhou, China. *Science of The Total Environment*, 304, pp.231–256.

Huang, M., Zhou, S., Sun, B. & Zhao, Q. (2008) Heavy metals in wheat grain: assessment of potential health risk for inhabitants in Kunshan, China. *Science of The Total Environment*, 405 (1-3), pp.54–61.

Huang, R., Gao, S., Wang, W., Staunton, S. & Wang, G. (2006) Soil arsenic availability and the transfer of soil arsenic to crops in suburban areas in Fujian Province, southeast China. *Science of The Total Environment*, 368 (2-3), pp.531–541.

Hudson-Edwards, K.A., Jamieson, H.E., Charnock, J.M. & Macklin, M.G. (2005) Arsenic speciation in waters and sediment of ephemeral floodplain pools, Ríos Agrio–Guadiamar, Aznalcóllar, Spain. *Chemical Geology*, 219 (1-4), pp.175–192.

Inglett, P.W., Reddy, K.R. & Corstanje, R. (2005) Anaerobic soils. In: D. Hillel ed. *Encyclopedia of Soils in the Environment*. Waltham MA, USA, Academic Press Inc, pp.71–78.

Isaure, M., Manceau, A., Geoffroy, N., Laboudigue, A., Tamura, N. & Marcus, M.A. (2005) Zinc mobility and speciation in soil covered by contaminated dredged sediment using micrometer-scale and bulk-averaging X-ray fluorescence, absorption and diffraction techniques. *Geochimica et Cosmochimica Acta*, 69 (5), pp.1173–1198.

Ishihara, T., Kobayashi, E., Okubo, Y., Suwazono, Y., Kido, T., Nishijyo, M., Nakagawa, H. & Nogawa, K. (2001) Association between cadmium concentration in rice and mortality in the Jinzu River Basin, Japan. *Toxicology*, 163 (1), pp.23–28.

Jackson, B.P. & Miller, W.P. (2000) Effectiveness of phosphate and hydroxide for desorption of arsenic and selenium species from iron oxides. *Soil Science Society of America*, 64, pp.1616–1622.

Järup, L. (2003) Hazards of heavy metal contamination. *British Medical Bulletin*, 68

(1), pp.167–182.

Jiang, W., Zhang, S., Shan, X.-Q., Feng, M., Zhu, Y.-G. & McLaren, R.G. (2005) Adsorption of arsenate on soils. Part 2: Modeling the relationship between adsorption capacity and soil physiochemical properties using 16 Chinese soils. *Environmental Pollution*, 138 (2), pp.285–289.

Joint Research Centre for Reference Materials (2012) Questions related to the use of reference materials [Internet]. Available from: <http://irmm.jrc.ec.europa.eu/reference_materials_catalogue/user_support/Pages/use.aspx> [Accessed March 2012].

Kibria, M.G. & Ahmed, M.J. (2006) Cadmium and lead uptake by rice (*Oryza Sativa L.*) grown in three different textured soils. *Soil & Environment*, 25 (2), pp.70–77.

Kim, C.S., Lowry, G.V., Shaw, S., Rytuba, J.J. & Brown, G.E., Jr (2001) Speciation of mercury-bearing mine wastes using X-ray absorption fine structure (XAFS) spectroscopy: physical and geochemical effects. In: Proceedings of the Eleventh Annual VM Goldschmidt Conference, Hot Springs, Virginia, USA. Cambridge, UK, Cambridge Publications.

Kim, C.S., Rytuba, J.J. & Brown, G.E. (2004) Geological and anthropogenic factors influencing mercury speciation in mine wastes: an EXAFS spectroscopy study. *Applied Geochemistry*, 19 (3), pp.379–393.

King, R.J. (1988) Minerals Explained 8: Sphalerite. *Geology Today*, 4, pp.67–70.

King, R.J. (2002) Minerals explained 37: Cinnabar. *Geology Today*, 18 (5), pp.195–199.

Kocman, D., Vreča, P., Fajon, V. & Horvat, M. (2011) Atmospheric distribution and deposition of mercury in the Idrija Hg mine region, Slovenia. *Environmental Research*, 111 (1), pp.1–9.

Kon, L.C., Durucan, S. & Korre, A. (2007) The development and application of a wind erosion model for the assessment of fugitive dust emissions from mine tailings dumps. *International Journal of Mining, Reclamation and Environment*, 21 (3), pp.198–218.

Kossoff, D., Hudson, D.K.A., Dubbin, W.E. & Alfredsson, M.A. (2011) Incongruent weathering of Cd and Zn from mine tailings: a column leaching study. *Chemical Geology*, 281 (1-2), pp.52–71.

Kossoff, D., Hudson-Edwards, K.A., Dubbin, W.E. & Alfredsson, M. (2012) Major and trace metal mobility during weathering of mine tailings: Implications for floodplain soils. *Applied Geochemistry*, 27, pp.562–576.

Krupp, E.M., Mestrot, A., Wielgus, J., Meharg, A.A. & Feldmann, J. (2009) The molecular form of mercury in biota: identification of novel mercury peptide complexes in plants. *Chemical Communications*, (28), pp.4257–4259.

la Campa, de, A.M.S., la Rosa, de, J.D., Fernández-Caliani, J.C. & González-Castanedo,

Y. (2011) Impact of abandoned mine waste on atmospheric respirable particulate matter in the historic mining district of Rio Tinto (Iberian Pyrite Belt). *Environmental Research*, 111 (8), pp.1018–1023.

Lancaster, N. (2009a) Aeolian features and processes. In: *Geological Monitoring*. Boulder, Colorado, USA, The Geological Society of America, pp.1–25.

Lancaster, N. (2009b) Aeolian features and processes. In: R. Young & L. Norby eds. *Geological Monitoring*. Boulder, Colorado, USA, The Geological Society of America.

Langmuir, D., Mahoney, J. & Rowson, J. (2006) Solubility products of amorphous ferric arsenate and crystalline scorodite ($FeAsO_4.2H_2O$) and their application to arsenic behavior in buried mine tailings. *Geochimica et Cosmochimica Acta*, 70 (12), pp.2942–2956.

Lavazzo, P., Adamo, P., Boni, M., Hillier, S. & Zampella, M. (2012) Mineralogy and chemical forms of lead and zinc in abandoned mine wastes and soils: An example from Morocco. *Journal of Geochemical Exploration*, 113, pp.56–67.

Lawrence, C.R. & Neff, J.C. (2009) The contemporary physical and chemical flux of aeolian dust: A synthesis of direct measurements of dust deposition. *Chemical Geology*, 267 (1-2), pp.46–63.

Lee, J., Lee, S., Chon, H. & Kim, K. (2008) Evaluation of human exposure to arsenic due to rice ingestion in the vicinity of abandoned Myungbong Au–Ag mine site, Korea. *Journal of Geochemical Exploration*, 98, pp.231–235.

Lengke, M.F., Sanpawanitchakit, C. & Tempel, R.N. (2009) The oxidation and dissolution of arsenic-bearing sulphides. *The Canadian Mineralogist*, 47, pp.593–613.

Li, B., Shi, J.B., Wang, X., Meng, M., Huang, L., Qi, X.L., He, B. & Ye, Z.H. (2013) Variations and constancy of mercury and methylmercury accumulation in rice grown at contaminated paddy field sites in three Provinces of China. *Environmental Pollution*, 181, pp.91–97.

Li, L., Wang, F., Meng, B., Lemes, M., Feng, X. & Jiang, G. (2010) Speciation of methylmercury in rice grown from a mercury mining area. *Environmental Pollution*, 158 (10), pp.3103–3107.

Li, P., Feng, X., Qiu, G., Shang, L. & Wang, S. (2012) Mercury pollution in Wuchuan mercury mining area, Guizhou, Southwestern China: The impacts from large scale and artisanal mercury mining. *Environment International*, 42, pp.59–66.

Li, R.Y., Stroud, J.L., Ma, J.F., McGrath, S.P. & Zhao, F.J. (2009) Mitigation of arsenic accumulation in rice with water management and silicon fertilization. *Environmental Science & Technology*, 43 (10), pp.3778–3783.

Limei, Z., Xiaoyong, L., Tongbin, C., Xiulan, Y., Hua, X., Bin, W. & Lixia, W. (2008) Regional assessment of cadmium pollution in agricultural lands and the potential health risk related to intensive mining activities: a case study in Chenzhou City, China. *Journal of Environmental Sciences*, 20 (6), pp.696–703.

Liu, C., Luo, C., Gao, Y., Li, F., Lin, L., Wu, C. & Li, X. (2010) Arsenic contamination and potential health risk implications at an abandoned tungsten mine, southern China. *Environmental Pollution*, 158, pp.820–826.

Liu, W.X., Shen, L.F., Liu, J.W., Wang, Y.W. & Li, S.R. (2007) Uptake of toxic heavy metals by rice (*oryza sativa L.*) cultivated in the agricultural soil near Zhengzhou City, People's Republic of China. *Bulletin of Environmental Contamination & Toxicology*, 79 (2), pp.209–213.

Lo, I.M.C. & Yang, X.Y. (1999) EDTA extraction of heavy metals from different soil fractions and synthetic soils. *Water, Air & Soil Pollution*, 109 (1), pp.219–236.

Lomax, C., Liu, W., Wu, L., Xue, K., Xiong, J., Zhou, J., McGrath, S.P., Meharg, A.A., Miller, A.J. & Zhao, F.-J. (2011) Methylated arsenic species in plants originate from soil microorganisms. *New Phytologist*, 193 (3), pp.665–672.

Lopez, M., Gonzalez, I. & Romero, A. (2008) Trace elements contamination of agricultural soils affected by sulphide exploitation (Iberian Pyrite Belt, Sw Spain). *Environmental Geology*, 54 (4), pp.805–818.

Loredo, J., Ordóñez, A. & Alvarez, R. (2006) Environmental impact of toxic metals and metalloids from the Munon Cimero mercury-mining area (Asturias, Spain). *Journal of Hazardous Materials*, 136 (3), pp.455–467.

Loredo, J., Ordóñez, A., Charlesworth, S. & De Miguel, E. (2003a) Influence of industry on the geochemical urban environment of Mieres (Spain) and associated health risk. *Environmental Geochemistry & Health*, 25 (3), pp.307–323.

Loredo, J., Pereira, A. & Ordóñez, A. (2003b) Untreated abandoned mercury mining works in a scenic area of Asturias (Spain). *Environment International*, 29 (4), pp.481–491.

Lovley, D.R. & Phillips, E.J.P. (1986) Availability of ferric iron for microbial reduction in bottom sediments of the freshwater tidal Potomac River. *Applied and Environmental Microbiology*, 52 (4), pp.751–757.

Lowry, G.V., Shaw, S., Kim, C.S., Rytuba, J.J. & Brown, G.E. (2004) Macroscopic and microscopic observations of particle-facilitated mercury transport from New Idria and Sulphur Bank mercury mine tailings. *Environmental Science & Technology*, 38 (19), pp.5101–5111.

Luo, C., Shen, Z.G. & Li, X. (2008) Root exudates increase metal accumulation in mixed cultures: implications for naturally enhanced phytoextraction. *Water, Air & Soil Pollution*, 193 (1-4), pp.147–154.

Luong, J.H.T., Majid, E. & Male, K.B. (2007) Analytical tools for monitoring arsenic in the environment. *Open Analytical Chemistry*, 1, pp.7–14.

Ma, J.F., Yamaji, N., Mitani, N., Xu, X., Su, Y., McGrath, S.P. & Zhao, F. (2008) Transporters of arsenite in rice and their role in arsenic accumulation in rice grain. *Proceedings of the National Academy of Sciences of the United States of America*, 105 (29), pp.9931–9935.

Magdoff, F.R. & Bartlett, R.J. (1985) Soil pH buffering revisited. *Soil Science Society of America Journal*, 49 (1), pp.145–148.

Martínez-Coronado, A., Oyarzun, R., Esbrí, J.M., Llanos, W. & Higueras, P. (2011) Sampling high to extremely high Hg concentrations at the Cerco de Almadenejos, Almadén mining district (Spain): The old metallurgical precinct (1794 to 1861 AD) and surrounding areas. *Journal of Geochemical Exploration*, 109 (1-3), pp.70–77.

McBride, M., Sauvé, S. & Hendershot, W. (1997) Solubility control of Cu, Zn, Cd and Pb in contaminated soils. *European Journal of Soil Science*, 48 (2), pp.337–346.

McLaughlin, M.J., Parker, D.R. & Clarke, J.M. (1999) Metals and micronutrients - food safety issues. *Field Crops Research*, 60, pp.143–163.

Meda, A.R., Scheuermann, E.B., Prechsl, U.E., Erenoglu, B., Schaaf, G., Hayen, H., Weber, G. & Wiren, von, N. (2007) Iron acquisition by phytosiderophores contributes to cadmium tolerance. *Plant Physiology*, 143 (4), pp.1761–1773.

Meers, E., Laing, Du, G., Unamuno, V., Ruttens, A., Vangronsveld, J., Tack, F.M.G. & Verloo, M.G. (2007) Comparison of cadmium extractability from soils by commonly used single extraction protocols. *Geoderma*, 141 (3-4), pp.247–259.

Mendez, M.O. & Maier, R.M. (2007) Phytostabilization of mine tailings in arid and semiarid environments—an emerging remediation technology. *Environmental Health Perspectives*, 116 (3), pp.278–283.

Meng, B., Feng, X., Qiu, G., Liang, P., Li, P., Chen, C. & Shang, L. (2011) The process of methylmercury accumulation in rice (*Oryza sativa L.*). *Environmental Science & Technology*, 45 (7), pp.2711–2717.

Meng, B., Feng, X., Qiu, G., Wang, D., Liang, P., Li, P. & Shang, L. (2012) Inorganic mercury accumulation in rice (*Oryza sativa L.*). *Environmental Toxicology and Chemistry*, 31 (9), pp.2093–2098.

Mertens, J. & Smolders, E. (2013) Zinc. In: B. J. Alloway ed. *Heavy Metals in Soils: Trace Metals and Metalloids in Soils and their Bioavailability*. Dordrecht, Nederlands, Springer, pp.465–493.

Mihaljevic, M., Ettler, V., Sebek, O., Drahota, P., Strnad, L., Prochazka, R., Zeman, J. & Sracek, O. (2010) Alteration of arsenopyrite in soils under different vegetation covers. *Science of The Total Environment*, 408 (6), pp.1286–1294.

Mikac, M., Foucher, D., Niessen, S., Lojen, S. & Fischer, J. (2003) Influence of chloride and sediment matrix on the extractability of HgS (cinnabar and metacinnabar) by nitric acid. *Analytical and Bioanalytical Chemistry*, 377, pp.1196–1201.

Miler, M. & Gosar, M. (2012) Characteristics and potential environmental influences of mine waste in the area of the closed Mežica Pb–Zn mine (Slovenia). *Journal of Geochemical Exploration*, 112, pp.152–160.

Miller, J.R., Hudson, D.K.A., Lechler, P.J., Preston, D. & Macklin, M.G. (2004) Heavy

metal contamination of water, soil and produce within riverine communities of the Río Pilcomayo Basin, Bolivia. *Science of The Total Environment*, 320 (2-3), pp.189–209.

Moreno, T., Higueras, P., Jones, T., McDonald, I. & Gibbons, W. (2005) Size fractionation in mercury-bearing airborne particles ($HgPM_{10}$) at Almadén, Spain: Implications for inhalation hazards around old mines. *Atmospheric Environment*, 39 (34), pp.6409–6419.

Moreno, T., Oldroyd, A., McDonald, I. & Gibbons, W. (2006) Preferential fractionation of trace metals–metalloids into PM_{10} resuspended from contaminated gold mine tailings at Rodalquilar, Spain. *Water, Air & Soil Pollution*, 179 (1-4), pp.93–105.

Navarro, A. (2008) Review of characteristics of mercury speciation and mobility from areas of mercury mining in semi-arid environments. *Reviews in Environmental Science and Bio/Technology*, 7 (4), pp.287–306.

Navarro, A., Cardellach, E. & Corbella, M. (2009) Mercury mobility in mine waste from Hg-mining areas in Almería, Andalusia (SE Spain). *Journal of Geochemical Exploration*, 101 (3), pp.236–246.

Navarro, M.C., Pérez-Sirventa, C., Martínez-Sáncheza, M.J., Vidala, J., Tovara, P.J. & Bech, J. (2008) Abandoned mine sites as a source of contamination by heavy metals: A case study in a semi-arid zone. *Journal of Geochemical Exploration*, 96, pp.183–193.

Niu, Z., Zhang, X., Wang, Z. & Ci, Z. (2011) Field controlled experiments of mercury accumulation in crops from air and soil. *Environmental Pollution*, 159 (10), pp.2684–2689.

Nordstrom, D.K. & Wilde, F.D. (2008) Reduction-oxidation potential (electrode method). In: F. D. Wilde ed. *National Field Manual for the Collection of Water Quality Data*. U.S. Geological Survey. Available from: <http://water.usgs.gov/owq/FieldManual/Chapter6/6.5_contents.html>. [Accessed October 2012].

Norton, G.J., Adomako, E.E., Deacon, C.M., Carey, A., Price, A.H. & Meharg, A.A. (2013) Effect of organic matter amendment, arsenic amendment and water management regime on rice grain arsenic species. *Environmental Pollution*, 177, pp.38–47.

Oyarzun, R., Martínez, J.I.M., García, J.A.L. & Carmona, C. (2013) An account of the events that led to full bay infilling with sulfide tailings at Portman (Spain), and the search for 'black swans' in a potential land reclamation scenario. *Science of The Total Environment*, 454-455, pp.245–249.

O'Reilly, S.E., Strawn, D.G. & Sparks, D.L. (2001) Residence time effects on arsenate adsorption/desorption mechanisms on goethite. *Soil Science Society of America*, 65, pp.67–77.

Paktunc, D. & Bruggeman, K. (2010) Solubility of nanocrystalline scorodite and amorphous ferric arsenate: Implications for stabilization of arsenic in mine

wastes. *Applied Geochemistry*, 25 (5), pp.674–683.

Pal, P., Sen, M., Manna, A., Pal, J., Pal, P., Roy, S. & Roy, P. (2009) Contamination of groundwater by arsenic: a review of occurrence, causes, impacts, remedies and membrane-based purification. *Journal of Integrative Environmental Sciences*, 6 (4), pp.295–316.

Paquette, K.E. & Helz, G.R. (1997) Inorganic speciation of mercury in sulfidic waters: the importance of zero-valent sulfur. *Environmental Science & Technology*, 31 (7), pp.2148–2153.

Parviainen, A., Isosaari, P., Loukola-Ruskeeniemi, K., Nieto, J.M. & Gervilla, F. (2012a) Occurrence and mobility of As in the Ylöjärvi Cu–W–As mine tailings. *Journal of Geochemical Exploration*, 114, pp.36–45.

Parviainen, A., Lindsay, M.B.J., Pérez-López, R., Gibson, B.D., Ptacek, C.J., Blowes, D.W. & Loukola-Ruskeeniemi, K. (2012b) Arsenic attenuation in tailings at a former Cu-W-As mine, SW Finland. *Applied Geochemistry*, pp.1–11.

Pedersen, H.D., Postma, D. & Jakobsen, R. (2006) Release of arsenic associated with the reduction and transformation of iron oxides. *Geochimica et Cosmochimica Acta*, 70 (16), pp.4116–4129.

Peralta-Videa, J.R., Lopez, M.L., Narayan, M., Saupe, G. & Gardea-Torresdey, J. (2009) The biochemistry of environmental heavy metal uptake by plants: Implications for the food chain. *The International Journal of Biochemistry & Cell Biology*, 41 (8-9), pp.1665–1677.

Ponnamperuma, F.N. (1972) The chemistry of submerged soils. *Advances in Agronomy*, 24, pp.29–88.

Pradhan, D., Kim, D.J., Chaudhury, G.R., Sohn, J.S. & Lee, S.W. (2010) Dissolution kinetics of complex sulfides using acidophilic microorganisms. *Materials Transactions*, 51 (2), pp.413–419.

Pueyo, M., Sastre, J., Hernandez, E., Vidal, M., Lopez-Sanchez, J.F. & Rauret, G. (2003) Prediction of trace element mobility in contaminated soils by sequential extraction. *Journal of Environmental Quality*, 32, pp.2054–2066.

Qiu, G., Feng, X., Meng, B., Sommar, J. & Gu, C. (2012) Environmental geochemistry of an active Hg mine in Xunyang, Shaanxi Province, China. *Applied Geochemistry*, 27 (12), pp.2280–2288.

Qiu, G., Feng, X., Wang, S. & Shang, L. (2006) Environmental contamination of mercury from Hg-mining areas in Wuchuan, northeastern Guizhou, China. *Environmental Pollution*, 142 (3), pp.549–558.

Qiu, G., Feng, X., Wang, S. & Shang, L. (2005) Mercury and methylmercury in riparian soil, sediments, mine-waste calcines, and moss from abandoned Hg mines in east Guizhou province, southwestern China. *Applied Geochemistry*, 20 (3), pp.627–638.

Quazi, S., Sarkar, D. & Datta, R. (2011) Changes in arsenic fractionation,

bioaccessibility and speciation in organo-arsenical pesticide amended soils as a function of soil aging. *Chemosphere*, 84 (11), pp.1563–1571.

Ramsey, P.W., Rillig, M.C., Feris, K.P., Moore, J.N. & Gannon, J.E. (2005) Mine waste contamination limits soil respiration rates: a case study using quantile regression. *Soil Biology and Biochemistry*, 37 (6), pp.1177–1183.

Rao, C., Sahuquillo, A. & Lopez Sanchez, J. (2008) A review of the different methods applied in environmental geochemistry for single and sequential extraction of trace elements in soils and related materials. *Water, Air & Soil Pollution*, 189 (1-4), pp.291–333.

Ravichandran, M. (2004) Interactions between mercury and dissolved organic matter-a review. *Chemosphere*, 55 (3), pp.319–331.

Ravichandran, M., Aiken, G.R., Reddy, M.M. & Ryan, R.N. (1998) Enhanced dissolution of cinnabar (mercury sulphide) by dissolved organic matter isolated from the florida everglades. *Environmental Science & Technology*, 32 (21), pp.3305–3311.

Ravichandran, M., Aiken, G.R., Ryan, J.N. & Reddy, M.M. (1999) Inhibition of precipitation and aggregation of metacinnabar (mercuric sulphide) by dissoved organic matter isolated from the florida everglades. *Environmental Science & Technology*, 33 (9), pp.1418–1423.

Razo, I., Carrizales, L., Castro, J., Fernando, D. & Monroy, M. (2004) Arsenic and heavy metal pollution of soil, water and sediments in a semi-arid climate mining area in Mexico. *Water, Air & Soil Pollution*, 152, pp.129–152.

Reddy, M.M. & Aiken, G.R. (2001) Fulvic acid-sulfide ion competition for mercury ion binding in the Florida Everglades. *Water, Air & Soil Pollution*, 132 (1/2), pp.89–104.

Revis, N.W., Osborne, T.R., Sedgley, D. & King, A. (1989) Quantitative method for determining the concentration of mercury(II) sulphide in soils and sediments. *Analyst*, 114 (7), pp.823–825.

Roberts, D.R., Scheinost, A.C. & Sparks, D.L. (2002) Zinc speciation in a smelter-contaminated soil profile using bulk and microspectroscopic techniques. *Environmental Science & Technology*, 36 (8), pp.1742–1750.

Robles-Arenas, V.M., Rodriguez, R., Garcia, C., Manteca, J.I. & Candela, L. (2006) Sulphide-mining impacts in the physical environment: Sierra de Cartagena-La Union (SE Spain) case study. *Environmental Geology*, 51 (1), pp.47–64.

Robson, T.C., Braungardt, C.B., Keith-Roach, M.J., Rieuwerts, J.S. & Worsfold, P.J. (2013) Impact of arsenopyrite contamination on agricultural soils and crops. *Journal of Geochemical Exploration*, 125, pp.102–109.

Rothenberg, S.E., Feng, X. & Li, P. (2011) Low-level maternal methylmercury exposure through rice ingestion and potential implications for offspring health. *Environmental Pollution*, 159 (4), pp.1017–1022.

Roussel, C., Néel, C. & Bril, H. (2000) Minerals controlling arsenic and lead solubility in an abandoned gold mine tailings. *Science of The Total Environment*, 263, pp.209–219.

Rumball, J.A. & Richmond, G.D. (1996) Measurement of oxidation in a base metal flotation circuit by selective leaching with EDTA. *International Journal of Mineral Processing*, 48 (1-2), pp.1–20.

Rytuba, J., Foster, A., Kim, C.S., Slowey, A.J., Lawler, D. & Forester, R. (2007) Arsenic contamination from the Kelly silver and Yellow Aster gold mine tailings, California: a potential health concern in the north-central Mojave desert. In: Proceedings of the GSA Denver Annual Meeting, Denver, CO, USA, p.31. Boulder, CO, USA, The Geological Society of America. Available from: <https://gsa.confex.com/gsa/2007AM/finalprogram/abstract_132396.htm>. [Accessed September 2013].

Rytuba, J.J. (2003) Mercury from mineral deposits and potential environmental impact. *Environmental Geology*, 43 (3), pp.326–338.

Rytuba, J.J. (2000) Mercury mine drainage and processes that control its environmental impact. *Science of The Total Environment*, 260 (1), pp.57–71.

Safari, V., Arzpeyma, G., Rashchi, F. & Mostoufi, N. (2009) A shrinking particle - shrinking core model for leaching of a zinc ore containing silica. *International Journal of Mineral Processing*, 93 (1), pp.79–83.

Salzsauler, K.A., Sidenko, N.V. & Sherriff, B.L. (2005) Arsenic mobility in alteration products of sulfide-rich, arsenopyrite-bearing mine wastes, Snow Lake, Manitoba, Canada. *Applied Geochemistry*, 20 (12), pp.2303–2314.

Sapsford, D.J., Bowell, R.J., Dey, M. & Williams, K.P. (2009) Humidity cell tests for the prediction of acid rock drainage. *Minerals Engineering*, 22 (1), pp.25–36.

Sarret, G., Balesdent, J., Bouziri, L., Garnier, J.-M., Marcus, M.A., Geoffroy, N., Panfili, F. & Manceau, A. (2004) Zn speciation in the organic horizon of a contaminated soil by micro-X-ray fluorescence, micro- and powder-EXAFS spectroscopy, and isotopic dilution. *Environmental Science & Technology*, 38 (10), pp.2792–2801.

Scherer, W.H. (2009) Sulfur in soils. *Journal of Plant Nutrition and Soil Science*, 172 (3), pp.326–335.

Schippers, A. (2004) Biogeochemistry of metal sulfide oxidation in mining environments, sediments, and soils. In: *Sulfur Biogeochemistry: Past and Present*. Boulder, Colorado, USA, The Geological Society of America, pp.49–62.

Schlüter, K. (2000) Review: evaporation of mercury from soils. an integration and synthesis of current knowledge. *Environmental Geology*, 39 (3-4), pp.249–271.

Schuster, E. (1991) The behavior of mercury in the soil with special emphasis on complexation and adsorption processes - A review of the literature. *Water, Air & Soil Pollution*, 56 (1), pp.667–680.

Schwertmann, U. & Murad, E. (1983) Effect of pH on the formation of goethite and

hematite from ferrihydrite. *Clays and Clay Minerals*, 31 (4), pp.277–284.

Shiomi, K. (1994) Arsenic in marine organisms; chemical forms and toxicological aspects. In: J. O. Nriagu ed. *Arsenic in the environment part II: Human health and ecosystem effects*. New York, USA, John Wiley & Sons, p.320.

Simmons, R.W., Pongsakul, P., Saiyasitpanich, D. & Klinphoklap, S. (2005) Elevated levels of cadmium and zinc in paddy soils and elevated levels of cadmium in rice grain downstream of a zinc mineralized area in Thailand: implications for public health. *Environmental Geochemistry & Health*, 27 (5-6), pp.501–511.

Simón, M., Martın, F., Ortiz, I., Garcıa, I., Fernández, J., Fernández, E., Dorronsoro, C. & Aguilar, J. (2001) Soil pollution by oxidation of tailings from toxic spill of a pyrite mine. *Science of The Total Environment*, 279 (1), pp.63–74.

Slowey, A.J. (2010) Rate of formation and dissolution of mercurysulfide nanoparticles: The dual role of natural organic matter. *Geochimica et Cosmochimica Acta*, 74 (16), pp.4693–4708.

Slowey, A.J., Rytuba, J.J. & Brown, G.E. (2005) Speciation of mercury and mode of transport from placer gold mine tailings. *Environmental Science & Technology*, 39 (6), pp.1547–1554.

Smolders, E. & Mertens, J. (2013) Cadmium. In: B. J. Alloway ed. *Heavy Metals in Soils: Trace Metals and Metalloids in Soils and their Bioavailability*. Dordrecht, Nederlands, Springer, pp.283–311.

Soghoian, S. & Sinert, R.H. (2009) Toxicity, Heavy Metals [Internet]. Available from: <http://emedicine.medscape.com/article/814960-overview> [Accessed 3 October 2012].

Stanton, M.R., Gemery-Hill, P.A., Shanks, W.C. & Taylor, C.D. (2008) Rates of zinc and trace metal release from dissolving sphalerite at pH 2.0–4.0. *Applied Geochemistry*, 23 (2), pp.136–147.

Stein, E.D., Cohen, Y. & Winer, A.M. (1996) Environmental distribution and transformation of mercury compounds. *Critical Reviews in Environmental Science & Technology*, 26 (1), pp.1–43.

Steinnes, E. (2013) Mercury. In: B. J. Alloway ed. *Heavy Metals in Soils: Trace Metals and Metalloids in Soils and their Bioavailability*. Dordrecht, Nederlands, Springer.

Stookey, L.L. (1970) Ferrozine-a new spectrophotometric reagent for iron. *Analytical and Bioanalytical Chemistry*, 42 (7), pp.779–781.

Takahashi, Y., Minamikawa, R., Hattori, K.H., Kurishima, K., Kihou, N. & Yuita, K. (2004) Arsenic behavior in paddy fields during the cycle of flooded and non-flooded periods. *Environmental Science & Technology*, 38 (4), pp.1038–1044.

Tchounwou, P.B., Ayensu, W.K., Ninashvili, N. & Sutton, D. (2003) Review: Environmental exposure to mercury and its toxicopathologic implications for public health. *Environmental Toxicology*, 18 (3), pp.149–175.

Ullrich, S.M., Tanton, T.W. & Abdrashitova, S.A. (2001) Mercury in the aquatic environment: a review of factors affecting methylation. *Critical Reviews in Environmental Science & Technology*, 31 (3), pp.241–293.

UNEP (2001) *Abandoned mines: Problems, issues and policy challenges for decision makers*. Paris, France, United Nations Environment Programme.

UNEP (2009) *Executive summary of the report on the extent of contaminated sites*. United Nations Environment Programme. Available from: <http://www.unep.org/gc/gcss-x/download.asp?ID=1074>. [Accessed July 2013].

United States Environmental Protection Agency (2004) Test methods for evaluating solid waste, physical/chemical methods [Internet], 4 ed. Available from: <http://www.epa.gov/epawaste/hazard/testmethods/sw846/online/index.htm> [Accessed 3 October 2012].

United States Geological Survey (2008) *Minerals Yearbook 2008 for Zinc*. Washington DC, U.S Geological Survey.

Uraguchi, S., Mori, S., Kuramata, M., Kawasaki, A., Arao, T. & Ishikawa, S. (2009) Root-to-shoot Cd translocation via the xylem is the major process determining shoot and grain cadmium accumulation in rice. *Journal of Experimental Botany*, 60 (9), pp.2677–2688.

US Geological Survey (2013) *Mineral commodity summaries 2013*. Reston, Virginia, U.S. Geological Survey. Available from: <http://minerals.usgs.gov/minerals/pubs/mcs/2013/mcs2013.pdf>.

USDA Foreign Agriculture Service (2010) GAIN report: National food safety standard - maximum levels of contaminants in food [Internet]. Available from: <http://gain.fas.usda.gov/Recent%20GAIN%20Publications/National%20Food%20Safety%20Standard-Maximum%20Levels%20of%20Contaminants%20in%20Food_Beijing_China%20-%20Peoples%20Republic%20of_8-19-2010.pdf> [Accessed 24 January 2013].

USGS (2010) *Mineral commodity summaries 2010*. U.SGeological Survey ed. Washington DC, USA, U.S Geological Survey.

Vazquez-Rodriguez, A.I., Santelli, C.M., Kim, C.S., Brooks, S.C. & Hansel, C.M. (2012) In situ colonization of HgS mineral by sulfur-oxidizing bacteria and the enhancement of HgS weathering. *Mineralogical Magazine*, 76 (6), p.2488.

Vazquez-Rodriguez, A.I., Zhang, T., Lamborg, C.H., Santelli, C.M., Brooks, S.C. & Hansel, C.M. (2013) Volatilization of Hg from HgS minerals mediated by the coupled activity of thiosulfate and a sulfur-oxidizing bacterium. In: Proceedings of Goldschmidt 2013, Florence, Italy, p.2404. Available from: <http://goldschmidt.info/2013/abstracts/finalPDFs/2404.pdf>. [Accessed September 2013].

Vela, N.P. & Caruso, J.A. (1993) Potential of liquid chromatography–inductively

coupled plasma mass spectrometry for trace metal speciation. Invited lecture. *Journal of Analytical Atomic Spectrometry*, 8, pp.787–794.

Voegelin, A., Jacquat, O., Pfister, S., Barmettler, K., Scheinost, A.C. & Kretzschmar, R. (2011) Time-dependent changes of zinc speciation in four soils contaminated with zincite or sphalerite. *Environmental Science & Technology*, 45 (1), pp.255–261.

Walker, F.P., Schreiber, M.E. & Rimstidt, J.D. (2006) Kinetics of arsenopyrite oxidative dissolution by oxygen. *Geochimica et Cosmochimica Acta*, 70 (7), pp.1668–1676.

Wang, M.Y., Chen, A.K., Wong, M.H., Qiu, R.L., Cheng, H. & Ye, Z.H. (2011) Cadmium accumulation in and tolerance of rice (*Oryza sativa L.*) varieties with different rates of radial oxygen loss. *Environmental Pollution*, 159 (6), pp.1730–1736.

Waples, J., Nagy, K., Aiken, G. & Ryan, J. (2005) Dissolution of cinnabar (HgS) in the presence of natural organic matter. *Geochimica et Cosmochimica Acta*, 69 (6), pp.1575–1588.

Weisener, C.G., Smart, R. & Gerson, A.R. (2003) Kinetics and mechanisms of the leaching of low Fe sphalerite. *Geochimica et Cosmochimica Acta*, 67 (5), pp.823–830.

Wenzel, W.W. (2013) Arsenic. In: B. J. Alloway ed. *Heavy Metals in Soils: Trace Metals and Metalloids in Soils and their Bioavailability*. Dordrecht, Nederlands, Springer.

WHO (2000) Arsenic. In: *Air Quality Guidelines for Europe*. Geneva, Switzerland, World Health Organisation.

WHO (2003) *Elemental mercury and inorganic mercury compounds: Human health aspects*. Geneva, Switzerland, World Health Organisation.

WHO (1999) *Evaluation of certain food additives and contaminants. 53rd Report of the Joint FAO/WHO Expert Committee on Food Additives*. Geneva, Switzerland, World Health Organisation.

WHO (2005) *Evaluation of certain food additives and contaminants. 64th Report of the Joint FAO/WHO Expert Committee on Food Additives*. Geneva, Switzerland, World Health Organisation.

WHO (1993) *Guidelines for drinking-water quality*. 2nd ed. Geneva, Switzerland, World Health Organisation.

WHO/FAO (1989) *Evaluation of certain food additives and contaminants*. Geneva, Switzerland, Food and Agriculture Organizaton of the United Nations & World Health Organization.

WHO/FAO (2006) *Report of the 38th session of the Codex Committee on Food Additives and Contaminants*. The Hague, Netherlands, Food and Agriculture Organizaton of the United Nations & World Health Organization.

WHO/FAO (2010) *Summary and Conclusions of the Seventy-Second Meeting of the Joint FAO/WHO Expert Committee on Food Additives*. Geneva, Switzerland, Food and Agriculture Organizaton of the United Nations & World Health Organization.

WHO/FAO (2003) *Summary and conclusions of the sixty-first meeting of the Joint FAO/WHO expert committee on food additives*. Geneva, Switzerland, Food and Agriculture Organizaton of the United Nations & World Health Organization.

Williams, P.N., Price, A.H., Raab, A., Hossain, S.A., Feldmann, J. & Meharg, A.A. (2005) Variation in arsenic speciation and concentration in paddy rice related to dietary exposure. *Environmental Science & Technology*, 39 (15), pp.5531–5540.

Williams, P.N., Villada, A., Deacon, C., Raab, A., Figuerola, J., Green, A.J., Feldmann, J. & Meharg, A.A. (2007) Greatly enhanced arsenic shoot assimilation in rice leads to elevated grain levels compared to wheat and barley. *Environmental Science & Technology*, 41 (19), pp.6854–6859.

Wojciechowska-Mazurek, M., Starska, K., Brulinska-Ostrowska, E., Plewa, M., Biernat, U. & Karlowski, K. (2006) Assessment of contamination of cereal products with elements noxious to human health. *Polish Journal of Environmental Studies*, 15, pp.546–549.

Xu, X.Y., McGrath, S.P., Meharg, A.A. & Zhao, F.J. (2008) Growing rice aerobically markedly decreases arsenic accumulation. *Environmental Science & Technology*, 42 (15), pp.5574–5579.

Yang, Z., Haneklaus, S., Singh, B. & Schnug, E. (2007) Effect of repeated applications of elemental sulfur on microbial population, sulfate concentration, and pH in soils. *Communications in Soil Science and Plant Analysis*, 39 (1-2), pp.124–140.

Yorks, T.E. & McHale, P.J. (2000) Effects of cold storage on anion, ammonium, and total nitrogen concentrations in soil water. *Communications in Soil Science and Plant Analysis*, 31 (1-2), pp.141–148.

Yu, H., Wang, J., Fang, W., Yuan, J. & Yang, Z. (2006) Cadmium accumulation in different rice cultivars and screening for pollution-safe cultivars of rice. *Science of The Total Environment*, 370 (2-3), pp.302–309.

Yu, Y., Zhu, Y., Gao, Z., Gammons, C.H. & Li, D. (2007) Rates of arsenopyrite oxidation by oxygen and Fe(III) at pH 1.8-12.6 and 15-45 ˚C. *Environmental Science & Technology*, 41, pp.6460–6464.

Yu-Hong, S., McGrath, S.P. & Fang-Jie, Z. (2010) Rice is more efficient in arsenite uptake and translocation than wheat and barley. *Plant & Soil*, 328 (1/2), pp.27–34.

Zarcinas, B.A., Pongsakul, P., McLaughlin, M.J. & Cozens, G. (2004) Heavy metals in soils and crops in Southeast Asia 2. Thailand. *Environmental Geochemistry & Health*, 26 (4), pp.359–371.

Zhang, H., Feng, X., Larssen, T., Qiu, G. & Vogt, R.D. (2010) In inland China, rice,

rather than fish, is the major pathway for methylmercury exposure. *Environmental Health Perspectives*, 118 (9), pp.1183–1188.

Zhang, W.D., Liu, D.S., Tian, J.C. & He, F.L. (2009) Toxicity and accumulation of arsenic in wheat (*Triticum aestivum L.*) varieties of China. *International Journal of Experimental Botany*, 78, pp.147–154.

Zhao, F., Stroud, J.L., Eagling, T., Dunham, S.J., McGrath, S.P. & Shewry, P.R. (2010a) Accumulation, distribution, and speciation of arsenic in wheat grain. *Environmental Science & Technology*, 44 (14), pp.5464–5468.

Zhao, H., Xia, B., Fan, C., Zhao, P. & Shen, S. (2012) Human health risk from soil heavy metal contamination under different land uses near Dabaoshan mine, southern China. *Science of The Total Environment*, 417-418, pp.45–54.

Zhao, L., Wu, L., Li, Y., Animesh, S., Zhu, D. & Uphoff, N. (2010b) Comparisons of yield, water use efficiency, and soil microbial biomass as affected by the system of rice intensification. *Communications in Soil Science and Plant Analysis*, 41 (1), pp.1–12.

Zhuang, P., McBride, M., Xia, H., Li, N. & Li, Z. (2009) Health risk from heavy metals via consumption of food crops in the vicinity of Dabaoshan mine, south China. *Science of The Total Environment*, 407 (5), pp.1551–1561.

Zota, A.R., Willis, R., Jim, R., Norris, G.A., Shine, J.P., Duvall, R.M., Schaider, L.A. & Spengler, J.D. (2009) Impact of mine waste on airborne respirable particulates in northeastern Oklahoma, United States. *Journal of the Air & Waste Management Association*, 59 (11), pp.1347–1357.

Publications

Robson, T.C. et al., 2014. Cadmium contamination of agricultural soils and crops resulting from sphalerite weathering. *Environmental Pollution*, 184, pp.283–289. DOI: http://dx.doi.org/10.1016/j.envpol.2013.09.001

Robson, T.C. et al., 2013. Impact of arsenopyrite contamination on agricultural soils and crops. *Journal of Geochemical Exploration*, 125, pp.102–109. DOI: http://dx.doi.org/10.1016/j.gexplo.2012.11.013